UNIVERSITY OF SOUTHAMPTON

Impact of Physiology, Ecology, and Trait Trade-offs on Marine Plankton Communities and the Carbon Cycle

by

Marco Puglia

A thesis submitted in partial fulfillment for the degree of Doctor of Philosophy

in the
Faculty of Environmental and Life Science
Ocean and Earth Science

15 October 2024

ORCID: 0000-0003-2357-013X

Contents

Abstract

Plankton modeling helps us understand how aquatic ecosystems and marine biogeochemistry interact. With observations and eco-physiological rules, it is possible to create simulations where plankton assemble their communities and shed light on the mechanisms that regulate the carbon cycle. Past literature assumed that plankton can be neatly categorized, according to the trophic strategy, into "phytoplankton" and "zooplankton". Autotrophic phytoplankton use photosynthesis and inorganic nutrients, while heterotrophic zooplankton consume other organisms or organic substances. However, in recent years, it has become apparent that trophic strategies exist on a spectrum, with many organisms occupying a continuous spectrum between strictly autotrophy and strictly heterotrophy. "Mixotrophs" are organisms capable of using both autotrophy and heterotrophy, and their role in the ecosystems increases size and carbon export. One of the main questions about mixotrophs is the role of their trophic "trade-off", where a trade-off is a compromise between different traits in the same organism (the autotrophic and heterotrophic traits in this case). In this thesis, through plankton modelling, I show that the trophic trade-off is slightly penalizing for mixotrophs, which decreases the capacity of mixotrophs to increase plankton average size and carbon export in a marine community. Another finding is that mixotrophs, through their flexible trophic strategy, survive better than zooplankton during the polar winter, which then increases the coupling between phytoplankton and mixotrophs blooms in the early spring, leading to a decrease in the strength of the carbon pump in the high latitudes. Furthermore, I explored the response of plankton to climate changes showing that mixotrophs increase community resistance to a warmer ocean by increasing average primary production, plankton size and carbon export. However, these increases are not sufficient to stop a possible positive feedback loop between carbon sequestration and climate warming, especially in the light of a sublinear trade-off that erodes the impact of the mixotrophic eco-physiology compared to the impact of phytoplankton and zooplankton. In summary, the higher the global average temperature will rise, the lower the carbon export will become, which in turn will decrease the capacity of plankton to sequester carbon from the atmosphere, and which ultimately feeds back on climate warming itself. This research also shows that the resolution of mixotrophs in computer models could improve the representation of biogeochemical cycles and community structure, which is relevant to the biogeochemistry field and the production of climate changes trajectories.

Chapter 1

Introduction

1.1 Marine Ecosystem Function

Marine microbial ecosystems are responsible for almost half of the global net primary production (Field et al., 1998) amounting to 50±10 Pg of carbon per year (Longhurst et al., 1995; Carr et al., 2006). This flux of carbon impacts biogeochemical cycles (Six and Maier-Reimer, 1996), constitutes the main source of food (directly and indirectly) for larger organisms such as fish and cetaceans, and thus influences human activities such as fisheries (Cheung et al., 2011; Hollowed et al., 2013). Marine plankton, which are mostly made of microbial organisms, exist as diverse communities made of numerous free-drifting populations. Collectively, these organisms form the base of oceanic food webs, where a food web is "a network of consumer–resource interactions among a group of organisms, populations, or aggregate trophic units" (Layman et al., 2015).

Plankton are a large and polyphyletic group with a diverse variety of forms. They include cyanobacteria (*Prochlorococcus*, *Synechococcus*, diazotrophs), photosynthetic protists (*Micromonas*, coccolithophores, diatoms, many dinoflagellates, Stoecker et al., 2017), protist predators (foraminifera, radiolaria, copepods), and the less studied, but not less important, groups such as viruses (Proctor and Fuhrman, 1990), archaea (Van Donk and Ringelberg, 1983) and fungi (Zhang et al., 2015). While the total number of species is unknown, global genomic surveys suggest that the eukaryotic species in the sunlit surface alone account for at least 150,000 different operational taxonomic units (a group of organisms with >97% of the sequence similarities in their 16S ribosomal RNA for prokaryotes and 18S for eukaryotes, De Vargas et al., 2015; Nguyen et al., 2016).

1.2 The biological carbon pump

Plankton drive carbon from the surface of the ocean to the depths in the more broad context of the ocean carbon pump. This pump can be divided (Volk and Hoffert, 1985; Sigman and Haug, 2003) into solubility pump, carbonate pump and biological carbon pump (or BCP). The solubility pump works in two steps: one, a decrease in surface water temperature increases the dissolvability of gaseous carbon in the medium, and two, cold waters are heavier than warm waters, therefore this additional absorbed carbon sinks at depth through the downwelling process.

The carbonate pump, or "hard tissue" pump, is driven by the formation of $CaCO_3$ made by calcifiers (especially coccolithophores) which trap inorganic carbon into shells and other hard structures. In the short term, this transformation releases carbon dioxide in the atmosphere (carbonate counter pump, Heinze et al., 1991), while, in the long term, it sequesters inorganic carbon from sea surface and accumulates carbonate in the ocean sediments.

The BCP, or "soft tissue" pump, is driven by photosynthesis that traps carbon from the atmosphere inside the living biomass (thus, it deals specifically with organic carbon). At surface level, carbon can be either respired back into the atmosphere, or sink in the aphotic zone, together with the rest of the organic matter, generating a downward flux of carbon.

It is estimated that the biological carbon pump accounts for an annual transfer of ∼9 Pg C (DeVries and Weber, 2017), while the total annual carbon sequestration rate in the ocean is of ∼90 Pg C (Prentice et al., 2001). The difference between the two numbers implies that most of the carbon sequestered in the oceans is moved by the solubility pump. However, the biological carbon pump still plays an important role in carbon sequestration and can help us to understand how marine biogeochemistry works.

The BCP acts against the homogenising tendency of ocean mixing to maintain a gradient in the partial pressure of CO_2 (Figure 1.1). It also operates on a timescales from hundreds to tens of thousands of years (DeVries et al., 2012) and is estimated to lower atmospheric CO_2 concentrations by 200 ppm (Parekh et al., 2006).

The photosynthetic conversion of inorganic carbon and nutrients into organic matter occurs only in the sunlit surface, while the remineralisation of organic matter back into inorganic forms occurs largely independently of light at all depths. As organic matter sinks gravitationally, this spatial decoupling of production and remineralisation drives a net flux of carbon into the ocean interior.

The primary production that maintains the BCP is driven by light, temperature, the supply of nutrients coming from vertical mixing, horizontal advection and wind deposition (Sarmiento, 2006; Coale et al., 1996). Phytoplankton photosynthesis fixes inorganic

carbon into organic carbon via the Calvin-Benson cycle, sustaining in this way their net growth, while producing O_2 (gross primary production) (Halsey and Jones, 2015). A part of this net growth and oxygen is used by phytoplankton autotrophic respiration (net primary production) (Roxburgh et al., 2005). The fate of the difference between net primary production and heterotrophic respiration (net community production) (Emerson, 2014) is that of sinking at depth as particulate organic matter (POM). A small portion of the POM, plus most of the dissolved organic matter (DOM), is quickly recycled by microscopic organisms in a process known as the "microbial loop" (Azam et al., 1983), and it is readily available for phytoplankton, while the rest of the organic material sink further in the water column (export production, which is recognised as just POM).

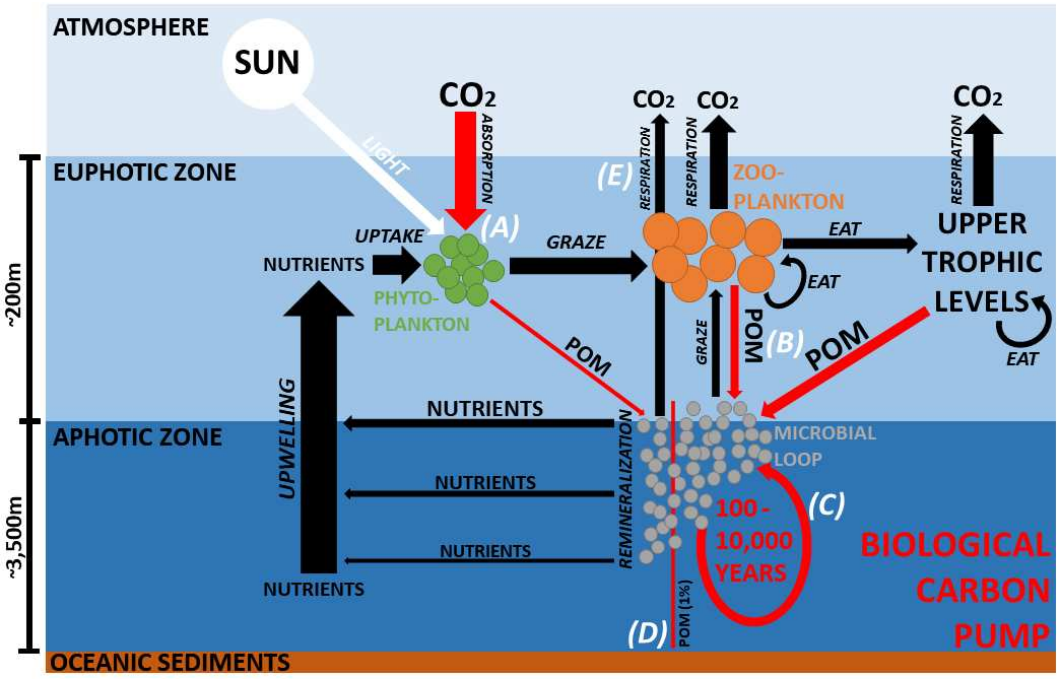

FIGURE 1.1: Schematic representation of the BCP (red arrows). Phytoplankton fix CO_2 using light and nutrients (a). Particulate organic matter (POM), containing carbon, is passed through the different trophic levels (b). Some of this POM sinks in the aphotic zone, and the associated carbon may reside here for thousands of years (c). Only ~1% (Hain et al., 2014) of the carbon reaches the oceanic sediments (d), while the rest is respired back into inorganic form by the microbial loop, in form of DIC (e).

The efficiency and the strength of the BCP is strongly dependent on the remineralisation process, since sensitivity analysis showed that an increase in the depth at which the microbial loop remineralises organic matter can decrease atmospheric carbon concentration of 27 ppm (Kwon et al., 2009). However, in the long term and at global scale, production must be always equal to export (which is mostly made of POM) to guarantee the stability of the system.

The BCP can be defined by its efficiency, or the export production divided by primary production (Ducklow et al., 2001) (to not be confused with "transfer efficiency", which is

the portion of the exported POC that reaches the 1,000 m, Wilson et al., 2022). Export production is defined as the fraction of primary production that is exported below the maximum annual mixed layer depth (Palevsky and Doney, 2021). The strength of the BCP is defined as the quantity of organic carbon transferred at depth (Sarmiento, 2006). Environmental factors and community structure impact efficiency and strength in complex ways. For example, higher temperatures can directly increase plankton metabolism, but may also indirectly suppress it through increased thermal stratification of the water column. Phytoplankton uptake of carbon directly depends on light, temperature and nutrient concentration, while predator's grazing rate depends directly on temperature and prey density.

1.3 Modelling the BCP and other ecosystem functions

Given the challenge of the complexity of this process and the challenges of making field observations in a marine environment, computer simulations have been used to help the study of marine biogeochemistry and plankton ecology. Such models go from non-mechanistic empirical relationships (Laws, 1975) to the explicit representation of the oceans through interconnected compartments, or a 3D grid, that resolves horizontal (latitude and longitude) and vertical (z-levels) portions of the seas (Ridgwell et al., 2007).

The first computer models to represent the BCP were the "nutrient restoring" models (Bacastow and Maier-Reimer, 1990; Najjar et al., 1992). The term nutrient restoring refers to the restoration of the concentration of nutrients to zero, or to values taken from observations, to simulate the effects of local plankton production. These values can be constant (steady state) or vary through time. As nutrients are mixed into the surface layer, such models bring simulated nutrient concentrations back to the observed values by exporting them to depth according to empirically-derived exponential remineralisation profiles (Najjar et al., 1992). Carbon is exported alongside the limiting nutrient, assuming a fixed "Redfieldian" export stoichiometry of 106 C, 16 N and 1 P (Redfield, 1934). Since nutrient restoring models rely on observations related to present time, it makes it difficult to apply this kind of model to scenarios (e.g. climate changes) where we have little or no data to use as input for the nutrient fields.

To allow the investigation of scenarios where observations are absent, models that explicitly resolve nutrient fields as prognostic variables were introduced. Such models can be called "nutrient limitation" models, which, together with nutrient restoring models, are known as models of "biologically-induced chemical fluxes" (Bacastow and Maier-Reimer, 1990; Heinze et al., 1991; Archer and Johnson, 2000). In both kinds of models, nutrients are removed from the surface and instantly redistributed to depth according to observed remineralisation profile, however in "nutrient limitation" models, the rate of

this flux is set by the surface nutrient concentrations, temperature and light availability. In models of biologically-induced chemical fluxes, feedbacks among production, nutrient concentrations and ecological populations are not explicitly resolved, and as such these models cannot represent changes driven by shifts in community composition and function.

The first global biogeochemistry models that allowed the explicit resolution of plankton communities were the so-called "NPZD" models standing for Nutrients, Phytoplankton, Zooplankton and Detritus (Oschlies et al., 2000; Levy et al., 1998). The nutrient compartment represented the available most-limiting nutrient in the environment, which was typically nitrogen or phosphorus, and occasionally also iron (Fiechter et al., 2009). The phytoplankton and zooplankton compartments represented the biomass of all phytoplankton and zooplankton as two homogeneous entities. The detrital compartment represented dead and decaying organic matter. All four compartments are represented in terms of a single nutrient currency, which moves through the four boxes according to the local ecological and environmental conditions, including temperature and light, that may change during the simulation.

While NPZD models can represent changes in the relative dominance of phytoplankton and zooplankton communities (and thus can crudely represent, for example, phytoplankton blooms), they are still unable to resolve changes in relative abundance among the diverse range of organisms within phytoplankton and zooplankton communities. To represent these shifts in community structure, new models (le Quéré et al., 2005) were introduced with explicit representations of multiple "Plankton Functional Types" (PFT). Commonly resolved PFTs include picophytoplankton, microzooplankton, diazotrophs, silicifiers, calcifiers, microzooplankton, and mesozooplankton (Moore et al., 2001; le Quéré et al., 2005).

Different groups have different functional roles, such as, for example, picophytoplankton which are the smallest size class that take up nutrients and fix carbon, and the detritus they produce is so small that it is quickly remineralised, microzooplankton which mediate the flux of biomass and energy from the smallest phytoplankton to higher trophic levels, diazotrophs which convert inert dinitrogen (N_2) into more readily bioavalable forms, silicifiers and calcifiers which take up dissolved silica and DIC, respectively, to build external cellular structures (and as a by-product generate a ballast effect that accelerates the sinking organic particulate, increasing the vertical carbon flux, Armstrong et al., 2001). Offset against this increase in ecological functionality and realism, the inclusion of greater complexity in PFT models also requires a larger number of parameters, which - assuming one additional parameter for each potential flux between state variables - increases approximately as the square of the number of PFTs included in the model (Denman, 2003).

It is possible to estimate some of these parameters from *in situ* or *in vitro* experiments, or by fitting models to data, but model fitting becomes numerically and computationally challenging as the number of unknown parameters increases because these parameters must also be constrained from observations (Denman, 2003; Anderson, 2005). Given the number of different functional groups, the challenges in making observations outside a laboratory and the difficulties of cultivating most of the known plankton, modern research lacks data regarding crucial parameters that are required for more complex models. This challenge becomes even more complex to face if it is considered that functional groups are not neatly restricted to single taxa of plankton, and their taxonomic composition is subject to change in time and space (Anderson, 2005).

1.3.1 Trait-based modelling

NPZD and PFT models both aggregate a large diversity of organisms into single state variables based on their exploitation of similar resources (e.g. light, nutrients and prey). As such, they can be described as models of ecological guilds (Simberloff and Dayan, 1991). As stated above, this neglects changes in community composition within these guilds. As an alternative approach, so-called "trait based" models (see Figure 1.2 for a brief list) attempt to decrease the role of discrete classifications and instead look to represent a diversity of organisms across a more-or-less continuous range of possible trait values.

A trait in this context is "a measurable characteristic of an organism" (Dawson et al., 2021) and traits can be added to models through the trait-based approach. Trait-based models consider generic populations across a range of traits, and each population has similar traits assigned according to observed or theoretical relationships between other traits. The simulated emergence of different trait combinations in different environmental contexts can then be assessed against observations and used to test the validity of the assumed trait relationships.

An important challenge in trait-based modeling is to identify and parameterise how different traits vary relatively to one another and to implement these relationships in an ecosystem model. These relationships are often referred to as trade-offs, under the assumption that organisms have limited resources that can be assigned to optimising particular traits, such as resource acquisition or growth (Follows et al., 2007; Litchman et al., 2007). In other words, a trade-off is a compromise between different functional aspects, or traits, of an organism.

One way to constrain such trade-offs is by taking into account organism size because size is considered a "master trait" (Menden-Deuer and Lessard, 2000; Litchman et al., 2007; Edwards et al., 2012; Marañón et al., 2013), or a trait that explains the majority

of variability in many other traits such as metabolic rate, growth, uptake rate, grazing rate and nutrient requirement (Ward et al., 2017).

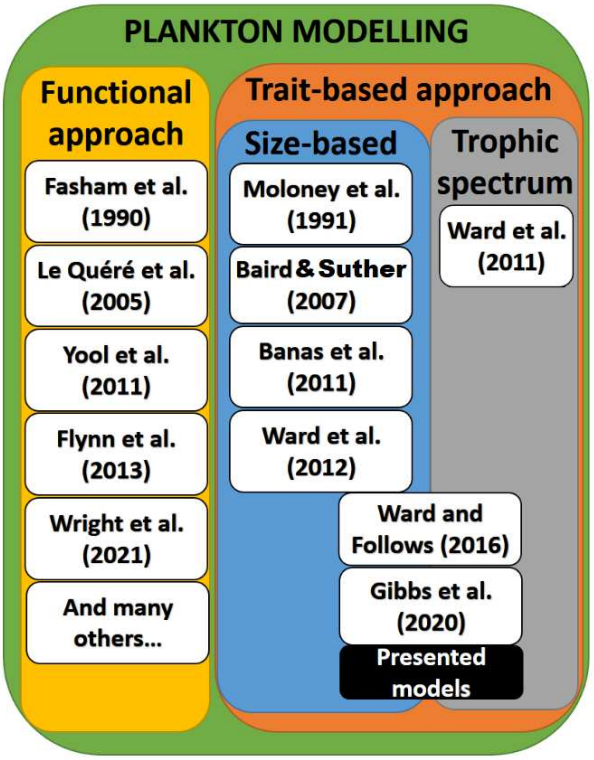

FIGURE 1.2: Plankton modelling can be classified in various categories. Two of these are the functional and the trait-based approach. The trait-based approach can be further divided according to the kinds of traits taken into consideration, in this case size and trophic strategy. The models used in this research belongs to both these sub-categories.

A first step toward a size-resolved model of a plankton community was made by Moloney et al. (1991). In this study each compartment was not a different species, but an agglomeration of different organisms of similar size. Size classes were further divided into separate functional categories of bacteria, phytoplankton and zooplankton. The main ecophysiological traits of each population were then assigned according to observed relationships between organism size, functional classification and key ecophysiological traits, including primary production, ingestion rate, sinking rate etc. This allowed a relatively large number of interacting populations to be efficiently represented with a small number of allometric parameters.

Baird and Suthers (2007) built a structurally similar model, where organisms are categorized and interact primarily based on their size, rather than having size as one of the many parameters. Another advantage of using size was reducing the number of model parameters, for each population, required to describe a complex ecosystem. Some examples of these parameters are the maximum nutrient uptake rate, the minimum quota, the uptake and grazing affinity (Litchman et al., 2007; Edwards et al., 2012; Ward, 2019; Gibbs et al., 2020b). Prey preference is an important factor related to plankton size,

as plankton predators tend to consume prey a certain number of times smaller than themselves. Prey must be sufficiently large to be detected, but not so large that they cannot be captured and ingested (Kiørboe, 2009). Banas (2011) developed a similarly size-structured model with 40 phytoplankton and 40 zooplankton size classes and investigated the effects of size-selective zooplankton predation. The high sensitivity of the emergent community structure to the width of the grazing preference function demonstrated the importance of this trait.

Ward et al. (2012) developed a size-structured ecosystem model within a global ocean circulation model, highlighting the importance of both bottom-up and top-down controls in setting the observed size biogeography of plankton. A common challenge among these approaches is to identify the most important rules and trade-offs that determine the relations between organism size and the modelled plankton traits.

1.4 Plankton physiology in models

Different approaches are used to simulate plankton physiology. Models with Monod (Monod, 1942) equations simulate microorganisms growth rate as a function of the environmental concentration of nutrients, with saturation of the growth at higher nutrient concentrations. However, these models typically use Redfieldian stoichiometry (Redfield, 1934) for the uptake of C:N:P, which is reflected on phytoplankton primary production (Geider and La Roche, 2002), and do not take into account internal cellular nutrient quotas, which determines growth rates. Quota models (Droop, 1968) are thus more biologically plausible, and reproduce changes in elemental ratio, which are observed to occur through time and space (Karl et al., 2001).

Quota models also allow observed temporal decoupling of nutrient uptake and population growth. Here growth rates are not a direct function of the environmental nutrient concentration, but instead of the cellular nutrient quota (defined in units of moles per cell or per mole of cellular carbon). The potential maximum growth rate can be reached only at a theoretical infinite quota. In these models, different nutrients have different internal quotas for each plankton class. These quota allow nutrient uptake to be a saturating function of environmental resource availability, rather than following the assumption that uptake and growth are constantly balanced.

Together with autotrophic uptake, predation (or more generally grazing, which here includes any trophic interactions including herbivory and carnivory) is another process that must be resolved to replicate food webs. Grazing is often represented by one of three so-called "functional responses" (Holling, 1959): Holling type I, where predation linearly increases with prey density without saturation at high prey abundance; Holling type II, where limits on the processing of food causes the grazing rate to saturate at high prey density; and Holling type III, where the type II response is further modified

at low prey abundance, with down-regulation of the predation rate affording scarce prey with a degree of "refuge" from attack (Kalinkat et al., 2023).

Modelled ecological dynamics will also typically include a representation of mortality. In its simplest form, losses to mortality will be a simple linear function of the population biomass. An additional quadratic mortality term can be added to the first mortality term to simulate the intensification of the competition at high population density that is attributable to grazing and viral infection. This additional loss term may help to prevent the potentially unrealistic collapse of both predator and prey populations (Gentleman and Neuheimer, 2008).

1.4.1 Plankton size and trophic strategy

The trait-based approach, used in this thesis, investigates mainly cellular size and trophic strategy in plankton communities.

Traditionally, plankton size has been discretized into few classes: picoplankton (0.2-2 μm), nanoplankton (2-20 μm), microplankton (20-200 μm), mesoplankton (200-2,000 μm) (Hu et al., 2015). All three size classes are distributed globally, however, in sub-tropical gyres >80% of the chlorophyll *a* belongs to picophytoplankton, half of the chlorophyll *a* in equatorial, temperate and polar regions belongs to nanophytoplankton while microphytoplankton is mostly distributed near the continental shelves (Roy et al., 2013).

By taking into account size, it is possible to account not only for the variability in a large number of other ecophysiologically important traits (as listed above) but also for biogeochemistry: larger plankton produce on average larger and denser sinking particles, which sink faster (Stokes' law) than smaller, less dense, particles, and which impacts the BCP. The addition of ballast, biogenic minerals produced by silicifier and calcifier, makes the particle sink faster (Armstrong et al., 2001). Therefore, in a size-based plankton model, it is possible to establish a direct link between eco-physiology and biogeochemical functions (Ward and Follows, 2016).

Together with size, also so-called trophic strategies play a role in defining how food webs work. Two trophic strategies are usually recognized in plankton: autotrophy - nutrition involving the synthesis of complex organic substances using inorganic compounds and photosynthesis and heterotrophy - nutrition involving the uptake of organic substances and capture of other organisms. The impact of size and trophic strategy on plankton community structure and biogeochemical cycles will be further dissected in the next subsection.

The trait-based approach has also been demonstrated to allow predictions about the correlation between trophic strategies and sizes, such for example the fact that the

smallest size classes prefer autotrophy as main way of feeding, while the largest size classes prefer heterotrophy (Andersen et al., 2015).

The two trophic strategies are linked to the concept of "bottom-up control" and "top-down control" (Benndorf et al., 2002). Bottom-up control, defined by environmental factors in the water, such as nutrient concentration, prey density, temperature and light level, controls plankton growth rate and therefore the total amount of primary production. Top-down control, defined by the mortality rate caused by, for example, grazing and infections (e.g. virus, bacteria etc.), controls the quantity of biomass in each size class and the number of phytoplankton and zooplankton species (Armstrong, 1994).

1.4.2 Mixotrophs

While the two trophic strategies are typically considered mutually exclusive, the clear-cut categorisation in plankton (i.e. phytoplankton versus zooplankton) is often a simplifications of a more complex observed phenomenon. These microscopic organisms can be more accurately arranged along a continuous mixotrophic gradient or spectrum (Sanders et al., 1990; Ward, 2019), between the two extremes.

Ecology has for long time underestimated the ubiquity and importance of mixotrophic organisms (Stoecker et al., 2017), their effects of their physiology on marine communities (Jones, 2000; Våge et al., 2013; Godrijan et al., 2020) and their impact on the biogeochemical cycles (Mitra et al., 2014; Ward and Follows, 2016). Mixotrophs can increase the total production of marine ecosystems (Baretta-Bekker et al., 1998; Mitra et al., 2014; Hammer and Pitchford, 2005) and decrease the primary production done by phytoplankton and recycling by bacteria (Stickney et al., 2000).

Primary production and consumption are strictly separated in a system populated only by phytoplankton and zooplankton (Figure 1.3a). This separation does not need to be the case in ecosystems where the first and second trophic levels in the food web are less neatly divided (Figure 1.3b). Mixotrophs, thanks to this trophic flexibility, increase biomass and energy transfers between different levels and changes how elements move in the biogeochemical cycles (Mitra et al., 2014; Stoecker et al., 2017).

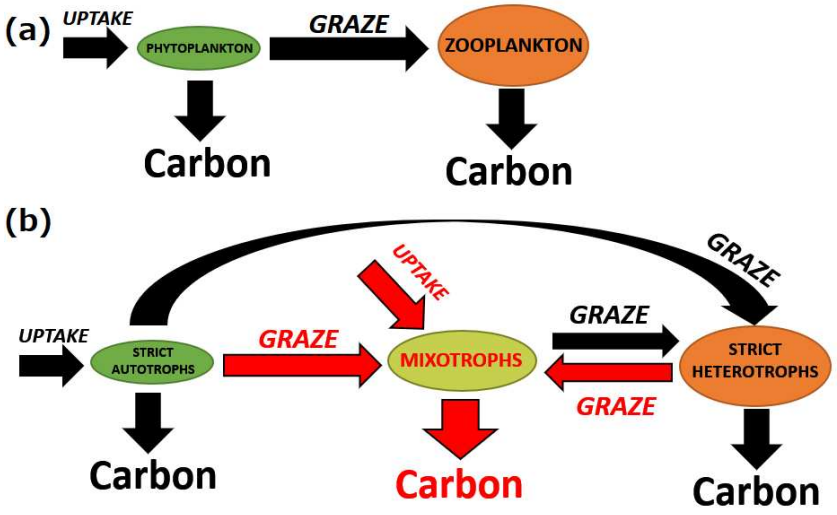

FIGURE 1.3: Schematic representation of the carbon fluxes in the plankton trophic web. **(a)** Web with only autotrophs and heterotrophs. **(b)** Web with strict autotrophs, mixotrophs and strict heterotrophs. Red arrows: crucial difference for the carbon cycle between the two models.

Ward and Follows (2016) showed that mixotrophy may be a globally significant feeding strategy which can change the relationship between nutrient supply and carbon export. The flexible physiology of the simulated mixotrophs allowed the community to achieve larger organisms sizes, which redistributed biomass in the community, and greater carbon assimilation for a given supply of limiting nutrient, which increased the DIC inventory. With larger organisms assumed to produce faster sinking organic detritus, these two shifts in the community lead to a stronger BCP with greater carbon export.

For the rest of this thesis, the mixotrophic strategy will be also called "generalist strategy", while strict autotrophy and strict heterotrophy will be also called "specialist strategies" (Fischer et al., 2017) to allow the comparison between mixotrophs and non-mixotrophs.

1.4.3 Trophic trade-offs in mixotrophs

The concept of "trophic trade-offs" is a useful tool to explore the potential advantages and disadvantages of mixotrophy (Våge et al., 2013). Mixotrophic trade-offs are widely assumed to be driven by the need to assign limited resources to the acquisition and use of light energy, inorganic nutrients and prey (Ward et al., 2011). Specifically, this has been suggested to relate to limited space on and within the organism for the cellular machinery required to acquire and process these different resources (Litchman et al., 2007; Raven, 1997).

Given these assumptions, theoretical studies of mixotrophy have often focused on the related costs that are assumed to offset the benefits of mixotrophy in different environments. For example, a strategy of "eating your competitor" has been argued to give an advantage to mixotrophs because it gives the double advantage of using prey as source of nutrient, alleviating nutrient limitation, and by decreasing competition for inorganic nutrients by increasing the competitor population mortality (Thingstad et al., 1996). Another possibility is that oligotrophic environments allow the coexistence of mixotrophs with phytoplankton because mixotrophs can sustain their phototrophic growth with prey (Stoecker, 1998; Stickney et al., 2000; Hartmann et al., 2012), which is still a relevant capacity if the environment is not constantly oligotrophic but changes in times between repleted and oligotrophic condition because mixotrophs can switch between different ways of feeding (Stoecker, 1998). However, Mitra et al. (2023) argue that the analysis of trade-offs can be done only on species belonging to the same environment and have a close evolutionary relationship, thus plankton mixotrophs do not have a comparable trophic trade-off when they compete with phylogenetically distant specialists.

The trophic trade-off was studied also with numerical experiments. For example, Våge et al. (2013) showed that mixotrophs can coexist with specialists, even with a very costly trade-off (Figure 1.4) if a highly resolved size-spectrum is applied in a nutrient limited environment. Ward et al. (2011) also showed that, when resources are diffusion limited, the disadvantage in mixotrophs of having less resource transporters on the cell surface, if compared to phytoplankton or zooplankton of same size, is absent. Edwards (2019) confirmed the diffusion limited results from previous research and added that the costs for the generalist trophic strategy can be overcome by the synergy (Ward, 2019) between carbon fixation through autotrophy (photosynthesis) and limiting nutrient acquisition through heterotrophy (grazing), at low resource concentration.

If the mixotrophic trade-off is slightly sublinear (see Figure 1.4), that would decrease the potential impact that mixotrophs have on ecosystems and biogeochemistry, as it was showed in the trophic trade-off sensitivity tests of Ward and Follows (2016), where mixotrophs with sublinear trade-off caused a lower increase in size and carbon export, in a simulated ocean, compared to mixotrophs with superlinear or without trade-off. The decrease in the impact is due to decrease in the feeding efficiency of mixotrophs if compared to the feeding strategies of the specialists, which causes a decrease in the abundance of mixotrophs in the community.

Additionally, mixotrophic physiology is more complex than a simple one-dimensional trade-off presented in Figure 1.4, as it is likely influenced by other environmental and eco-physiological factors such as light availability, growth and competitive pressure, but for the aims of this research, the change in shape was limited to the competition between different trophic modes (see Chapter 2).

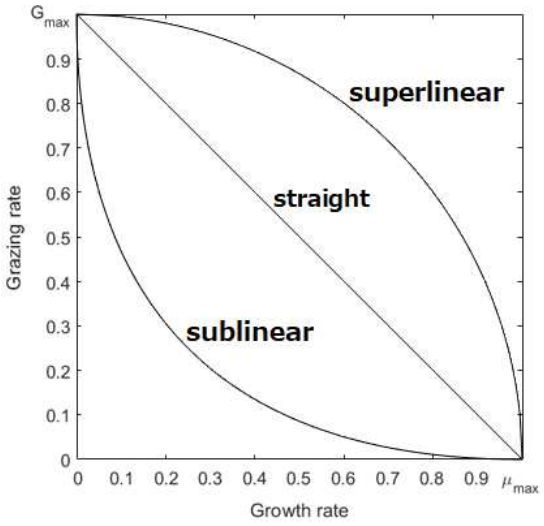

FIGURE 1.4: Visualization of the mixotrophic trade-off function. The sublinear line corresponds to a costly trade-off, while the superlinear line correspond to an advantageous trade-off.

Given the observations that mixotrophs are ubiquitous in the oceans, uncertainties concerning the reaction of mixotrophs to a change in physiology, ecology, water physics and temperature, and uncertainties regarding trade-offs between trophic strategies, an outstanding question is what will be the response in term of average size, biomass and carbon export, of plankton community with mixotrophs in a warmer 21^{st} century.

1.4.4 Mixotrophs and climate changes

The Intergovernmental Panel on Climate Change (IPCC) defines climate change as "*a change in the state of the climate that can be identified ... by changes in the mean and/or the variability of its properties, and that persists for an extended period, typically decades or longer*" (Pachauri et al., 2014). The primary cause of this change is anthropogenic greenhouse gasses, dominated by carbon dioxide (CO_2), with a following increase in the average global temperatures.

Many questions (Bopp et al., 2001; Sarmiento et al., 2004; Henson et al., 2022; Wilson et al., 2022) are still under study while we talk about the relation between climate changes, plankton communities and BCP. For example, what will be the plankton response (quantitative and qualitative) to climate change? What will be the impact of climate changes on plankton biogeography? Will the BCP become weaker or stronger? Will a positive feedback loop be established between increasing concentration of atmospheric CO_2 and a weaker BCP?

Of the four Representative Concentration Pathways (RCP2.6, RCP4.5, RCP6.0, RCP8.5, where the numbers is the difference in radiative forcing, measured in watts per m^2, between the year 2100 and pre-industrial era) proposed by the IPCC, this thesis uses only

the RCP8.5 pathway. Despite its improbability and being considered misleading (Hausfather and Peters, 2020), this trajectory was nonetheless the best pattern to underline the potential changes in plankton community structure and ocean biochemistry because with an increased intensity of climate changes there is also an increased biogeochemical response in the ocean under the assumption that the impact on ocean physics and biogeochemistry is linear across the different scenarios.

Literature has already analysed the impact of increasing temperatures on mixotrophs. For example, Wilken et al. (2013) concluded that increasing temperatures cause mixotrophs to become more heterotrophic due to the differential temperature sensitivity of proteins responsible for autotrophic and heterotrophic metabolism. Subsequently Wilken et al. (2018) added that, in shallow lakes, due to increasing temperatures, but also to decreasing water transparency ("brownification", Kritzberg and Ekström, 2012), bacterivore phytoplankton increase their predation rate. Chan et al. (2019) and González-Olalla et al. (2019) also concluded that increasing temperatures drive mixotrophs toward an increase in the heterotrophic uptake, however González-Olalla et al. (2019) underlined that waters exposed to higher temperatures and higher ultraviolet levels (condition typical for plankton in a water column with a shallower mixed layer), actually drives plankton toward autotrophy. Princiotta et al. (2016) instead founded that a mixotrophic chrysophyte increases its phototrophic and grazing rate between 8° and 16°C, while at 20°C, the rates decline.

Jassey et al. (2015) suggested that increasingly warmer summers negatively impact mixotrophs in peatlands, causing a decrease in biomass (50%) and net carbon uptake (13%). Lepori-Bui et al. (2022) took into consideration the rapid evolution rate of microorganisms, and showed that mixotrophs increase their carbon use efficiency and decreased their photosynthetic rate in favour of their grazing rate in a warmer environment. In a numerical experiment, despite the lack of resolved size and trophic strategy resolution, Wieczynski et al. (2023) underlined the possibility of abrupt and less reversible changes of trophic strategy in mixotrophs, from autotrophy to heterotrophy, with higher temperatures.

In this thesis, one of the major focuses is on climate changes and it's impact on mixotrophs. The relation between these two is little understood, but given the importance of mixotrophs in the carbon cycle and in plankton communities, this study can provide new insights in this subject.

1.5 Thesis objectives and chapters

The aim of this thesis is to shed light on the rules that define plankton community assembly, how mixotrophs impact this process, and what is the final impact of these organisms on the carbon cycle, especially in the light of future climate warming.

The thesis is made of 7 chapters. Excluding the Introduction, the EcoGEnIE model presentation and the Discussion chapter, there are 4 research chapters explicitly dedicated to my research: the first chapter (Chapter 2) will be about how environmental variables impact plankton community structure in a 0D model, and how different values of mixotrophic trade-offs play a role in this; the other three chapters (Chapters 4, 5 and 6) will be about a global ocean simulation and how mixotrophs and/or climate changes scenario will impact the carbon cycle.

1.5.1 Chapter 2: A trait-based model of a plankton food web for the Gulf of Naples

This chapter explores how the organization of plankton communities is determined by environmental parameters and the trophic strategies in the mixotrophic spectrum. This spectrum goes from strict autotrophy, gaining energy and nutrients from inorganic nutrients and sunlight, to strict heterotrophy, gaining energy and nutrients from feeding on other organisms, with intermediate, mixotrophic, organisms using a combination of both strategies. Mixotrophy is still a poorly understood nutritional strategy in plankton communities, from its ecological drawbacks and strengths, to its overall biogeochemical impacts. To gain insights on the role of mixotrophic physiology in the assembly of communities, and to constrain the shape of the mixotrophic trade-off, computer simulations made with different environmental and plankton physiological parameters were performed and compared with observations of taxonomic abundance and trophic interactions from the Gulf of Naples. The final results show that phytoplankton perform better at cold temperatures, zooplankton perform better warm temperatures, while mixotrophs perform better at intermediate temperatures. The best fits between observations and simulations show a mixotrophic trade-off slightly sublinear.

1.5.2 Chapter 3: The EcoGEnIE global plankton ecology model

This chapter introduces to the reader the EcoGEnIE model, its development history, how it works, why it was used for this research and what are the ecological configuration and the simulated scenario used in the rest of the thesis.

1.5.3 Chapter 4: The biogeochemical impacts of mixotrophy over long timescales

Mixotrophs have previously been shown to increase mean organism size and carbon export in the ocean. While this suggests that mixotrophy may serve to increase the ocean's capacity to store inorganic carbon, global modelling studies have been limited to relatively short time scales, on the order of a decade. Such time scales are insufficient to

investigate the impacts of mixotrophy on the ocean's long term capacity for carbon storage, as they cannot fully resolve important feedbacks between surface plankton ecology and the biogeochemistry of the ocean interior, which equilibrate over multi-millennial periods. Here, a relatively low resolution coupled model of ocean ecology, biogeochemistry and circulation was used to explore the possible impacts of mixotrophy on the marine ecosystem over these longer timescales. To achieve this, the model was compared in two configurations: one with separate phytoplankton and zooplankton populations, and one where no such distinction is made (i.e. with all plankton populations characterised as potential mixotrophs). In line with previous studies, it was found that mixotrophy was associated with an increase in carbon export at equatorial and temperate latitudes, but also with a decrease in biomass and carbon export at higher latitudes. The model simulations suggest that this additional effect is driven by tighter coupling between production and grazing in the mixotrophic model, which serves to suppress plankton blooms. Over thousands of years, this cyclical bloom suppression decreases carbon export and leads to a relative decrease in the strength of the BCP, compared to the low latitudes, over much longer timescales, as export carbon is transported through ocean interior by overturning circulation.

1.5.4 Chapter 5: The impacts of anthropogenic climate change on a simulated global plankton community

Plankton play a major role in carbon cycles, and are sensitive to the change of their environment. This chapter focuses on how autotrophic and heterotrophic plankton regulate marine community function such as export production, and how this is affected by the global warming. To gain insights over this issue, two experiments were performed through the use of the EcoGEnIE model: a Control scenario with steady carbon dioxide atmospheric concentrations, and a RCP8.5 scenario with increasing carbon dioxide atmospheric concentrations. The final comparison between these two models shed light on the possible future changes in environmental conditions, plankton population distribution and decrease in the strength of the the carbon biogeochemical cycle in the 21^{st} century. Explicit examples are: a global decrease in phosphorus concentrations, especially at high latitudes; a poleward expansion of the warmer environments, with conditions typical of the equatorial regions characterizing temperate regions, and temperate regions characterizing the polar regions; plankton carbon biomass will move toward the smallest plankton size classes at low latitude and in the larger plankton size classes at high latitudes. Overall, these alterations will cause a decrease in the strength of the BCP.

1.5.5 Chapter 6: The biogeochemical impacts of mixotrophy in a future warmer world

There have been numerous research that combine the study of mixotrophs and warming environmental temperatures in the most recent decade. Modelled mixotrophs have been shown to increase trophic transfer efficiency and export production at the global scale. This has the potential to impact the marine ecosystem's response to environmental changes over the 21^{st} century. This study shows, using a coupled ecosystem and Earth system model, that mixotrophy may enhance the impacts of climate change on mean organism size and carbon export, increasing the magnitude of predicted increases at high latitudes and decreases at low latitudes, relative to a model where mixotrophy is not accounted for. It further showed how an increase of the strength of the trade-off corresponds to a decrease in the relative change in mean organism size and carbon sequestration rate. This change has a potential detrimental effect the global carbon export. All these results suggest that mixotrophy should be included in other Earth system models used to study the carbon cycle and climate in the 21^{st} century.

1.5.6 Chapter 7: Discussion

In the Discussion chapter, the wider implications of the findings will be explored and summarised. Emphasis will be also put on the connections between the findings of different chapters. Lastly, there will be a summary of potential future works that can be started from the experience acquired during this project.

Chapter 2

A trait-based model of a plankton food web for the Gulf of Naples

2.1 Introduction

Export production, that is the part of primary production that sinks into the dark layer of the water column (Falkowski et al., 2003), is often assumed to be balanced over long timescales by the exogenous supply of limiting nutrients to the sunlit ocean surface (Eppley and Peterson, 1979). If it is further assumed that organic carbon is exported alongside nutrients with a fixed Redfieldian stoichiometry (Redfield, 1934) the strength of the BCP can be assumed to be set primarily by the physical processes that deliver nutrients to the surface ocean, with ecological complexity taking a secondary role. However, we now know that mixotrophic organisms can decouple carbon fixation from the supply of limiting nutrients, and can also modify the elemental stoichiometry of plankton and associated organic matter.

Mixotrophs acquire limiting nutrients from prey (Nygaard and Tobiesen, 1993), and offset carbon losses that occur through respiration thanks to photosynthesis (Stoecker, 1998; Stoecker et al., 2017). Furthermore, Ward and Follows (2016) showed that these changes may fundamentally change the relationship between nutrient supply and carbon export. In their model, mixotrophs' more flexible physiology allowed an inrease in plankton average sizes and an increase in carbon acquisition for a given supply of limiting nutrient. Larger and more carbon rich organisms sank deeper in the water column and transported more carbon to depth, which was assumed to increase the oceanic capacity for carbon storage.

As discussed in Chapter 1, Ward and Follows (2016) also showed that the influence on the carbon cycle was strongly dependent not only on the absence/presence of mixotrophs but also on a mixotrophic feeding trade-off (Våge et al., 2013). This trade-off is a

compromise given by the capacities of maintaining both autotrophic and heterotrophic nutrition. This compromise is assumed to be related to space and energy consumption of the different cellular machineries in the same limited cellular space (Raven, 1997). The "shape" of this trade-off is still unknown, but it may have a role in determining community structure and function, which then influences the carbon cycle.

The main traits that vary along the trophic spectrum (between the extremes of photoautotrophic phytoplankton and predatory zooplankton) are the capacities to photosynthesise, to take up inorganic nutrient and to capture and consume prey. Given the size dependence of trophic interactions, this trade-off needs to be understood in the context of a size-structured ecosystem, in which both phytoplankton and zooplankton traits vary strongly as a function of organism size.

To encode the degree to which phytoplankton and zooplankton traits can be combined in the same organism, the shape of the trade-off can be assumed to be linear, superlinear or sublinear (Figure 1.4). A linear trade-off implies that any gain in phytoplankton traits is accompanied by a linearly proportional decline in zooplankton traits, and *vice versa*. A superlinear trade-off represents a synergistic situation in which gains in the traits for one trophic strategy are associated with proportionally smaller losses in the other (mixotrophs thus being "more than the sum of their parts", Ward, 2019). Conversely, a sublinear trade-off represents a situation in which gains in one trophic strategy are offset by disproportionately larger losses in the other (Edwards, 2019).

Regardless of the shape of the trade-off, mixotrophs may benefit from the combined use of multiple resources that were previously assumed to be mutually exclusive. For example, the potential use of nutrients from predation to sustain photosynthesis, and the use of photosynthesis to sustain predatory activity. Different shapes can be mathematically defined by equations 2.1 and 2.2, where μ_{max} and g are the maximum autotrophic growth rate and the grazing rate, ω ($0 \leq \omega \leq 1$) is the balance between phytoplankton ($\omega = 1$) and zooplankton ($\omega = 0$) traits, τ (Castellani et al., 2012) is a scalar number that can be: 1 (a linear trade-off), <1 (a superlinear trade-off - favouring mixotrophs), or >1 (a sublinear trade-off - favouring specialists).

$$\mu_{max}(\tau) = \omega^{\tau} \cdot \mu_{max} \tag{2.1}$$

$$g(\tau) = (1 - \omega)^{\tau} \cdot g \tag{2.2}$$

To understand the influence of mixotrophy on plankton community structure, and to investigate the likely shape of potential trade-offs between phytoplankton and zooplankton traits, the plankton community model of Gibbs et al. (2020a) was applied to simulate the observations made by D'Alelio et al. (2016a). By comparing the model to observations under different assumed values for τ, we can infer the most likely shape of the mixotrophic trade-off for the system in question. The Gibbs et al. (2020a) model is a

trait-based ecosystem model that simulates a plankton community across a range of sizes and trophic strategies, from picoplankton to mesoplankton, and from strict autotrophy to strict heterotrophy. The trait-based approach of Gibbs et al. (2020a) permits a simplified representation of the ecosystem by focusing on the traits of interest and to ignore more complex taxonomic classifications.

This chapter will analyse how the plankton community self assembles according to different environmental parameters. Temperature and light availability will be the main focus because they heavily impact plankton community structure. Investigation on mixotrophic physiology will also shed light on the extent to which mixotrophy is effectively more or less than the sum of its parts (Castellani et al., 2012; Våge et al., 2013; Ward, 2019), and what this means for the carbon cycle in the oceans (Baretta-Bekker et al., 1998; Mitra et al., 2014; Hammer and Pitchford, 2005).

To examine how trophic strategy and organism size are distributed in a real-world plankton community, a useful dataset is given by D'Alelio et al. (2016a). The study analysed the differences in community structure and carbon flux in the Gulf of Naples under bloom and non-bloom scenarios. For this reason D'Alelio et al. (2016a) reported plankton sizes, trophic strategies, biomass and carbon fluxes. Tables 2.1, 2.2 and 2.3 summarise the original dataset, collected at the MareChiara station (LTER-MC, 40°48.5'N, 14°15'E; Zingone et al., 2010) in the Gulf of Naples (GoN), Mediterranean Sea. The sampling was performed at 0.5, 2, 5, 10, 20, 40, 60 m of depth with Niskin bottles on a Rosette sampler. Mesozooplankton were captured with a net between 50m and the surface. Captured organisms were fixed in formaldehyde (D'Alelio et al., 2015). The collected data were integrated into two layers, the surface layer (0-5m) and the deep layer (5-60m). The average temperature was 20°C (±10°C, Stabile et al., 2007). During summer, the season in which the observations were made, two phases alternated between mid-June and late-August (summer seasons 2002–2009): a plankton blooming phase and a stable (non-bloom) phase (D'Alelio et al., 2016a). The oscillations in bloom state are due to the location, which is at the interface between coastal (eutrophic) and open-sea (oligotrophic) environment, and this interface changes location due to seasonality and local circulation (D'Alelio et al., 2015).

Original dataset from D'Alelio et al. (2016a)

All observations presented in this chapter are taken from the non-bloom phase, which, unlike the bloom phase observations, can reasonably be approximated with a steady state model. Additionally, the observations were made during the summers of different non-consecutive years: 1984-1988 for primary production; 2007 and 2009 for carbon biomass; 2002-2009 for physics (salinity) and ecology (taxa, chlorophyll *a*, biomass, DOC concentration). Given the gap in time, the data from 1984-1988 were not used in the final comparison with the results of the model.

D'Alelio et al. (2016a) calculated the carbon biomass of 56 different groups of taxa (called Functional Nodes), and assigned to each a characteristic average size according to the literature (between 1 μm and 28 mm) and similarly assigned trophic strategies (between 1, phytoplankton, and 0, zooplankton).

Feeding interactions between taxa, in terms of carbon biomass fluxes, were calculated through Ecopath (Christensen and Pauly, 1992), a mass-balanced (consumption = production + respiration + unassimilated food) ecosystem model that generate food webs. Primary production for each group was estimated using both literature data (characteristic maximum growth rate of each species) and the growth rate of the whole community measured *in situ*. Consumption rate was as well calculated by considering data from literature and observations, with the inclusion of the feeding preference (i.e. diet), which allowed to determine the contribution, in percentage, of the biomass and energy coming from each prey-group. The unique physiology of mixotrophs required both primary production and consumption esteems, taking into account the characteristic uptake to grazing ratio of each group, assigned as well from literature and observations (for a complete explanation, refer to D'Alelio et al., 2016b). Gibbs et al. (2020a) and D'Alelio et al. (2016a) organized their simulated community in two different ways: Gibbs et al. (2020a) produced a trophic network according to plankton traits, while D'Alelio et al. (2016a) presented a network with different groups/species. Thus, making a comparison between the two different choices of community representation, in this Chapter, biomass had to be reorganized from a taxonomic to a functional point of view.

Tables 2.1 lists the 56 Functional Nodes of the original dataset. Each group is distinguished by its position on the mixotrophic spectrum (ω), its size and carbon biomass. Tables 2.2 and 2.3 show the feeding interactions between the different functional groups listed in Tables 2.1, prey on row and predators on column. Each number corresponds to the quantity of biomass transferred between two different groups.

TABLE 2.1: Original "non-bloom phase" biomass data from D'Alelio et al. (2016a), descriptions from the original paper. Abbreviations and symbols: FN=Functional Node from the original paper, ω=Trophic Strategy (1 = phytoplankton, 0 = zooplankton), (s)=surface, (d)=depth, (a)=water column. The size column may be Equivalent Spherical Diameter (*) or maximum length (†).

FN	Classification according to D'Alelio et al. (2016a)	Description	ω (-)	Size (μm)	Carbon biomass (mg C m^{-2})
1	Cyanobacteria (s)	Mainly Synechococcus	1	1^*	3.2
2	Prochlorophytes (s)	Mainly Prochlorococcus	1	1^*	0.3
3	Phyto-nanoflagellates (s)	Several species	1	1.9^*	22
4	Chaetoceros spp. (s)	Diatom genus	1	2.4^*	4.2
5	Leptocylindrus spp. (s)	Diatom genus	1	5.8^*	31.3
6	Skeletonema spp. (s)	Diatom genus	1	3.1^*	5.7
7	Small diatoms (s)	Several species	1	3.2^*	4.3
8	Pennate diatoms (s)	Pennate diatoms	1	3.3^*	1.2
9	Pseudo-nitzschia spp. (s)	Diatom genus	1	3^*	2.9
10	Centric diatoms (s)	Centric diatoms	1	12^*	19.7
11	Coccolithophores (s)	Mainly Emiliania huxleyi	1	4.3^*	3.9
12	Phyto-microflagellates (s)	Several species	1	4^*	3.9
13	Mixotrophic nanoflagellates (s)	Mainly Ollicola vangorii	0.5	1.5^*	0.1
14	Small dinoflagellates (s)	Several species	0.59	4.5^*	6.6
15	Medium dinoflagellates (s)	Several species	0.59	9^*	4.1
16	Myrionecta rubra (a)	Ciliate species	0.9	10^*	0.6
17	Tontonia spp. (s)	Oligotrichous ciliate genus	0.83	40^*	9.5
18	Laboea spp. (s)	Oligotrichous ciliate genus	0.64	22^*	1.8
19	Strombidium spp. (s)	Oligotrichous ciliate genus	0.81	38^*	11.6
20	HNF (s)	Agglutinated nanoflagellates	0	2.4^*	0.4
21	Hetero-dinoflagellates (s)	Several species	0	11.1^*	7.7
22	Prostomatids (s)	Agglutinated ciliates	0	26.8^*	1.7
23	Strobilidium spp. (s)	Ciliate genus	0	26.8^*	4.3
24	Tintinnids (s)	Agglutinated ciliates	0	11^*	0.2
25	Nanociliates (s)	Agglutinated ciliates	0	8^*	0.7
26	Cyanobacteria (d)	Mainly Synechococcus	1	1^*	108.4
27	Prochlorophytes (d)	Mainly Prochlorococcus	1	1^*	10.8
28	Phyto-nanoflagellates (d)	Several species	1	1.9^*	33.6
29	Coccolithophorids (d)	Mainly Emiliania huxleyi	1	4.3^*	166.2
30	Diatoms (d)	Several species	1	3.2^*	10.3
31	Mixotrophic nanoflagellates (d)	Several species	0.5	1.5^*	0.1
32	Small dinoflagellates (d)	Several species	0.59	4.5^*	85.5
33	Medium dinoflagellates (d)	Several species	0.59	9^*	52.9
34	HNF (d)	Agglutinated nanoflagellates	0	2.4^*	0.1
35	Hetero-dinoflagellates (d)	Several species	0	11.1^*	34.2
36	Prostomatids (d)	Agglutinated ciliates	0	26.8^*	7.3
37	Strobilidium spp. (d)	Ciliate genus	0	26.8^*	19.1
38	Tintinnids (d)	Agglutinated ciliates	0	11.4^*	1
39	Nanociliates (d)	Agglutinated ciliates	0	8^*	3
40	Heterotrophic bacteria (s)	-	0	0.5^*	32.7
41	Heterotrophic bacteria (d)	-	0	0.5^*	373.5
42	Penilia avirostris (a)	Cladoceran species	0	$800^\dagger$	96.1
43	Cladocerans (a)	Evadne & Pseudevadne spp.	0	$900^\dagger$	33.8
44	Paracalanus parvus (a)	Calanoid copepod species (adults)	0	$850^\dagger$	25.5
45	Acartia clausii (a)	Calanoid copepod species (adults)	0	$1,150^\dagger$	7.5
46	Temora stylifera (a)	Calanoid copepod species (adults)	0	$1,000^\dagger$	39.1
47	Centropages typicus (a)	Calanoid copepod species (adults)	0	$1,000^\dagger$	12.2
48	Other calanoids (a)	Agllutinated genera (adults)	0	$1,050^\dagger$	8.7
49	Juvenile calanoids (a)	Juveniles of calanoid copepod	0	$450^\dagger$	14.6
50	Appendicularia (a)	-	0	$3,000^\dagger$	36.1
51	Doliolids (a)	Agglutinated species	0	$1,500^\dagger$	2
52	Salps (a)	Agglutinated species	0	$10,000^\dagger$	16.2
53	Meroplankton (a)	Agglutinated species	0	$250^\dagger$	3.5
54	Oithona spp. (a)	Agglutinated larvae	0	$675^\dagger$	1.4
55	Detritivora (a)	Cyclopoid copepod genus	0	$650^\dagger$	7.4
56	Carnivora (a)	Cyclopoid copepod genera	0	$28,000^\dagger$	276.3
57	Appendicularia houses (a)	Mainly chaetognats	-	$3,000^\dagger$	113.8
58	Small faecal pellets (a)	Faecal pellets of small animals	-	$< 200^\dagger$	81.5
59	Salp faecal pellets (a)	Faecal pellets of salps	-	$> 200^\dagger$	3.8
60	Carnivores faecal pellets (a)	Faecal pellets of carnivores	-	$> 200^\dagger$	0.6
61	DOC (s)	Dissolved Organic Carbon	-	–	16.6
62	DOC (d)	Dissolved Organic Carbon	-	–	58.3
63	Generic particulate detritus (a)	Amorphous particulate detritus	-	$< 200^\dagger$	4,486.80

TABLE 2.2: Carbon biomass fluxes (mg C m^{-2} d^{-1}) inferred by D'Alelio et al. (2016a). Predators in rows, prey in columns. Part I

FN	13	14	15	16	17	18	19	20	21	22	23	24	25	31	32	33	34	35	36	37
1	0	0.21	0.13	0	0.28	0.16	0	0.14	0.3	0.08	0.07	0	0.58	0	0	0	0	0	0	0
2	0.02	0	0	0	0	0	0.06	0.02	0	0	0	0	0	0	0	0	0	0	0	0
3	0	6.87	0.21	0	3.46	0.27	4.31	0.24	1.78	0.48	0.36	0.07	0.09	0	0	0	0	0	0	0
4	0	0.29	0.21	0	0.5	0.19	0.82	0	1.13	0.1	0.18	0.01	0.01	0	0	0	0	0	0	0
5	0	7.38	0.21	0	3.68	0.27	0.58	0	4.13	0.14	0.19	0	0	0	0	0	0	0	0	0
6	0	4	0.11	0	0.12	0.11	0.72	0	0.32	0.05	0.14	0	0.01	0	0	0	0	0	0	0
7	0	1.39	0.11	0	0.5	0	0.44	0	0.76	0.08	0.09	0.05	0	0	0	0	0	0	0	0
8	0	0	0.1	0	0	0	0	0	0.23	0.03	0.11	0	0	0	0	0	0	0	0	0
9	0	0.97	0.11	0	0	0	0	0	0.65	0.09	0.13	0	0	0	0	0	0	0	0	0
10	0	3.84	0.13	0	0.45	0	1.04	0	4.09	0.08	0.13	0	0	0	0	0	0	0	0	0
11	0	0.03	0.19	0	0	0.01	0	0	1.14	0.34	1.3	0.07	0	0	0	0	0	0	0	0
12	0	0.28	0.13	0.04	0.08	0	0.42	0	0.9	0.36	0.66	0.02	0.05	0	0	0	0	0	0	0
13	0	0	0	0	0	0	0	0	0	0.01	0	0	0.01	0	0	0	0	0	0	0
14	0	1.08	0.15	0	0	0	0	0	3.94	0.22	0.59	0.05	0.01	0	0	0	0	0	0	0
15	0	0	0.09	0	0	0	0	0	0.82	0.02	1.99	0	0	0	0	0	0	0	0	0
16	0	0	0	0	0	0	0	0	0	0	0.01	0	0	0	0	0	0	0	0	0
17	0	0	0	0	1.42	0.26	1.3	0	0.9	0.22	0.19	0	0	0	0	0	0	0	0	0
18	0	0	0	0	0	0	0	0	0	0	0	0	0	0	0	0	0	0	0	0
19	0	0	0	0	1.53	0.26	1.77	0	1.1	0.26	0.21	0	0	0	0	0	0	0	0	0
20	0	0	0	0	0	0	0	0	0	0	0	0	0	0	0	0	0	0	0	0
21	0	0	0.68	0	0	0	0	0	0.23	0.2	1.63	0	0	0	0	0	0	0	0	0
22	0	0	0	0	0	0	0	0	0.2	0.07	0.12	0	0	0	0	0	0	0	0	0
23	0	0	0	0	0	0	0	0	0.74	0.07	0.05	0	0	0	0	0	0	0	0	0
24	0	0	0.01	0	0	0	0	0	0	0.03	0	0	0	0	0	0	0	0	0	0
25	0	0	0	0	0	0	0	0	0	0	0	0	0	0	0	0	0	0	0	0
26	0	0	0	0	0	0	0	0	0	0	0	0	0	0	24.36	0.78	0	2.13	1.09	7.9
27	0	0	0	0	0	0	0	0	0	0	0	0	0	0	0.56	0.84	0.06	0.66	1.2	3.17
28	0	0	0	0	0	0	0	0	0	0	0	0	0	0	21.86	1.31	0.05	7.91	1.36	4.89
29	0	0	0	0	0	0	0	0	0	0	0	0	0	0	33.02	2.06	0	12.35	1.59	8.08
30	0	0	0	0	0	0	0	0	0	0	0	0	0	0	1.15	0	0	1.26	0.04	0.04
31	0	0	0	0	0	0	0	0	0	0	0	0	0	0	0	0	0	0	0	0
32	0	0	0	0	0	0	0	0	0	0	0	0	0	0	31.61	2	0	8.1	1.92	5.15
33	0	0	0	0	0	0	0	0	0	0	0	0	0	0	0	0	0	0.22	0	0.2
34	0	0	0	0	0	0	0	0	0	0	0	0	0	0	0	0	0	0	0	0
35	0	0	0	0	0	0	0	0	0	0	0	0	0	0	0	0.69	0	0.24	0.48	0.57
36	0	0	0	0	0	0	0	0	0	0	0	0	0	0	0	0	0	0	0	0
37	0	0	0	0	0	0	0	0	0	0	0	0	0	0	0	0	0	0.02	0.02	0.08
38	0	0	0	0	0	0	0	0	0	0	0	0	0	0	0	0.08	0	0	0.11	0.06
39	0	0	0	0	0	0	0	0	0	0	0	0	0	0	0	0.5	0	0.1	0	003
40	0.13	0	2.29	0	2.8	0	6.77	0	10.85	1.44	1.6	0.57	0.08	0	0	0	0	0	0	0
41	0	0	0	0	0	0	0	0	0	0	0	0	0	0.08	0.61	3.23	0	10.24	0.5	12.96
42	0	0	0	0	0	0	0	0	0	0	0	0	0	0	0	0	0	0	0	0
43	0	0	0	0	0	0	0	0	0	0	0	0	0	0	0	0	0	0	0	0
44	0	0	0	0	0	0	0	0	0	0	0	0	0	0	0	0	0	0	0	0
45	0	0	0	0	0	0	0	0	0	0	0	0	0	0	0	0	0	0	0	0
46	0	0	0	0	0	0	0	0	0	0	0	0	0	0	0	0	0	0	0	0
47	0	0	0	0	0	0	0	0	0	0	0	0	0	0	0	0	0	0	0	0
48	0	0	0	0	0	0	0	0	0	0	0	0	0	0	0	0	0	0	0	0
49	0	0	0	0	0	0	0	0	0	0	0	0	0	0	0	0	0	0	0	0
50	0	0	0	0	0	0	0	0	0	0	0	0	0	0	0	0	0	0	0	0
51	0	0	0	0	0	0	0	0	0	0	0	0	0	0	0	0	0	0	0	0
52	0	0	0	0	0	0	0	0	0	0	0	0	0	0	0	0	0	0	0	0
53	0	0	0	0	0	0	0	0	0	0	0	0	0	0	0	0	0	0	0	0
54	0	0	0	0	0	0	0	0	0	0	0	0	0	0	0	0	0	0	0	0
55	0	0	0	0	0	0	0	0	0	0	0	0	0	0	0	0	0	0	0	0
56	0	0	0	0	0	0	0	0	0	0	0	0	0	0	0	0	0	0	0	0
57	0	0	0	0	0	0	0	0	0	0	0	0	0	0	0	0	0	0	0	0
58	0	0	0	0	0	0	0	0	0	0	0	0	0	0	0	0	0	0	0	0
59	0	0	0	0	0	0	0	0	0	0	0	0	0	0	0	0	0	0	0	0
60	0	0	0	0	0	0	0	0	0	0	0	0	0	0	0	0	0	0	0	0
61	0	0	0	0	0	0	0	0	0	0	0	0	0	0	0	0	0	0	0	0
62	0	0	0	0	0	0	0	0	0	0	0	0	0	0	0	0	0	0	0	0
63	0	0	0	0	0	0	0	0	0	0	0	0	0	0	0	0	0	0	0	0

TABLE 2.3: Carbon biomass fluxes (mg C m^{-2} d^{-1}) inferred by D'Alelio et al. (2016a). Predators in rows, prey in columns. Part II

FN	38	39	40	41	42	43	44	45	46	47	48	49	50	51	52	53	54	55	56
1	0	0	0	0	0.13	0.06	0	0	0	0	0	0	0.08	0.06	0.04	0	0	0	0
2	0	0	0	0	0.02	0	0	0	0	0	0	0	0	0.02	0.01	0	0	0	0
3	0	0	0	0	1.8	0.68	0.3	0.02	0.06	0.01	0.14	0.27	5.74	0	0.7	1.1	0	0	0
4	0	0	0	0	1.26	0.62	0.3	0.05	0.06	0.01	0.14	0.29	1.25	0.18	0.27	0.49	0	0	0
5	0	0	0	0	7.24	0.2	0.35	0.05	0.18	0.04	0.14	0.27	4.12	0.17	0.86	0.88	0	0	0
6	0	0	0	0	1.92	0.39	0.28	0.03	0	0	0.09	0.25	0.54	0.14	0.09	0.08	0	0	0
7	0	0	0	0	1.42	0.48	0.26	0.03	0	0	0.09	0.25	0.54	0.14	0.04	0.07	0	0	0
8	0	0	0	0	0.3	0	0.28	0.02	0.01	0	0.09	0.25	0.34	0.14	0	0	0	0	0
9	0	0	0	0	0.55	0.58	0.28	0.03	0	0	0.09	0.25	0.01	0.14	0	0	0	0	0
10	0	0	0	0	0.89	0.06	0.05	0.03	0.12	0.02	0.01	0.05	0.07	0.06	0.29	0.37	0	0	0
11	0	0	0	0	1.28	0	0.53	0.05	0.03	0	0.12	0.43	0.71	0.22	0	0	0	0	0
12	0	0	0	0	1.93	0.01	0.36	0.03	0.01	0	0.09	0.25	0	0.14	0	0.03	0	0	0
13	0	0	0	0	0.01	0	0	0	0	0	0.01	0.01	0	0.01	0	0	0	0	0
14	0	0	0	0	0.34	0	0.36	0.04	0.01	0	0.12	0.26	0.3	0.15	0	0	0	0	0
15	0	0	0	0	0.6	0.01	0.01	0.04	0.13	0.05	0	0.01	0.15	0.07	0	0	0	0	0
16	0	0	0	0	0.02	0	0	0.02	0.07	0.04	0	0	0.05	0	0	0.01	0	0	0
17	0	0	0	0	0.82	0.07	0.04	0.05	0.18	0.07	0.05	0.03	1.02	0.08	0.38	0.75	0	0	0
18	0	0	0	0	0	2.16	0	0.06	0.22	0.07	0	0	0	0.08	0	0	0	0	0
19	0	0	0	0	0.9	0.08	0.04	0.05	0.18	0.07	0.05	0.04	1.88	0.08	0.42	0.74	0	0	0
20	0	0	0	0	0	0.05	0.11	0	0	0	0.02	0.12	0	0	0	0	0	0	0
21	0	0	0	0	1.48	0.02	0.02	0	0.15	0.05	0	0.02	0	0.06	0	0.02	0	0	0
22	0	0	0	0	0	0.02	0	0.04	0.14	0.05	0	0	0.34	0.06	0	0	0	0	0
23	0	0	0	0	0.08	3.16	0	0.03	0.12	0.05	0	0	0	0.07	0	0	0	0	0
24	0	0	0	0	0	0	0	0.01	0.04	0.03	0	0	0	0.04	0	0	0	0	0
25	0	0	0	0	0	0	0.18	0.02	0.08	0.04	0.07	0.18	0.1	0.05	0	0	0	0	0
26	0	0	0	0	4.54	0	0	0	0	0	0	0	67.13	0.01	2.97	0	0	0	0
27	0.02	0.02	0	0	0.45	0.08	0	0	0	0	0	0	0.4	0.06	0.45	0	0	0	0
28	0.3	0.92	0	0	2.27	3.13	0.3	0.03	0.09	0	0.13	0.35	7.61	0.17	1.05	1.48	0	0	0
29	0.64	0.93	0	0	9.09	0.67	0.3	0.05	0.07	0.01	0.14	0.27	73.32	0.13	3.23	4.99	0	0	0
30	0	0	0	0	6.08	1.42	0.54	0.06	0.02	0	0.03	0.52	1.91	0.2	0.15	0	0	0	0
31	0	0.01	0	0	0.01	0.01	0	0	0	0	0	0	0.01	0	0	0	0	0	0
32	0	0.34	0	0	4.86	0	0	0.06	0	0	0	0	0.92	0.05	1.75	2.06	0	0	0
33	0	0	0	0	4.07	0.03	0.14	0.03	0.15	0.05	0.01	0.15	14.62	0.05	0.53	0.04	0.01	0	0
34	0	0.01	0	0	0.01	0	0	0	0	0	0	0	0	0.01	0	0	0	0	0
35	0	0	0	0	7.3	0.03	0.16	0.07	0.16	0.06	0	0.2	4.67	0.06	0	0.03	0.01	0	0
36	0	0	0	0	0.01	1.94	0.02	0.03	0.12	0.04	0	0.01	0.15	0.03	0.12	0	0	0	0
37	0	0	0	0	0.01	5.83	0.06	0.05	0.21	0.05	0	0.06	4.09	0.05	0.06	0.01	0.01	0	0
38	0	0	0	0	0.03	0.02	0	0.02	0.07	0.02	0	0	0	0.03	0.06	0.05	0	0	0
39	0	0	0	0	0.01	0.01	0.32	0.03	0.13	0.04	0.09	0.24	0	0.03	0.05	0.05	0	0	0
40	0	0	0	0	0	0	0	0	0	0	0	0	0	0	0	0	0	0	0
41	0.42	0.99	0	0	0	0	0	0	0	0	0	0	0.9	0.02	2.5	0	0	0	0
42	0	0	0	0	0	0	0	0	0	0	0	0	0	0	0	0	0	0	0.46
43	0	0	0	0	0	0	0	0	0	0	0	0	0	0	0	0	0	0	0.16
44	0	0	0	0	0	0	0	0	0	0	0	0	0	0	0	0	0	0	0.18
45	0	0	0	0	0	0	0	0	0	0	0	0	0	0	0	0	0	0	0.18
46	0	0	0	0	0	0	0	0	0	0	0	0	0	0	0	0	0	0	1.08
47	0	0	0	0	0	0	0	0	0	0	0	0	0	0	0	0	0	0	0.54
48	0	0	0	0	0	0	0	0	0	0	0	0	0	0	0	0	0	0	018
49	0	0	0	0	0	0	0	0	0	0.12	0	0	0	0	0	0	0.01	0	0.18
50	0	0	0	0	0	0	0	0	0	0.12	0	0	0	0	0	0	0	0	0.17
51	0	0	0	0	0	0	0	0	0	0	0	0	0	0	0	0	0	0	0
52	0	0	0	0	0	0	0	0	0	0	0	0	0	0	0	0	0	0	007
53	0	0	0	0	0	0	0	0	0	0	0	0	0	0	0	0	0	0	0.01
54	0	0	0	0	0	0	0	0	0	0	0	0	0	0	0	0	0	0	0
55	0	0	0	0	0	0	0	0	0	0	0	0	0	0	0	0	0	0	0.18
56	0	0	0	0	0	0	0	0	0	0	0	0	0	0	0	0	0	0	0.18
57	0	0	2.93	3.52	0	0	0	0	0	0	0	0	0	0	0	0	0	5.23	0
58	0	0	4.32	5.2	0	0	0	0	0	0	0	0	0	0	0	0	0.05	0	0
59	0	0	0	0	0	0	0	0	0	0	0	0	0	0	0	0	0	0	0
60	0	0	0.07	0.08	0	0	0	0	0	0	0	0	0	0	0	0	0	0	0
61	0	0	51.3	0	0	0	0	0	0	0	0	0	0	0	0	0	0	0	0
62	0	0	0	61.74	0	0	0	0	0	0	0	0	0	0	0	0	0	0	0
63	0	0	14.65	17.64	0	0	0	0	0	0	0	0	0	0	0	0	0	0	0

Trait-based reorganisation

To allow easier comparison with the trait-based model, the individual groups listed in Table 2.1 were aggregated according to size class and trophic strategy. The groups were aggregated to one of the closest 25 size classes (logarithmically spaced between 0.2 and 2,000 μm), and to one of the closest 25 trophic strategies (linearly space between 1, phytoplankton, and 0, zooplankton). The various degrees of mixotrophy were assigned using the fraction, assigned (through literature) by D'Alelio et al. (2016a), of the growth rate in mixotrophs due to autotrophy. The structure of the aggregated data set is given in Tables 2.4 and 2.5

TABLE 2.4: Same dataset from Table 2.1 after the carbon biomass data (mg C m^{-2}) were moved into logarithmically spaced size classes. ω=Trophic Strategy (1 = phytoplankton, 0 = zooplankton)

Size (μm)	ω (-)	Biomass (mg C m^{-2})
0.93	1	122.78
2	1	59.82
2.94	1	23.81
4.31	1	174.07
6.32	1	31.35
13.63	1	19.64
1.36	0.5	0.13
4.31	0.59	92.1
9.28	0.59	57.03
9.28	0.9	0.57
20	0.64	1.77
43.09	0.83	9.47
43.09	0.81	11.58
0.43	0	406.21
2	0	0.49
9.28	0	46.76
29.36	0	32.44
293.56	0	3.47
430.89	0	14.58
632.46	0	8.79
928.32	0	215.43
1,362.58	0	9.46
2,000	0	328.56

TABLE 2.5: Same dataset from Table 2.2, 2.3 after the carbon flux data (mg C m^{-2} d^{-1}) was assigned to the functional groups. Predators on row, prey on column.

μm		0.43	1.36	2	4.31	9.28	9.28	9.28	20	29.36	43.09	43.09	293.56	430.89	632.46	928.32	1,362	2,000
	ω	0	0.5	0	0.58	0.91	0.58	0	0.65	0	0.83	0.79	0	0	0	0	0	0
0.43	0	0	0.21	0	0.61	0	5.52	23.15	0	16.5	2.8	6.77	0	0	0	0	0.020	3.4
0.93	1	0	0.020	0.22	25.13	0	1.75	3.71	0.16	13.51	0.28	0.060	0	0	0	5.28	0.15	71.08
1.36	0.5	0	0	0	0	0	0	0.020	0	0.010	0 2	0	0	0.010	0	0.040	0.010	0.010
2	0	0	0	0.29	29.02	0	1.73	12.22	0.46	7.37	3.96	5.13	3.07	0.91	0	11.3	0.45	16.62
2	1	0	0	0	0	0	0	0.010	0	0	0	0	0	0.12	0	0.19	0.010	0
2.94	1	0	0	0	7.51	0	0.43	3.28	0.11	0.80	0.62	1.16	0.15	1.52	0	15.2	0.93	3.62
4.31	1	0	0	0	33.33	0.040	2.38	16.1	0.010	12.33	0.080	0.42	5.02	0.95	0	14.64	0.62	77.26
4.31	0.58	0	0	0	32.69	0	2.15	12.44	0	7.88	0	0	2.06	0.26	0	5.69	0.30	2.97
6.32	1	0	0	0	7.38	0	0.21	4.13	0.27	0.33	3.68	0.58	0.88	0.27	0	8.15	0.22	4.98
9.28	0.91	0	0	0	0	0	0	0	0	0.010	0	0	0.010	0	0	0.13	0.020	0.050
9.28	0.58	0	0	0	0	0	0.090	1.04	0	2.21	0	0	0.040	0.16	0.010	5.25	0.19	15.3
9.28	0	0	0	0	0	0	1.96	0.57	0	6.08	0	0	0.15	0.64	0.010	10.61	0.42	4.88
13.63	1	0	0	0	3.84	0	0.13	4.09	0	0.21	0.45	1.04	0.37	0.050	0	1.15	0.090	0.36
20	0.65	0	0	0	0	0	0	0	0	0	0	0	0	0	0	2.45	0.14	0
29.36	0	0	0	0	0	0	0	0.96	0	0.41	0	0	0.010	0.070	0.010	11.91	0.36	4.76
43.09	0.83	0	0	0	0	0	0	0.90	0.26	0.41	1.42	1.3	0.75	0.030	0	1.23	0.13	1.4
43.09	0.79	0	0	0	0	0	0	1.1	0.26	0.47	1.53	1.77	0.74	0.040	0	1.32	0.13	2.3
293.56	0	0	0	0	0	0	0	0	0	0	0	0	0	0	0	0	0	0.010
430.89	0	0	0	0	0	0	0	0	0	0	0	0	0	0	0.010	0.12	0	0.18
632.46	0	0	0	0	0	0	0	0	0	0	0	0	0	0	0	0	0	0.18
928.32	0	0	0	0	0	0	0	0	0	0	0	0	0	0	0	0	0	20.42
1,362	0	0	0	0	0	0	0	0	0	0	0	0	0	0	0	0	0	0.18
2,000	0	0	0	0	0	0	0	0	0	0	0	0	0	0	0	0.12	0	7.35

Aggregated biomass and grazing data are shown as a food web in Figure 2.1. The coordinates of the nodes in the food web correspond to the size and trophic strategy of the aggregated groups, while the sizes of the nodes correspond to the aggregated biomass (Table 2.4). The widths of the edges between the nodes describe magnitude of the trophic fluxes between the aggregated groups (Table 2.5). Each node therefore represents a group of plankton of similar size and trophic strategy, and each line is a grazing interaction between the different groups.

Figure 2.1 shows that the phytoplankton portion of the community is made by pico-phytoplankton and nanophytoplankton. These organisms are grazed by mixotrophs and zooplankton. Mixotrophs are mostly distributed between 5 and 50 μm and eat phytoplankton together with bacteria (the red spot in the bottom right corner). Most of the zooplankton are mesozooplankton, but there are also some zooplankton populations between 20 and 30μm. The flux of biomass moves mostly from phytoplankton to mixotrophs to zooplankton. Mesozooplankton feed mostly on phytoplankton, while nanozooplankton and picozooplankton feed on both phytoplankton and mixotrophs.

2.2 Model description

The aim of this chapter is to study the impact of mixotrophy on plankton community structure and the associated trade-offs between trophic strategies. The dataset compiled by D'Alelio et al. (2016a) provides a useful overview of the community in terms of average size, carbon biomass and plankton position on the trophic spectrum. It cannot - by itself - provide information on the shape of the trophic trade-off, or inform us on how

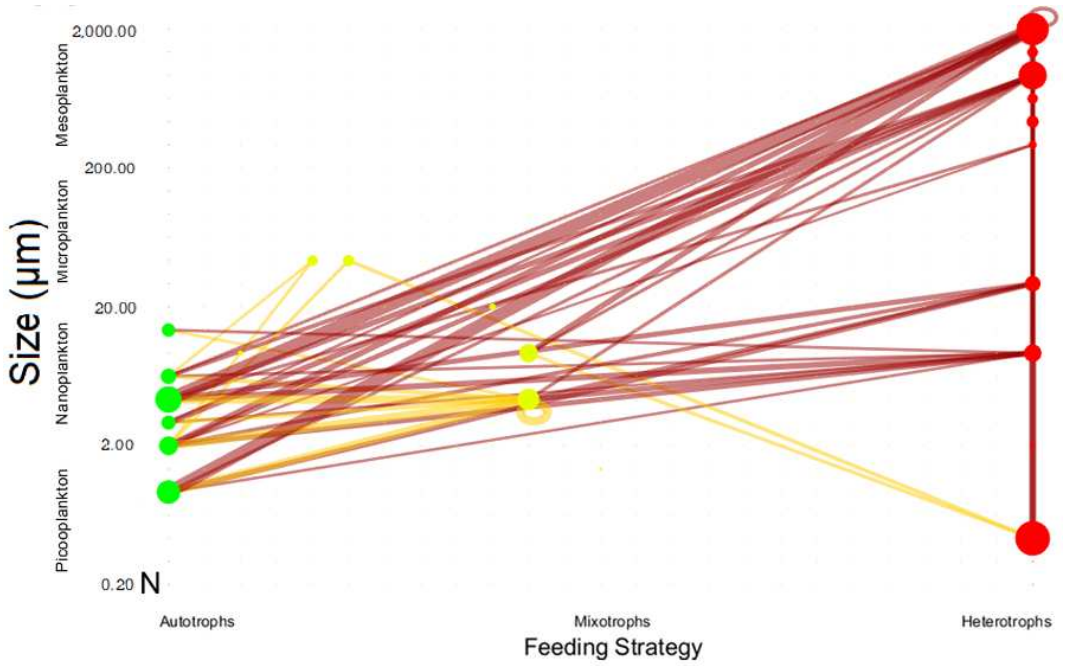

FIGURE 2.1: Food web generated from Tables 2.4 - 2.5. The size of the circles (nodes) represents the cubic root of biomass inside the different functional groups, the thickness of the edges represents the amount of grazing. Green circles: Phytoplankton. Yellow circles: Mixotrophs. Red circles: Zooplankton. Orange edges: mixotrophic grazing/predation. Red edges: zooplankton grazing/predation. Loop edges represent grazing within the same functional node and possibly cannibalism.

the ecosystem will respond to changing environmental parameters, such as temperature. To this end, we can apply a trait-based model that resolves plankton size and trophic strategy.

2.2.1 Model overview

The model proposed by Gibbs et al. (2020a) permits the simulation of different interactions between species of different sizes across the full trophic spectrum. The model is equivalent to a laboratory chemostat, to which a nutrient rich resource medium is added at a constant rate, with growth medium (including the plankton community) washed out at an equivalent rate. This system is also broadly analogous to a stratified ocean ecosystem, in which nutrient rich water is supplied from depth as surface waters are transported downwards at the same rate. The model resolves a single nitrogen nutrient element and has no spatial structure.

The model simulates the transfer of nutrients from the abiotic environment to the organisms and *vice versa*. The photosynthetic growth of plankton is represented by the light-, temperature- and nutrient-limited uptake of inorganic nitrogen. Biomass is subsequently transferred between populations by grazing (i.e. predation). Mortality is included as a fixed linear fraction of plankton biomass, and an additional quadratic mortality term

is included as a representation of viral lysis and other density-dependent loss terms. A fixed fraction of grazing interactions and mortality is passed directly back to the inorganic nutrient pool, as a crude representation of the microbial loop, while the rest is washed out. For the sake of simplicity, organic detritus is not included.

The modelled system includes multiple discrete size classes and trophic strategies. L discrete size classes are logarithmically-spaced between 0.2 and 2,000 μm, while M discrete trophic classes are linearly spaced between phytoplankton (1) and zooplankton (0). An exploration of the sensitivity of the model to the value of L and M is performed. With a "trait space" (an abstract space that resolves different possible combination of ecophysiological traits), of $L \times M$ discrete populations, the model can be described as a Multi-Compartment Model (MCM from now on).

The original model from Gibbs et al. (2020a) was developed to reproduce the evolution of a plankton communities over extended timescales of thousands to millions of years. In this study there was an interest toward much shorter periods of time relating to ecological timescales. As such, the evolutionary components of Gibbs et al. (2020a) were removed, with all possible populations in the $L \times M$ trait-space maintained above a low threshold biomass of 10^{-16}. This baseline value ensures that no population can go completely extinct, allowing each population to establish whenever conditions favourable to its growth arise in the model. At the same time, the threshold is sufficiently small that it does not meaningfully influence the biomass of successful populations in the model. By keeping all unsuccessful populations alive, it is not only possible to build a complete community in a reasonably short amount of time, but also to mimic the high resilience, dispersion and re-colonization capacities of the microscopic plankton (Martiny et al., 2006; Telford et al., 2006).

2.2.2 Generic population equations

The model includes state variables for inorganic nutrient (N) and $L \times M = j$ plankton populations (B_j). These two categories of state variables are represented in units of nitrogen concentration (mmol N m^{-3}). A simplified form of the equations for J generic plankton populations is

$$\frac{dN}{dt} = k(N_0 - N) - \sum_{j=1}^{J} \mu_j B_j \tag{2.3}$$

$$\frac{1}{B_j}\frac{dB_j}{dt} = \mu_j + \lambda \cdot G_j^+ - G_j^- - \delta - B_j \delta_q \tag{2.4}$$

In Equation 2.3, k is the incoming and outgoing flow rate, μ_j is the gross autotrophic growth rate of the population j and B_j is the biomass of population j. In Equation 2.4,

G_j^+ and G_j^- are the integrated biomass gains from prey (Equation 2.7) and losses to predators (Equation 2.8), respectively. Here λ is the grazing efficiency, δ is the basal mortality rate and δ_q is the quadratic mortality rate related to the biomass. Units are as shown in Table 2.6, Table 2.6 and 2.9.

TABLE 2.6: State variables.

Symbol	Unit	Description
N	mmol N m^{-3}	Quantity of nutrient
B_j	mmol Nm^{-3}	Quantity of biomass in each population, j

2.2.3 Growth equations

Phytoplankton growth, μ_j, is calculated as a saturating Monod function (Monod, 1959) of nutrient availability.

$$\mu_j = \frac{\mu_{max,j}(\tau) \cdot \alpha_j \cdot N}{\mu_{max,j} + \alpha_j \cdot N} \cdot \gamma_I \cdot \gamma_T \tag{2.5}$$

Here $\mu_{max,j}$ is the maximum autotrophic growth rate and α_j is the biomass-specific nutrient affinity (Figure 2.2). Temperature and light limitation are included as adimensional scalars γ_T and γ_I. These are equal for all populations. γ_T is set as an exponential function of environmental temperature T (Li and Dickie, 1987; Dutkiewicz et al., 2012)

$$\gamma_T = e^{(0.05 \cdot T - 20)} \tag{2.6}$$

The pre-assimilation gains to population j by grazing on other plankton j_{prey} are written as

$$G_j^+ = \gamma_T \cdot g'_j(\tau) \cdot \sum_{j_{prey}=1}^{J} \phi_{j,j_{prey}} \cdot B_{j_{prey}} \tag{2.7}$$

The total losses from population j to grazing by other plankton j_{pred} are written as

$$G_j^- = \gamma_T \cdot \sum_{j_{pred}=1}^{J} g'_{j_{pred}}(\tau) \cdot \phi_{j_{pred},j} \cdot B_{j_{pred}} \tag{2.8}$$

Here $\phi_{j_{pred},j_{prey}}$ is the fraction of each prey population available to each predator population. The effective grazing clearance rate g'_j includes a prey refuge effect that decreases a predators grazing rate as the total amount of available prey becomes small.

$$g'_j = g_j(\tau) \cdot (1 - e^{-\Lambda \cdot \sum_{jprey=1}^{J} \phi_{j,jprey} \cdot B_{jprey}}) \tag{2.9}$$

In this function Λ is the prey refuge coefficient, with smaller values increasing the size of the prey refuge and also model stability (Gibbs et al., 2020b).

TABLE 2.7: Auxiliary variables.

Symbol	Unit	Description
G^+	day^{-1}	Gains from predation.
G^-	day^{-1}	Losses from predation.
μ	day^{-1}	Growth Rate.
α	m^3 $(mmol\ N)^{-1}$ day^{-1}	Uptake rate of the phototrophs.
g	m^3 $(mmol\ N)^{-1}$ day^{-1}	Grazing rate.
γ_T	–	Exponential temperature function.

2.2.4 Parameterisation

Many ecophysiological traits are strongly correlated with organism size (Edwards et al., 2012; Marañón et al., 2013; Ward et al., 2017). Example of these are maximum growth rate, nutrient affinity, prey size-preference, sinking rate and light utilization (Hansen et al., 1994; Litchman et al., 2007; Litchman and Klausmeier, 2008; Edwards et al., 2012; Marañón et al., 2013; Ward et al., 2017). These traits change with size according to the factor

$$aV^b \tag{2.10}$$

where V is cellular volume, a is the coefficient and b is the exponent (or slope of the change). The values of a and b, for each parameter, are listed in Table 2.8.

TABLE 2.8: Size-dependent ecophysiological parameters and their coefficients. Source: Gibbs et al. (2020b)

Parameter	Symbol	coefficients		Units
		a	b	
Uptake rate of phototrophs	α	794	-0.63	m^3 $(mmol\ N)^{-1}$ d^{-1}
Grazing rate	g	6.48	-0.16	m^3 $(mmol\ N)^{-1}$ d^{-1}
Maximum growth rate	μ_{max}	See Equation 2.11		d^{-1}
Growth rate at infinite quota	μ^{∞}	4.70	-0.26	d^{-1}
Maximum cellular uptake rate	ρ_{max}	0.024	1.10	mmol N $cell^{-1}$ d^{-1}
Cell quota	Q_{min}	0.032	0.76	mmol N $cell^{-1}$

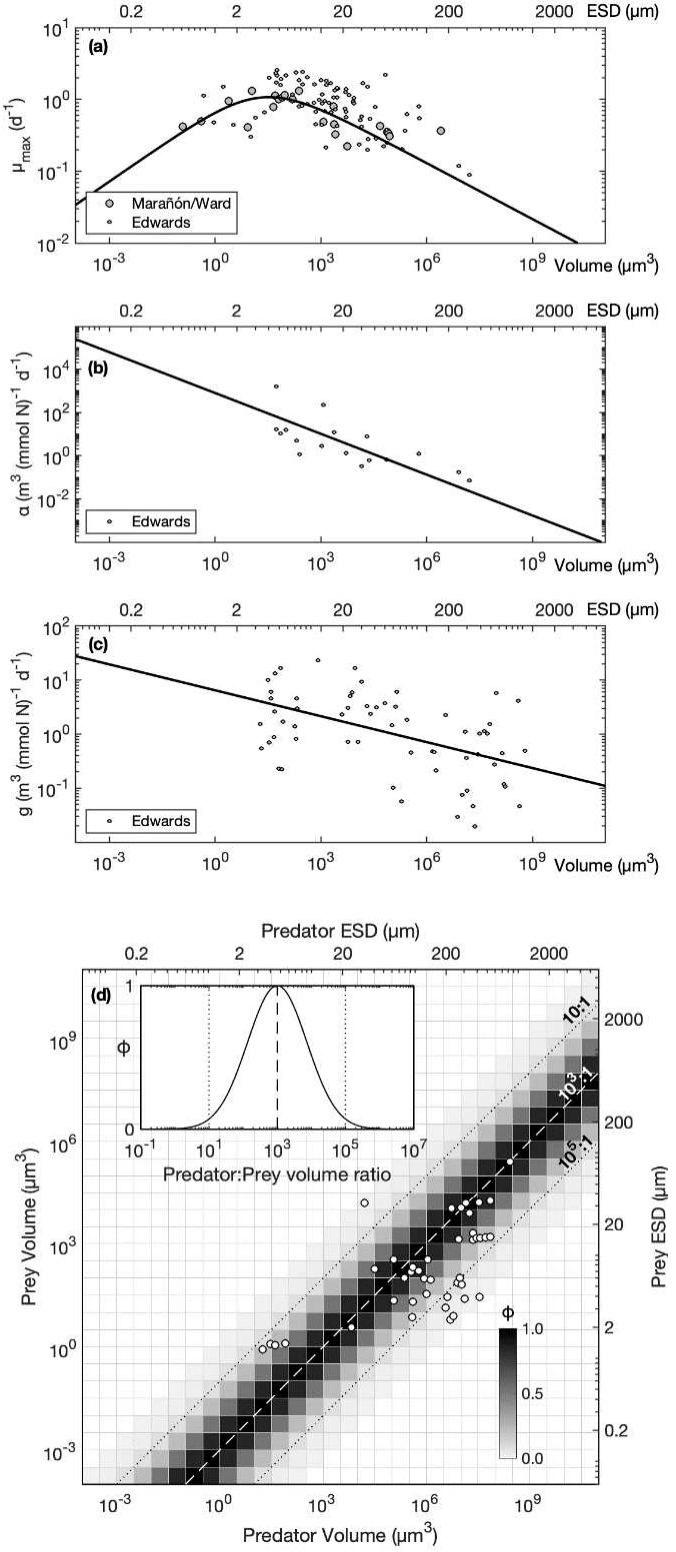

FIGURE 2.2: Scaling functions used for the ecophysiological parameters, from Gibbs et al. (2020b) Figure S7. The spots represent observations, while the lines represent the scalings given in Tables 2.8. **(a)**: Maximum growth rate μ_{max}. **(b)**: Affinity for the inorganic nutrients α. **(c)**: Grazing clearance rate g. **(d)**: Predator-prey size preference range ϕ. Sources: (Edwards et al., 2012; Marañón et al., 2013; Ward et al., 2017)

The affinity for the inorganic nitrogen, α, is higher for the smallest cells due to their high surface/volume ratio (Edwards et al., 2012). However it is important to note that in the larger cells, it is size of the diffusive boundary layer that limits uptake rate (Armstrong, 2008). Additionally, according to the dataset of Hansen et al. (1997), zooplankton grazing clearance rate, g, decrease with body size, even if this increase is not constant among different taxa. The potential maximum growth rate, μ^{∞}, decreases with size (Ward et al., 2017). Maximum cellular uptake rate, ρ_{max}, and cellular quota, Q_{min}, grow with size (Marañón et al., 2013).

The monomodal size-dependence of the maximum growth rate, μ_{max}, is a compromise between nutrient uptake (ρ_{max}) relative to the basal nutrient requirement (Q_{min}) and the maximum potential metabolic rate (μ^{∞}). Larger cells have higher uptake rate than smaller cells, relative to their basal nutrient requirements, whereas smaller cells have faster maximum metabolic rate than larger cells (Ward et al., 2017). These opposing trends lead to growth rates declining either side of an optimum at around 6 μm (Marañón et al., 2013). μ_{max} of the j population is equal to

$$\mu_{max,j} = \frac{\mu_j^{\infty} \cdot \rho_{max,j}}{\mu_j^{\infty} \cdot Q_{min,j} + \rho_{max,j}} \tag{2.11}$$

Where Q_{min} is minimum cellular nitrogen quota, μ^{∞} is the theoretical maximum growth rate at infinite cellular quota and ρ_{max} is the maximum cellular nutrient uptake rate.

Grazing interactions are also related to (relative) size, as the availability of prey to predators ($\phi_{j_{pred},j_{prey}}$) decreases either sides of an optimal ratio. Observations suggest that each plankton taxonomic group has a different optimal predator-prey size ratio, ranging from 1:1 to 30:1 (Hansen et al., 1994). Given that the model does not resolve taxonomic identity, a single general grazing preference is used. The grazing preference declines either side of an optimal predator-prey ESD (equivalent spherical diameter) ratio of 10:1, according to an approximately log-normal function with a geometric standard deviation of $\overset{\times}{\div}100$.

Size-independent parameters are listed in Table 2.9.

TABLE 2.9: Values for the size-independent model parameters.

Symbol	Unit	Value	Description
k	day^{-1}	0.01	Incoming flow rate.
δ	day^{-1}	0.025	Basal mortality rate.
δ_q	$\text{m}^3\ (\text{mmol N})^{-1}\ \text{day}^{-1}$	0.025	Quadratic mortality rate.
Λ	$\text{m}^3\ (\text{mmol N})^{-1}$	-10	Prey refuge coefficient.
λ	–	0.7	Grazing assimilation efficiency.

The temperatures chosen to perform the comparison with the observation of the D'Alelio et al. (2016a) dataset were 20°C and 25°C. The 25°C was suggested in D'Alelio et al. (2016b) as the average summer temperature of the surface layer of the GoN, however,

this number was given in the supplementary information file without specifying what "surface layer" means or when (what year) the temperature was measured. By looking at Stabile et al. (2007)(Fig. 3), and using a plot digitizer, it was possible to establish a more reliable (albeit not perfect) average temperature, in the first 60m of depth (the specified maximum sampling depth of D'Alelio et al., 2016a), of ∼20°C during the summer of 2002. Given the scarcity of the sources of the original claim, it was reputed more thorough to proceed with temperature analysis at 20 and 25°C.

Trait-space resolution

Size classes are geometrically spaced between 0.2 μm and 20 mm, while trophic classes are linearly spaced between 0 and 1. Each population has assigned traits according to its size (Equations 2.11 and 2.10) and trophic strategy (Equations 2.1 and 2.2). Together the two traits define all the possible populations that the community can generate. The $L \times M$ resolution of the trait space was selected by increasing the values of L and M together until the changes no longer affected community structure. It was found that consistent results were achieved once L and M reached 25, as shown in (Figure 2.3) and that simulations with 25×25 (= 625 possible populations) provided a reasonable compromise between computational burden and community resolution.

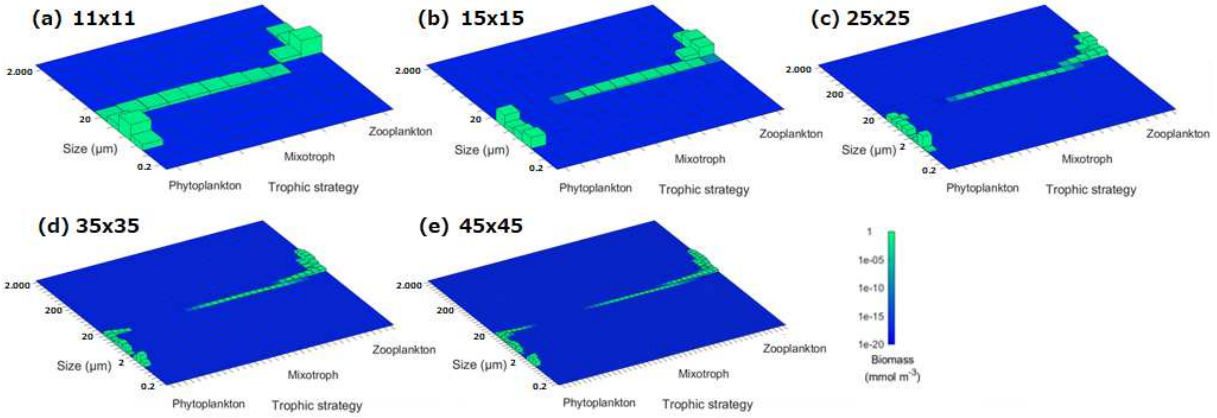

FIGURE 2.3: Equilibrium solutions of the model with different $L \times M$ resolution (the bold numbers above each panel). The blue square represents the trait space, and each green shape represents the biomass assigned to each trait.

2.2.5 Confirming a steady state

All simulations ran for 1,000 years and temperature, trade-off and light limitation did not change throughout the simulation. This time frame was sufficient for the model to approach equilibrium, as shown by Figure 2.4. Within 200 years of the 10,000 year simulation all populations had reached a steady state.

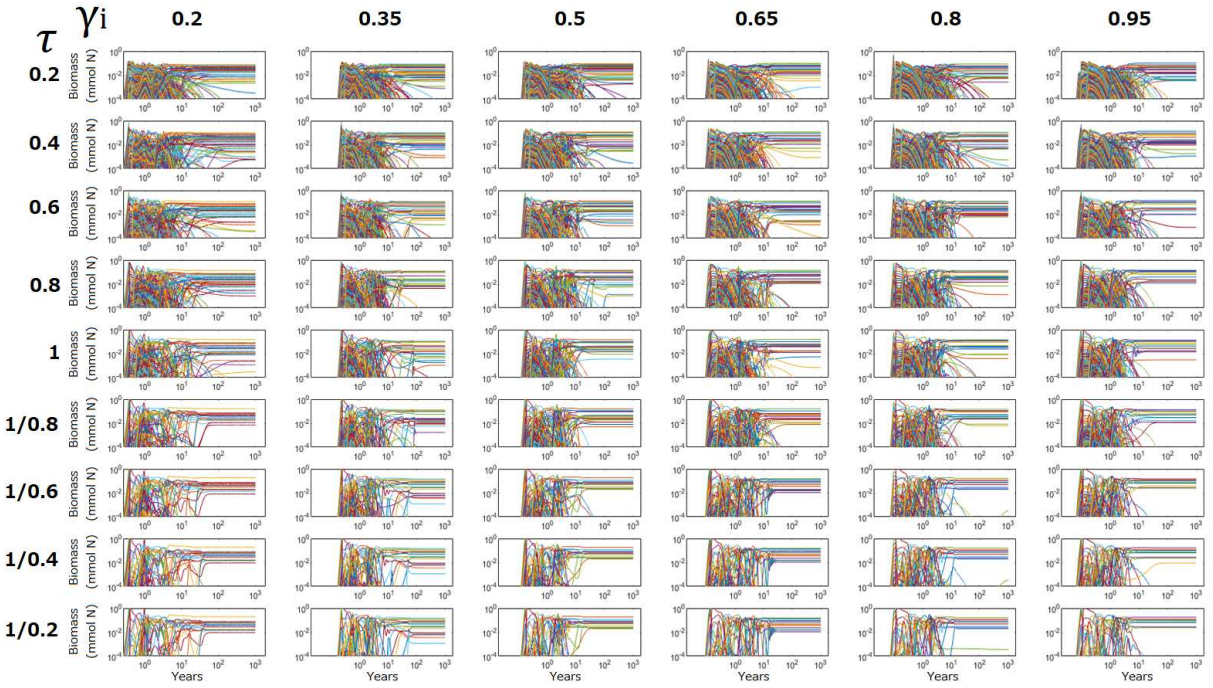

FIGURE 2.4: Temporal development of the behaviour of the biomass in the model. The steady state is reached by the end of the simulation (flat lines after year 100). The x-axis is on a log scale. Each line represents the biomass of each single population through the simulation.

2.2.6 Model-observation comparison

Simulations and observations were compared in terms of the relative proportion of phytoplankton, mixotrophs and zooplankton in the modelled and observed communities. The mismatch between model and observations was quantified in terms of the euclidean distance in a three-dimensional space defined by the relative biomass of the phytoplankton, mixotrophic and zooplankton populations.

$$J = \sqrt{\sum_{i=1}^{n}(O_i - Q_i)^2} \tag{2.12}$$

Here O is the observed percentage of biomass belonging to the trophic strategy i of D'Alelio et al. (2016a), and Q is the simulated percentage of biomass belonging to the same trophic strategy i of the model. n is equal to 3 because there are three different trophic strategies (phytoplankton, mixotrophs and zooplankton). It is possible to see the relative proportions between the trophic strategies, in the simulations and the dataset, in the ternary plots of Figure 2.5, which shows τ (from 0.2 to 1/0.2) versus γ_I (from 0.2 to 0.95) at 20 and 25°C.

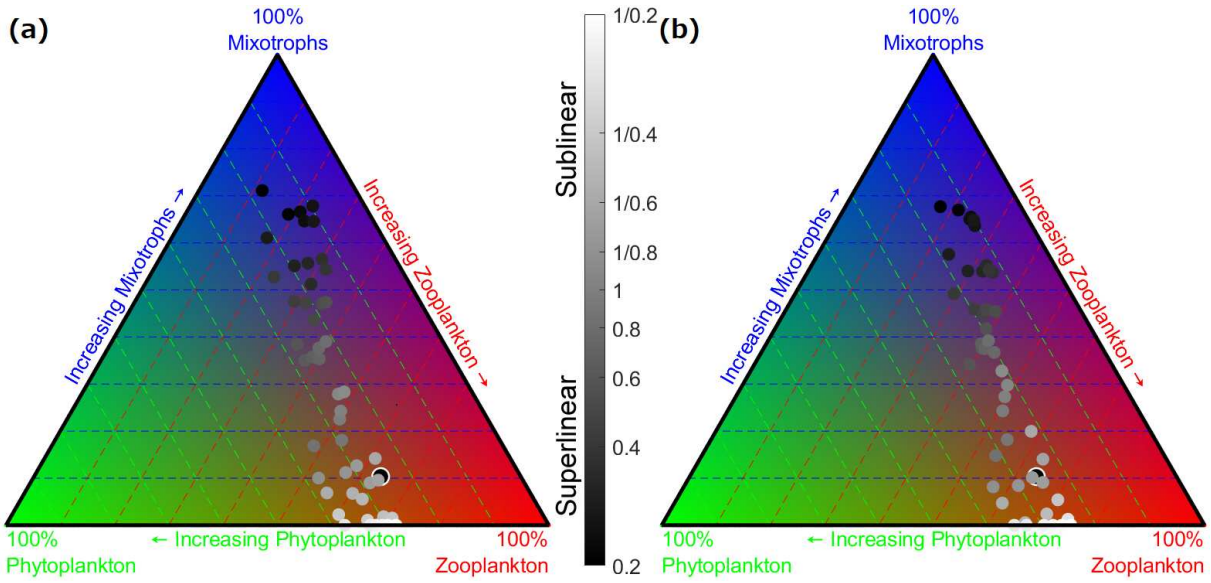

FIGURE 2.5: Ternary plots showing community composition (percentage P:M:Z) as a function of the shape of the trophic trade-off. The simulation had different values of trophic trade-off and light limitation factor. **(a)** 20°C. **(b)** 25°C. The black dot circled with white represents the observations from D'Alelio et al. (2016a). The other dots are shaded by the shape of the trophic trade-off (τ) (see inset scale bars).

2.2.7 Sensitivity analysis

The model was tested across a range of values for nutrient (N_0), temperature (T), light (γ_I) and the value that defines the shape of the trade-off (τ) (see Table 2.10 for a complete list). Only temperature and light limitation values were uniformly spaced. The different temperatures were used only for the sensitivity tests, while, for the fitting, nutrient and temperature were kept constant (5 mmolN m^{-3}, 20°C and 25°C).

TABLE 2.10: Summary of the variables tested.

Input used	**Values**	**Total**	**Description**
N_0 (mmolN m^{-3})	{1, 2, 5, 10, 100}	5	Incoming nutrient concentration
T (°C)	{0, 5, ..., 40}	9	Environmental temperature
γ_I (-)	{0.20, 0.35, ..., 0.95}	6	Light limitation factor
τ (-)	{0.2, 0.4, 0.6, 0.8, 1, 1/0.8, 1/0.6, 1/0.4, 1/0.2}	9	Trophic trade-off parameter

The trophic trade-off was applied only to the maximum uptake and grazing rates (Equations 2.1 and 2.2). This choice was made under the assumption that there is no trade-off in resource affinity when resources are encountered at very low rates (Ward et al., 2011).

2.3 Experimental Design

The model described in the Method section was tested for temperature (9 different single values) versus trophic trade-off configurations (9 different single values) for a total of 81 experiments. Light limitation (6 different single values) was as well tested with different temperatures and trade-off, however light was not showed to change the community as drastically as temperature and trade-off, which caused the results to be omitted in this thesis. The exclusion of the findings on light limitations is driven also by the need for brevity in this thesis, while nutrient sensitivity is discussed in the next section.

A second set of simulations counted 108 iterations comparing temperature (9 different single values) versus light limitation (6 different single values) at 2 different temperatures: 20°C and 25°C as per Stabile et al. (2007) and D'Alelio et al. (2016a).

The ranges of values of the parameters for the various combination are found in Table 2.10, testing the sensitivity of community composition to the shape of the mixotrophic trade-off and the degree of temperature and light limitation. Solutions that most closely matched the observed community (Equation 2.12) were then used to infer the shape of the trade-off and to explore the sensitivity of the system to changes in environmental temperature.

2.4 Results

2.4.1 Sensitivity to nutrient

Different sensitivity tests were run with different nutrient concentrations (Figure 2.6) using τ equal to 1, temperature equal to 20°C and γ_I equal to 0.1.

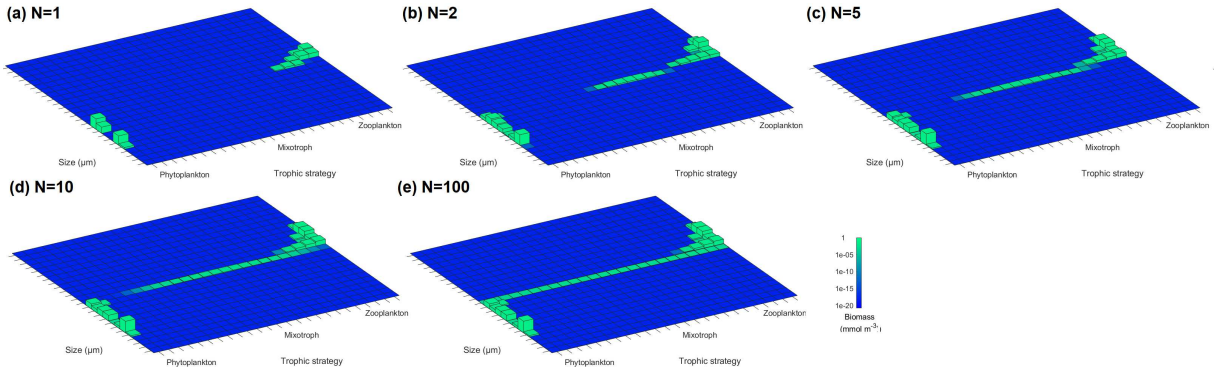

FIGURE 2.6: Equilibrium solutions of the model with different values of N (the bold numbers above each panel) in mmolN m^{-3}. The blue square represents the trait space, and each green shape represents the biomass assigned to each trait.

The tests showed that going below 2 mmolN m^{-3}, the size of the mixotrophic community is progressively reduced, which is a result not suitable for this research. Meanwhile, above 10, the system increases the size of the mixotrophic community until, at 100 mmolN m^{-3}, all the possible positions on the mixotrophic spectrum are occupied by a population. Above 10 mmolN m^{-3} mixotrophs' biomass is so spread that it does not give any useful information on the mixotrophic spectrum. For this reason it was chosen 5 mmolN m^{-3} as a conservative compromise between a very small and a too spread mixotrophic strategy.

2.4.2 Sensitivity to temperature and the trophic trade-off

Figure 2.7 shows how the community composition varied according to τ (from 0.2 to 1/0.2) and temperature (from 0 to 40°C). Each ternary plot corresponds to the same exact set of simulations (trophic trade-off versus temperature), but with scale bars showing the change in trophic trade-off (a) and temperature (b).

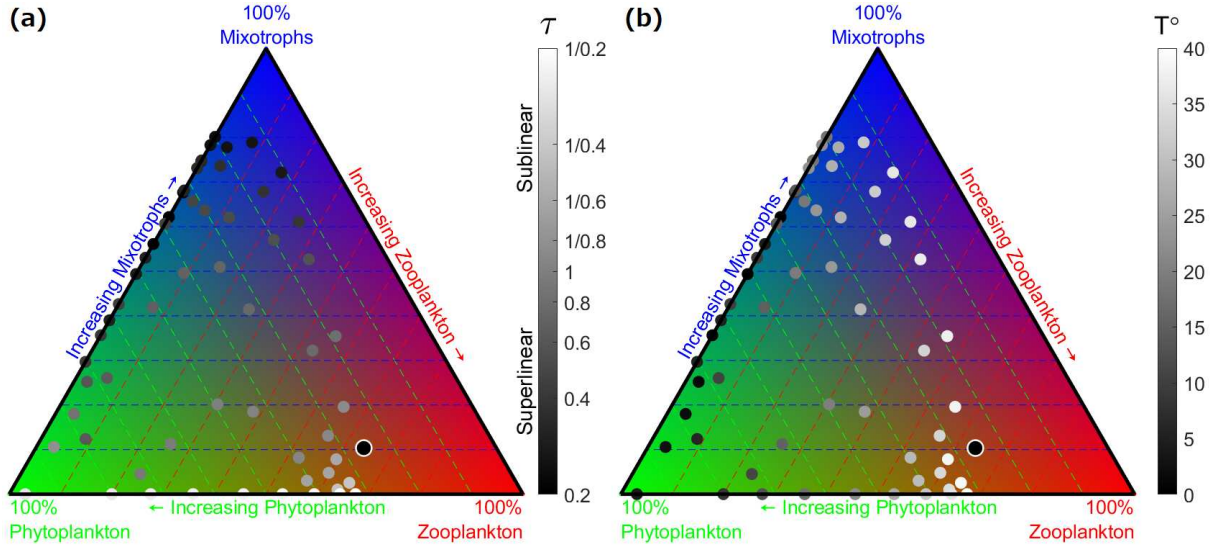

FIGURE 2.7: Ternary plot showing community composition (percentage P:M:Z) as a function of the shape of the trophic trade-off and temperature. The black dot circled with white represents the observations from D'Alelio et al. (2016a). Both panels show the same simulations with different temperatures and trophic trade-off, but in panel **(a)** the dots are shaded by the environmental trophic trade-off (τ), while in **(b)** the dots are shaded by the shape of the temperature (see inset scale bars).

Figure 2.7(a) shows the relation between community composition (P:M:Z) and tropic trade-off. As expected, superlinear trophic trade-offs favour mixotrophs, while linear and sublinear trade-offs favour specialists. Figure 2.7(b) shows the relation between community composition (P:M:Z) and temperature. Phytoplankton clearly prevail at low temperatures (<20°C), while zooplankton prevail at high temperatures (>20°C).

Mixotrophs prevail at temperatures above 15°C. Together, these two ternary plots suggest that mixotrophs increase in relative abundance at high temperatures and when there is a superlinear trade-offs.

2.4.3 Misfit quantification

After establishing how temperature and trophic trade-off impact community composition, the simple misfit function (Equations 2.12) was applied to test which parameter combinations allowed the model to minimise the euclidean distance between model and observation. Figure 2.8 shows model-data misfit as a function of the tested parameters at temperatures of (a) 20°C and (b) 25°C. In each panel the background colour shows the euclidean distance between the observations and the model as a function of τ (from 0.2 to 1/0.2, rows) and γ_I (from 0.2 to 0.95, columns). Figure 2.8 clearly shows that the shortest euclidean distances (indicative of the best-fit model) are associated with approximate values of $\tau = 1/0.8$ and γ_I=0.5-0.8. Given the difference in light limitation between the two results, it is possible to attest that this parameter has less impact than the trade-off.

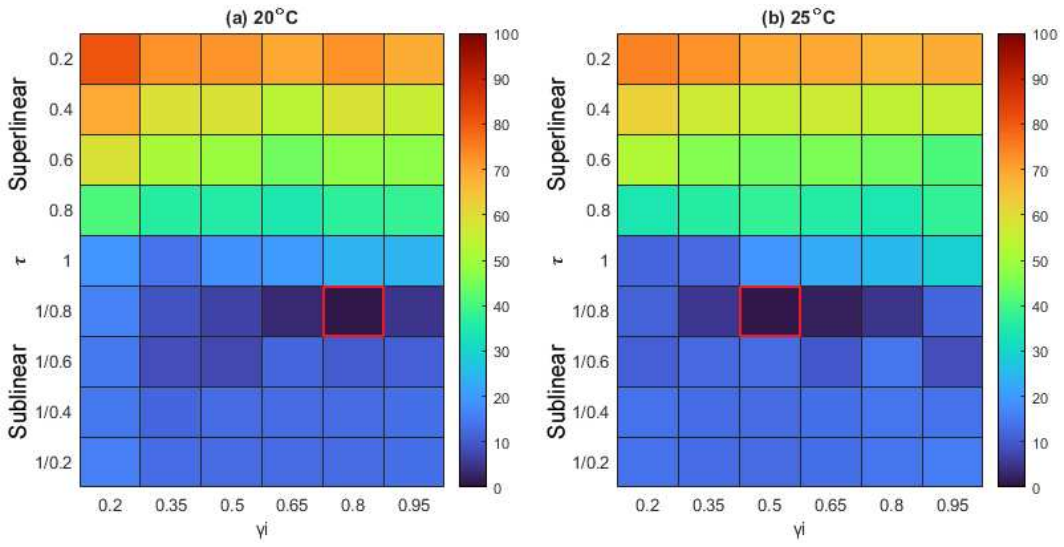

FIGURE 2.8: Dissimilarity between model and observations as a function of τ and γ_I. **(a)**: simulations performed at 20°C as indicated by Stabile et al. (2007), **(b)**: simulations performed at 25°C as indicated by D'Alelio et al. (2016a). The red outlined blue square indicates the closest simulations to the observations.

After the quantification of the distances between the observations and the simulations, the closest matches in terms of the relative proportions of phytoplankton, mixotrophs and zooplankton (Figure 2.8, blue squares underlined in red) are shown in a network format and compared with an equivalent network based on the observed community (Figure 2.9).

The networks in Figure 2.9 are organized in a similar way to Figure 2.1. Figure 2.9(e) is the same picture of Figure 2.1. In both steady state model solutions (Figure 2.9 a and c), picoplankton dominate the phytoplankton. Figure 2.9(a, c, e) all show a similar size distribution among the community of zooplankton. The main differences are in the absence from the simulations (Figure 2.9 a and c) of the detritivorous bacteria that are present in the observed community (panel e). This is to be expected because the model does not resolve organic detritus or its consumption. Mixotrophic populations are very small in the simulations as in the observed community. The observed mixotrophs (panel e) are generally more autotrophic than their simulated equivalents (panels a and c), however it is important to note that the misfit equation did not penalize the position on the mixotrophic spectrum.

The simulated and observed systems also differ in terms of the trophic interactions. In the simulations (Figure 2.9 a and c), grazing fluxes are dominated by nanozooplankton feeding on picophytoplankton, while in the observed system (Figure 2.9 e), it is mesozooplankton that feed most prominently on nano and microphytoplankton. This is probably due to the narrowness of the predator-prey size preference parameter, that does not allow properly the interactions between populations of such different average size. Although, in all cases, energy and biomass flow from small to large plankton, and from phytoplankton to zooplankton. In order to quantify the role of the mixotrophs in the simulated ecosystems, an additional set of experiments was performed.

2.4.4 Comparing simulations with and without mixotrophy

Figure 2.9(b, d) presents results from simulations with the same parameters as used for Figure 2.9(a, c), respectively, but with all mixotrophic plankton excluded at the start of the simulation. This community composition was achieved by decreasing the number of trophic strategies, M, from 25 to just the two specialist strategies.

Figure 2.9(a) presents the same size classes of phytoplankton populations of Figure 2.9(b). The differences are in the number of zooplankton populations: in the 25×2 model, it is possible to see the development of smaller mesozooplankton populations, that substitute mixotrophs of similar sizes. The biomass fluxes connect the same nodes, however, in Figure 2.9(b) the mixotrophs fluxes are made by the smallest zooplankton. The same similarities and differences are visible between Figure 2.9(c) and (d).

Figure 2.10 shows the differences in the community size distribution for simulations with and without mixotrophy. The figure indicates very little difference in the size class distribution between the mixotrophic and non-mixotrophic models, but in Figure 2.10(b) it is possible to notice a small increase in the quantity of biomass at 2 and at 2,000 μm. Biomass at 2 μm corresponds mostly to the largest phytoplankton, while biomass at 2,000 μm corresponds to the largest zooplankton.

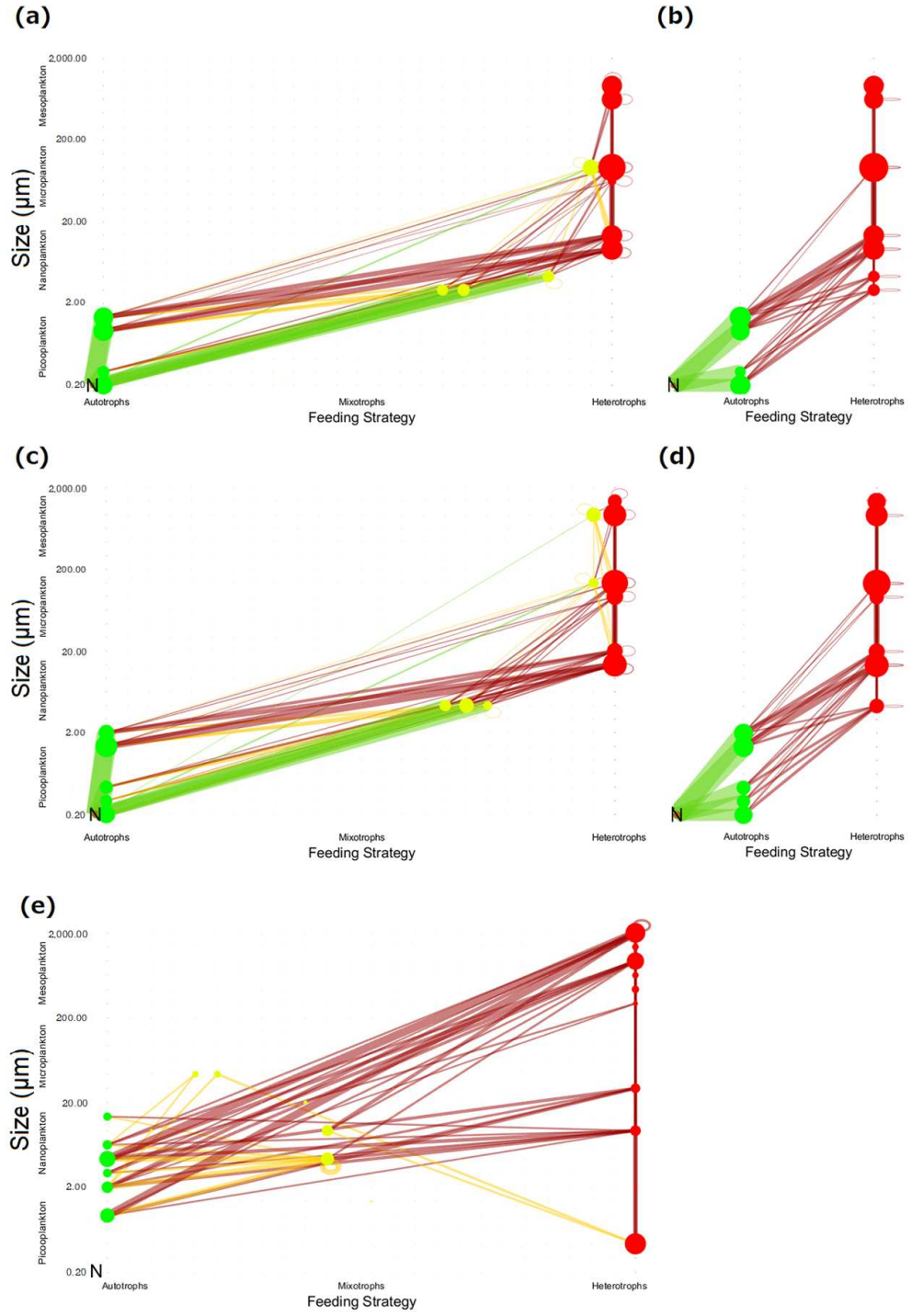

FIGURE 2.9: Trophic webs of the simulations and observations. The radius of the nodes represent the cubic root of the quantity of biomass for that population, while the edges between these nodes represent a trophic interaction. The thickness of these edges is proportional to the nitrogen flux into and out of each population. Green corresponds to phytoplankton biomass, red to zooplankton biomass and yellow to mixotrophic biomass. Primary production is shown in green, while grazing interactions are shown in orange (for mixotrophs) and red (for zooplankton). Panel **(b)** shows a similar simulation to (a) but run without the resolution of the mixotrophic populations. Panel **(a)** shows the best-fit food web for T=20°C (T=20°C, γ_I=0.8, τ=1/0.8). Panel **(c)** shows the best-fit network for T=25°C (T=25°C, γ_I=0.5, τ=1/0.8). Panel **(d)** run a similar simulation to (c) but without the resolution of the mixotrophic spectrum. Panel **(e)** shows the observed biomasses and empirically-modelled fluxes from the non-bloom phase of D'Alelio et al. (2016a).

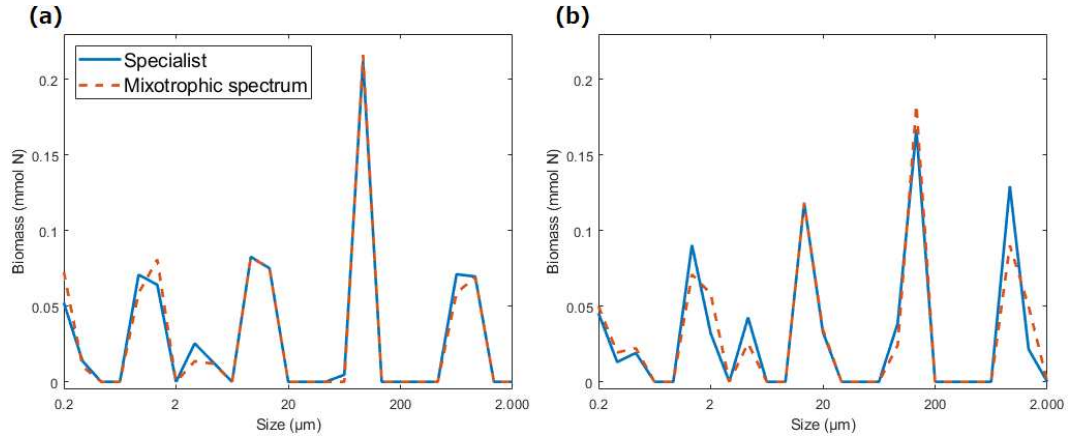

FIGURE 2.10: Comparing the integrated biomass in each size class for simulated ecosystems with (solid blue line) and without (dashed red line) mixotrophs. Cell diameter is shown on the x-axis and biomass abundance on the y-axis. The biomass in each size class shows the integral across all trophic strategies. **a)**: T=20°C, γ_I=0.8, τ=1/0.8 **b)**: T=25°C, γ_I=0.5, τ=1/0.8

2.5 Discussion

The aim of this chapter is to address the three following questions: How do temperature and the shape of the trophic trade-off impact the simulated balance of phytoplankton, mixotrophy and zooplankton? What shape of trophic trade-off allows the model to best approximate the observed data? Is mixotrophy less or more than the sum of its parts (Ward, 2019)?

Since the strength of trade-offs and environmental constraints are largely unknown, and since different mixotrophic taxa are very likely differentially influenced by these trade-offs (Stoecker, 1998), this chapter applied a model to investigate the rules that describe the development of a diverse plankton community, from the smallest to the largest, and from strictly autotrophic phytoplankton to strictly heterotrophic zooplankton, with a particular focus on how the community composition responds to the adjustment of key parameters.

According to literature (Rose and Caron, 2007; Gillooly et al., 2001; Allen et al., 2005; Wilken et al., 2013), photoautotrophic and heterotrophic metabolic rate should differentially change according to increasing temperatures. This chapter used a model that considered no such difference, however, the results clearly show that the dominance of certain trophic strategies changes with different temperatures. If physiology alone is not sufficient to explain how temperature impact plankton community assembly, ecology can be used to explain temperature related patterns. At low temperature, phytoplankton do not produce enough biomass to sustain the rest of the community. When then temperature goes up, this biomass increases, and allows mixotrophs and zooplankton to grow. Mixotrophs dominate the community only at superlinear trade-off. Thus, ecology,

together with physiology, must be taken into account when it is necessary to explain in nature how temperature shapes plankton community structure.

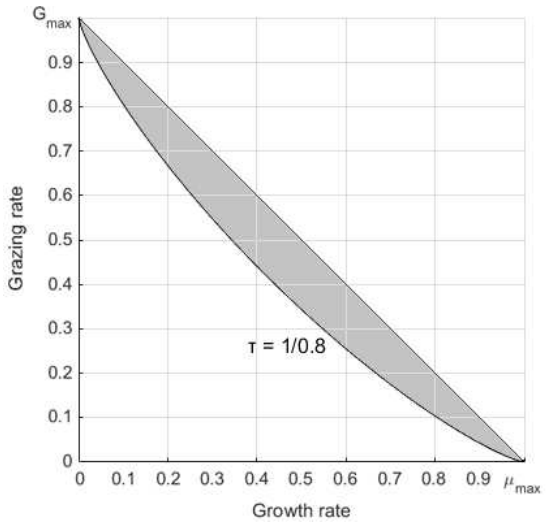

FIGURE 2.11: The shape of the trophic trade-off suggested by the best-fit models.

According to Figure 2.8, the GoN, during summer, presents an ecosystem characterized by a sublinear trophic trade-off ($\frac{1}{0.8}$) (Figure 2.11). This result suggests that mixotrophs can be a part of a community even when penalised by a costly trade-off, relative to the specialists (Våge et al., 2013). Ward et al. (2011) showed that mixotrophs coexist with the specialists, even when mixotrophy is a less efficient trophic strategy than strict autotrophy and heterotrophy. By assuming that the autotrophic uptake rate and the heterotrophic grazing rate are limited by cell surface area, trophic success is achieved when resources are diffusion limited. Mixotrophs hosts both trophic systems on their surfaces, thus they have half the transport rate for a single resource, but contemporary, they can outcompete the specialists when both resources are at low concentration (i.e. when the slower transport rate is less penalizing).

Edwards (2019) showed that the nutrient-carbon co-limitation is another key factor that allows mixotrophs to coexist with specialists. Phytoplankton and zooplankton growth rates are respectively limited by water nutrient concentration and by carbon assimilation, due to photosynthesis and grazing on nutrient-enriched prey. Mixotrophs do not have such limitation, and when nutrient or prey become scarce in their surrounding, they can survive by switching between trophic systems.

Although the best-fit models were not fully able to reproduce the observed system, they showed how the presence of the mixotrophs leads to a change in the biomass of the whole ecosystem (Figure 2.10). The magnitude of the change is very small because the trophic trade-off is sublinear, and sublinear trade-off decrease the potential impact of mixotrophs (Ward and Follows, 2016). A more thorough study of this effect is illustrated in Figure 2.12(a), where τ (from 0.2 to 1/0.2) and temperature (from 0 to 40°C) were checked against each other, like in Figure 2.7 but with a heatmap this time. Here

the absolute difference in the quantity of biomass between models with and without mixotrophs are shown as a function of environmental temperature and the strength of the mixotrophic trade-off parameter, τ. This picture shows that a superlinear trade-offs, and a temperature between 25° and 30°C causes the largest difference in biomass. This parameter combination is optimal for showing the difference because mixotrophs are more abundant around intermediate temperatures and with very superlinear trade-off. The combination allows mixotrophs to vary more and show more difference in the heatmap.

Figure 2.12(b) shows the two simulations with the largest difference ($\tau = 0.2$ T=25°C, black dot in Figure 2.12(a). These simulations indicate that the difference is actually an increase in biomass in the largest size classes. In comparison with the mixed results of Figure 2.10, the larger shift of biomass toward the larger size classes is due to the superlinear trophic trade-off. This result confirms the conclusions from Ward and Follows (2016) that indicates a general increase in the average size when mixotrophs are added to a size-structured plankton model.

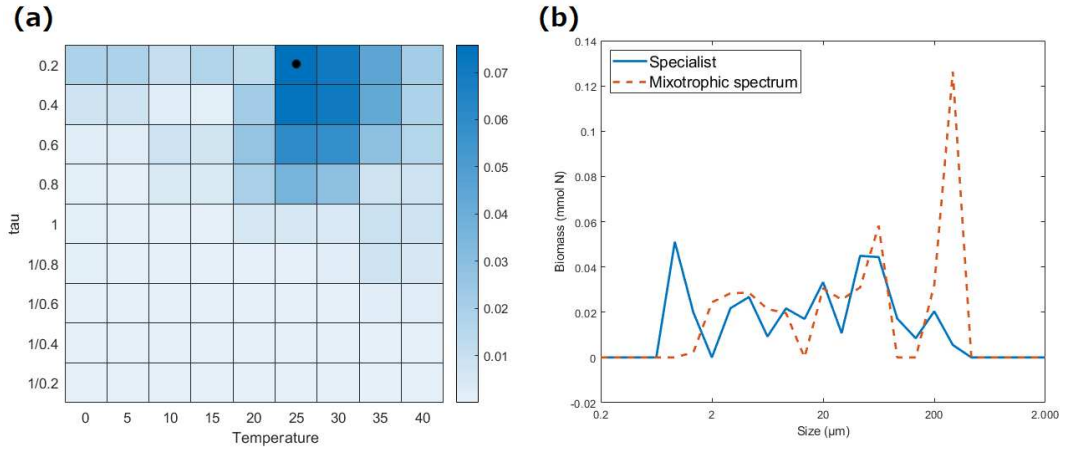

FIGURE 2.12: **(a)**: The intensity of the colour corresponds to the simulations where the presence of mixotrophy caused the largest change in the quantity of biomass in the populations. This is evident in zone between T=25-30°C and τ=02-0.8. **(b)**: example from T=25°C, τ=0.8, the maximum distance (black dot in **a**).

The results from the sensitivity tests with and without mixotrophy have important implications for the carbon cycle. Given that it is expected that future oceans will become warmer (Pachauri et al., 2014), the findings of this chapter suggest that plankton ecosystems may shift toward more mixotrophic and heterotrophic communities (Wilken et al., 2013). Heterotrophic plankton will also have larger, on average, cell sizes, and this in turn will increase the average rate of sinking and thus the strength of the BCP. However, the suggested sub-optimal trade-off may limit the capacity of mixotrophs to impact the community as it responds to climate change since, by going from a mixotroph without trade-off to a mixotroph with the trade-off, the final result will start to resemble

the result from a system with only specialists. (See Figure 6.5, this idea is further explored in Chapter 6)

It is also important to underline the problems caused by the predator-prey size preference. Observations lead to a flux distribution that covered the top-right portion of Tables 2.5, however, given the assumption made by Gibbs et al. (2020b), the predator-prey size preference allowed to fill just a diagonal of the predator versus prey Table (Tables 2.11), which caused a different distribution in size. This approximation should not be underestimated, and future models should keep into account the possibility of extending the possible range of the predator-prey size preference.

TABLE 2.11: Impact of the predator-prey size preference range on one of the final results (T=20°C, γ_I=0.8, τ=1/0.8).

μm		0.29	0.29	4.31	9.28	13.63	92.83	92.83	632.46	928.32
	ω	0.29	0.33	0.13	0	0	0.04	0	0	0
0.2	1	0.00069	0.00046	0.00043	0.0004	0	0	0	0	0
0.93	1	0	0	0.00058	0.00758	0.0049	0	0	0	0
2.94	0.29	0	0	0	0.00036	0.00063	0	0	0	0
2.94	0.33	0	0	0	0	0.00045	0	0	0	0
4.31	0.13	0	0	0	0	0	0	0.00053	0	0
6.32	1	0	0	0	0.0058	0.0053	0	0	0	0
9.28	0	0	0	0	0	0	0.0012	0.00672	0	0
13.63	1	0	0	0	0	0	0.00094	0.00517	0	0
92.83	0	0	0	0	0	0	0	0	0.00208	0.00208
92.83	0.04	0	0	0	0	0	0	0	0.0004	0.0004

To conclude, this chapter shows how, an observation dataset, has a plankton community with mixotrophs that coexist with the specialists despite a costly (sublinear trade-off) combination of autotrophic and heterotrophic resource acquisition (Figure 2.8). It is important for modellers to take this cost into account, because the strength of the trade-off has a large impact on plankton community composition and ecosystem function, in terms of average plankton cell size and carbon uptake (Ward and Follows, 2016). Together with temperature (Figure 2.7) and light limitation (Figure 2.5), trophic trade-offs affect the community carbon export, and therefore the BCP, a process that plays a role in the regulation of the quantity of carbon in our atmosphere.

This research was able to show how community structure changes according to different temperatures and trophic trade-off. Next chapters will expand on this body of research by adding other findings related to the analysis of model simulating plankton communities on a global scale and their relation to the global biogeochemical cycles.

Chapter 3

The EcoGEnIE global plankton ecology model

The model used for the rest of the thesis is EcoGEnIE (Ward et al., 2018), an ecological extension of GEnIE (Grid Enabled Integrated Earth system model, Ridgwell et al., 2007). GEnIE is an Earth System Model of Intermediate Complexity (Claussen et al., 2002), and will be used for the rest of the thesis because it will allow to simulate, on a global scale, changes in plankton community structure and the carbon cycle.

Since EcoGEnIE incorporates a trait-based approach, with the use of size and trophic strategy, and since the relation between biogeochemistry and plankton is ruled by eco-physiological traits (i.e. carbon export related to average plankton size; Ward and Follows, 2016), the model has the potential of exploring the relation between carbon cycle and ecology. This model will also allow to simulate a future, warmer, 21^{st} century, with interactions between ocean physics, chemistry and biology. By simulating in parallel different scenarios with different ecological configurations, the role of each element (ocean circulation, stratification, nutrient concentration, phytoplankton, mixotrophs, zooplankton etc...) will be untangled by the final results.

EcoGEnIE is only one of the latter expansions to the original framework called GEnIE, which was developed to flexibly permit the addition of different modules that can simulate ocean, atmosphere, and ice sheets (Marsh et al., 2011). GEnIE spatial resolution is set as a compromise between low resolution and computationally efficient energy balance models, and higher resolution and more computationally expensive general circulation models (Marsh et al., 2011).

The circulation component of GEnIE and EcoGEnIE is based on the frictional geostrophic 3D ocean circulation model C-GOLDSTEIN (Edwards and Shepherd, 2002; Edwards and Marsh, 2005). This representation of the ocean circulation facilitates the movement of tracers around the ocean on a large scale, but lacks the resolution to account for

smaller scale patterns such as turbulent mixing and small-scale eddies, which are known to impact the global biogeochemical cycles (Lévy et al., 2012, 2014). Atmospheric processes are simulated by a 2D Energy and Moisture Balance Model (Weaver et al., 2001), which represents heat and water in the atmosphere and at the ocean-air interface. This submodel impacts the representation of thermohaline circulation and cloud formation, which feeds back on the entire system. Spatial and temporal resolution are low to limit computational costs. The dynamic-thermodynamic sea-ice model simulates the icecaps (Semtner Jr, 1976), which are sensitive to local changes in temperature and moisture, and which influence Earth's energy balance by moderating the planetary albedo.

Ocean biogeochemical fluxes were added to the model, as described in Lenton et al. (2006) and Ridgwell et al. (2007). The inclusion of the BCP was initially represented as a nutrient-restoring approach, in which phosphate concentrations were restored to zero (Lenton et al., 2006). This model was later revised so that phosphate uptake (and thus carbon export) was represented as a function of nutrient availability, light and temperature (Ridgwell et al., 2007).

Ridgwell et al. (2007) calibrated GEnIE parameters to fit marine geochemical data (Conkright et al., 2002; Key et al., 2004), thus allowing and improving data-constraining representation of the ocean carbon cycle. This carbon-centric version of the model was called cGEnIE. At this stage it was possible to simulate biogeochemical cycles, and their relative feedback, on time frames up to 10,000 years, which are also relevant to the BCP.

The GEnIE framework was extended by Ward et al. (2018) to include an explicit representation of plankton communities throughout the ocean surface layer. This expansion required the addition of new state variables representing plankton carbon, chlorophyll and nutrient biomasses with flexible stoichiometry, and allowed the investigation of how relatively complex plankton ecology can feedback on ocean biogeochemical cycles and climate over very long timescales, that would be extremely slow and difficult to compute in more highly resolved global ocean models.

In this chapter there will be an overview of EcoGEnIE, an explanation on how the biogeochemical and ecological modules (BIOGEM and ECOGEM) interact, an introduction to the ecophysiological parameterisations that define the simulated plankton and a list of the parameters used in the model simulations. There will also be a description of the possible ecological configurations and trade-offs used, a list of the main numerical experiments used in the thesis, and details of how some unexpected and undesirable behaviours were fixed after some initial numerical experiments.

3.1 The physical environment

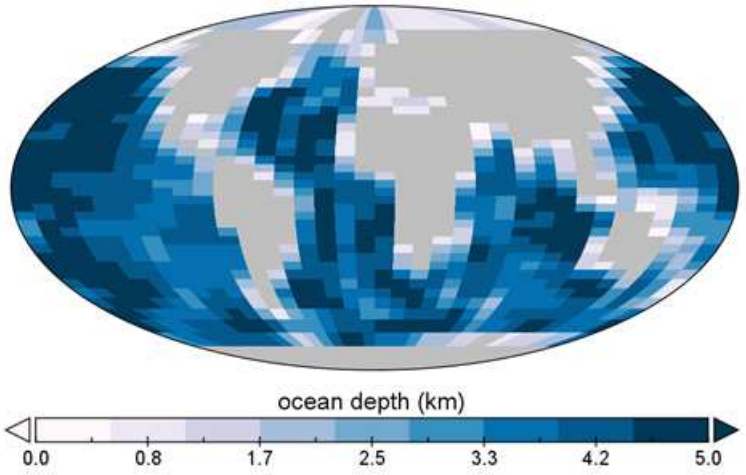

FIGURE 3.1: GEnIE bathymetry on a 36×36 grid.

The simulation environment uses a configurable resolution grid that is set here to $36 \times 36 \times 16$ in latitude, longitude and depth (Figure 3.1). The horizontal grid is uniformly separated in longitude and in the sine of latitude (such that all grid boxes have equal area). The vertical grid is resolved into 16 layers that progressively increase in thickness from 80.8 m at the surface to 766 m at the deepest layer. Currents are simulated by diffusion and advection equations (Edwards et al., 1998) that exchange heat, salinity and tracers among the compartments, horizontally and vertically.

The atmosphere is a single homogeneous compartment, and simulates air temperature and moisture which are vertically exchanged with ocean (by precipitation and evaporation), ice sheets and land (prescribed runoff map, Edwards and Marsh, 2005). The melting/forming of the ice covered part of the polar seas is simulated by taking into account the heat flux between the atmosphere and ocean.

3.2 Biogeochemical fluxes (BIOGEM)

The BIOGEM module simulates biogeochemical transformations of P, C, O and alkalinity (ALK) in the ocean (Ridgwell et al., 2007) (Figure 3.2). In the standard configuration of cGEnIE, nutrients and carbon are taken up from the water in the surface layer, with a fraction going to dissolved organic matter and the remainder being instantly exported and remineralised at depth. This process happens without the presence of simulated organisms.

Production in cGEnIE is limited by the availability of phosphorus and iron. The phosphorus and iron cycles are represented because biological productivity is assumed to be

regulated by these nutrients in the long term (Falkowski, 1997; Tyrrell, 1999). In the original Ridgwell et al. (2007) paper, the model was calibrate using phosphate observations (Conkright et al., 2002). Fluxes of dissolved inorganic carbon (DIC), oxygen and ALK, are subsequently calculated using an assumed fixed stoichiometry of C:P:Fe:O (Redfield, 1934). Despite the importance of nitrogen as a directly limiting nutrient to phytoplankton growth, this element was not represented in the model because it requires a representation of nitrogen fixation that is not included in the standard version of the model (Ridgwell et al., 2007). All biogeochemical tracers in the model move following simulated currents.

Carbon and oxygen are also exchanged with the atmosphere, moving as functions of the difference in the partial pressure of CO_2 between the atmosphere and the ocean. Phosphate and iron are supplied to the productive ocean surface via upwelling and mixing of deeper waters. Iron is additionally scavenged from the water column, leading to a general deficit of iron relative to phosphorus. This loss term is balanced at steady state by atmospheric deposition according to a predetermined distribution (Mahowald et al., 2005).

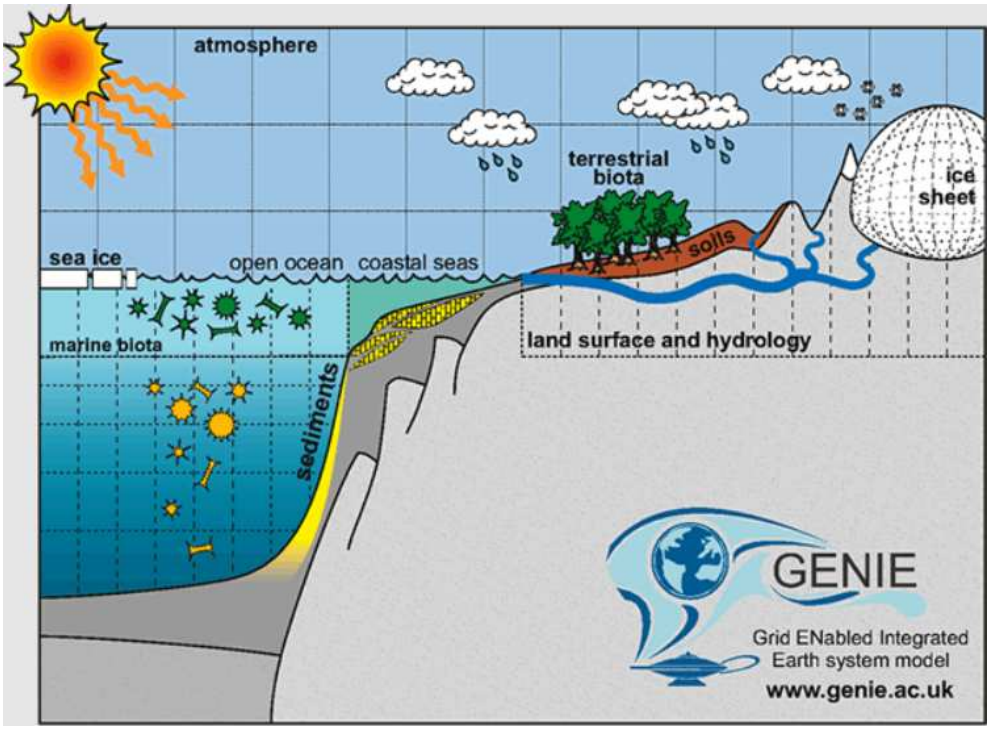

FIGURE 3.2: Schematic representation of cGenie. Light and heat from the sun impact atmosphere, sea ice and ocean. The BIOGEM module transforms these elements between their inorganic and organic form, simulating the role of marine biota without explicitly resolving plankton populations. A portion of the produced organic matter is exported and remineralised at depth. Source: www.genie.ac.uk

Despite the presence of organic matter, at no point is ecology explicitly represented. As said before, uptake, and thus production, is reproduced in proportion of the influence

of temperature, nutrients and light, and these these processes happen only in the ocean surface boxes of the grids. Then, a fraction of the organic matter produced is instantaneously remineralised while it is still at surface, while the rest sinks and then decays by following a double-exponential decay in function of depth (Ridgwell et al., 2007).

3.3 Plankton ecology (ECOGEM)

ECOGEM is the module used to explicitly simulate plankton populations in the cGEnIE environment (Ward et al., 2018) (Figure 3.3). Plankton populations reside in the surface compartments of the ocean, and exchange C, P, Fe and O with the BIOGEM module. The rate of primary production is a function of plankton biomass and the availability of nutrients, light and temperature (as determined by the interactions of ECOGEM, BIOGEM and C-GOLDSTEIN). Nutrient elements are taken up during primary production, and biomass is exchanged between populations during grazing. Plankton mortality is then partitioned into dissolved organic matter (DOM) and (implicit) particulate organic matter pools. These fractions are passed back to BIOGEM, where DOM is remineralised at a fixed rate and POM is instantly exported to depth.

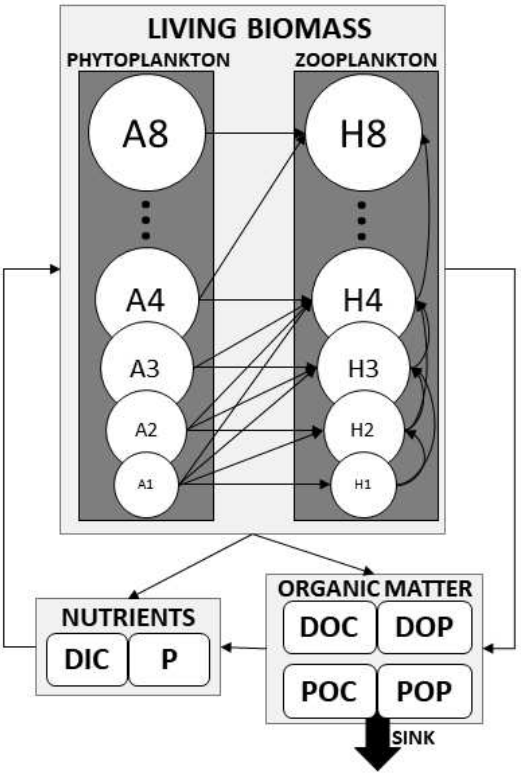

FIGURE 3.3: Model representation of the state variables, the size classes and their interconnections. Each circle represents a plankton population with logarithmically increasing size. A for autotrophs, H for heterotrophs.

The oceanic plankton communities, and their interactions with the abiotic environment, are explicitly resolved by the ECOGEM package using three state variables: R, B and D. At each point in the surface ocean grid, R is a local vector containing the three dissolved inorganic elements used by plankton: carbon, phosphate and iron. B is a local matrix representing plankton populations, with the biomass of each population represented as three resource elements (C, P and Fe) and chlorophyll *a* (Chl). D is a local matrix that represents the amount of dissolved and particulate carbon, phosphorus and iron produced by plankton and messy feeding.

$$\mathbf{R} = \begin{pmatrix} R_{DIC} & R_{PO_4} & R_{Fe} \end{pmatrix} \tag{3.1}$$

$$\mathbf{B} = \begin{pmatrix} B_{1,C} & B_{1,P} & B_{1,Fe} & B_{1,Chl} \\ B_{2,C} & B_{2,P} & B_{2,Fe} & B_{2,Chl} \\ \vdots & \vdots & \vdots & \vdots \\ B_{J,C} & B_{J,P} & B_{J,Fe} & B_{J,Chl} \end{pmatrix} \tag{3.2}$$

$$\mathbf{D} = \begin{pmatrix} D_{1,C} & D_{1,P} & D_{1,Fe} \\ D_{2,C} & D_{2,P} & D_{2,Fe} \end{pmatrix} \tag{3.3}$$

As is the case in BIOGEM, primary production (and the ecological community) are restricted to the surface layer of the model. The inorganic elements are taken from the BIOGEM module and passed to the **R** variable of ECOGEM. Then, through differential equations representing primary production and grazing, the simulated nutrient elements are redistributed in the **B** variable, which contains J different populations characterized by different traits (size and trophic strategy) and 4 different kinds of biomass (C, P, Fe, chlorophyll *a*). At each time step mortality and unassimilated feeding are passed to the detrital variable **D**, which is passed back to BIOGEM for remineralisation and export.

The main advantage of using this model is the settable space resolution given by cGEnIE, which allows to run 10^4 year-long simulations in a reasonably short amount of time, which is in turn a time-frame useful for achieving the biogeochemical steady state in a simulated global ocean (Ward et al., 2018). Furthermore, the trait-based approach gives the advantage of limiting the number of plankton types used, and to automatize the assignation of plankton traits through empirically estimated allometric relationships (Ward et al., 2012). The main disadvantage of this model, instead, is the weak upwelling that causes a decrease in the average global concentration of DIC in the model (Wilson et al., 2018; Ward et al., 2018). Additionally, the trait-based approach allows ecological analysis on plankton communities but it does not allow species resolution, which precludes analysis on biodiversity and its impact on the biogeochemical cycles.

3.4 Plankton ecophysiology

Plankton populations are assigned to a number of different size classes and three feeding categories: autotrophy, mixotrophy and heterotrophy (i.e. $\omega = 1$, 0.5 and 0). Next equations will provide the background to understand the simulated physiology behind nutrient and carbon acquisition/storage and temperature dependence, since it is the impact of these processes, at global scale, that drives the differences between ecological configurations and scenarios. Clear examples are mixotrophs with higher carbon to limiting nutrients ratio (Ward and Follows, 2016) and metabolic rates proportional to environmental temperature (Brown et al., 2004). For a complete description of all EcoGEnIE equations see Ward et al. (2018).

Nutrient uptake and carbon assimilation are separated processes, with nutrient uptake regulated by the environmental concentration of nutrients, and carbon assimilation regulated by the cellular nutrient-to-carbon ratio (or quota) and the availability of light. The nutrient quota for each population j is defined by

$$Q_{j,i_r} = \frac{B_{j,i_r}}{B_{j,C}}$$

where i_r is P or Fe. Each population has a maximum and minimum quota of phosphorus and iron to carbon. Carbon assimilation is a function of the internal nutrient quotas, temperature and light. Nutrient uptake, V, is a Michaelis-Menten-like function of nutrient availability and temperature, assigned to each population j with

$$V_{j,i_r} = \frac{V_{j,i_r}^{max} \alpha_{j,i_r} [R_{i_r}]}{V_{j,i_r}^{max} + \alpha_{j,i_r} [R_{i_r}]} Q_{j,i_r}^{stat} \cdot \gamma_T$$

Where V_{j,i_r}^{max} is the maximum autotrophic growth, α is the affinity for inorganic nutrient R_{i_r}, Q_{j,i_r}^{stat} is the degree of cellular "satiation" that down-regulates uptake as the cellular quota approaches its maximum. γ_T is temperature limitation term, as defined by

$$\gamma_T = e^{S \cdot (T-20)} \tag{3.4}$$

Where T is environmental temperature in °C, and S is a constant that can be modified to asses the differential impact of temperatures on the autotrophic and heterotrophic metabolism (Wilken et al., 2013).

The net carbon uptake rate is modified by the light-limitation term, a variable that changes according to a Poisson function of local irradiance, chlorophyll quota to carbon ratio, and, since chlorophyll production is heavily iron-limited, a photosynthesis-irradiance curve with a initial slope limited by this element (Geider et al., 1998). Another factor that impacts photosynthesis is the size of the phosphorus quota.

Photoacclimation is the process by which photosynthetic organisms adjust their chlorophyll to carbon ratio according to irradiance and nutrient availability. According to this ratio, a certain amount of nutrients are diverted to make new chlorophyll. However, in the model, while chlorophyll quota is proportional to the phosphorus quota, the ratio does not directly decreases by consuming phosphorus, but changes as it is needed (with an associated cost). The attenuation of light with depth is calculated as the sum of light attenuation by water and by chlorophyll, and so more light is attenuated in high biomass systems (Shigesada and Okubo, 1981).

Heterotrophic plankton are assumed to graze prey most efficiently when they are 10 times smaller then themselves in length (Hansen et al., 1994). Additionally, prey caught by predators are not completely assimilated ("messy feeding"), and the assimilated elements, P and Fe, are assimilated as function of how much each quota is full: if the quota is full, the element is not assimilated, if the quota is empty then assimilation reaches the maximum efficiency. Mortality is a linear function of plankton biomass, but under a certain threshold it is decreased to prevent local and global extinctions (Baas-Becking, 1934, i.e. "everything is everywhere"). This threshold is low enough to not directly impact the biomass of abundant populations (Ward et al., 2018).

From a biogeochemical perspective, the losses of biomass in the plankton population, by means of mortality and messy feeding by zooplankton, are divided into dissolved and particulate matter (DOM and POM). DOM is remineralised at constant rate, while POM is instantly converted into its inorganic form and export at depth. The proportion of mortality and unassimilated grazing going to POC and DOC is dependent on the population size class: the smallest size classes produce a 4:1 ratio of DOM/POM, the intermediate size classes (100 μm) produce a 1:1 ratio, while the largest size class produce a 2:3 ratio (Ward et al., 2018).

3.5 Parameterisation

The populations are placed into eight size classes of 0.6, 1.9, 6.0, 19.0, 60.0, 190.0, 600.0 and 1,900.0 μm equivalent spherical diameter (ESD; Figure 3.3). The ecophysiological parameters used by the model can be categorized according to whether or not they are dependent on organism size, as shown in Tables 3.1 and 3.2.

Plankton size-dependent traits are scaled for different sizes following allometric power-law relationships (Chisholm, 1992) (Figure 3.4). These traits are the maximum nutrient uptake rate (V_P^{max}) and cellular carbon quota (Q_c), which increase with size (Marañón et al., 2013). Nutrient affinity (α) decreases with size while according to Hansen et al. (1997), the maximum prey ingestion rate G_C^{max} also decreases with size.

The maximum photosynthetic growth rate P_C^{max} has a monomodal behaviour with peak around 6 μm (Marañón et al., 2013), a size corresponding to nanophytoplankton. This monomodal shape is likely the compromise between the maximum uptake normalised relative the minimum quota, which grows with size, and the maximum metabolic rate, which decreases with size (Ward et al., 2017). Predation is also established by size through a grazing matrix based on the predator:prey size ratio, where the optimal grazing preference is reached when the ratio is 10:1, with a standard deviation of $\overset{\times}{\div}10$.

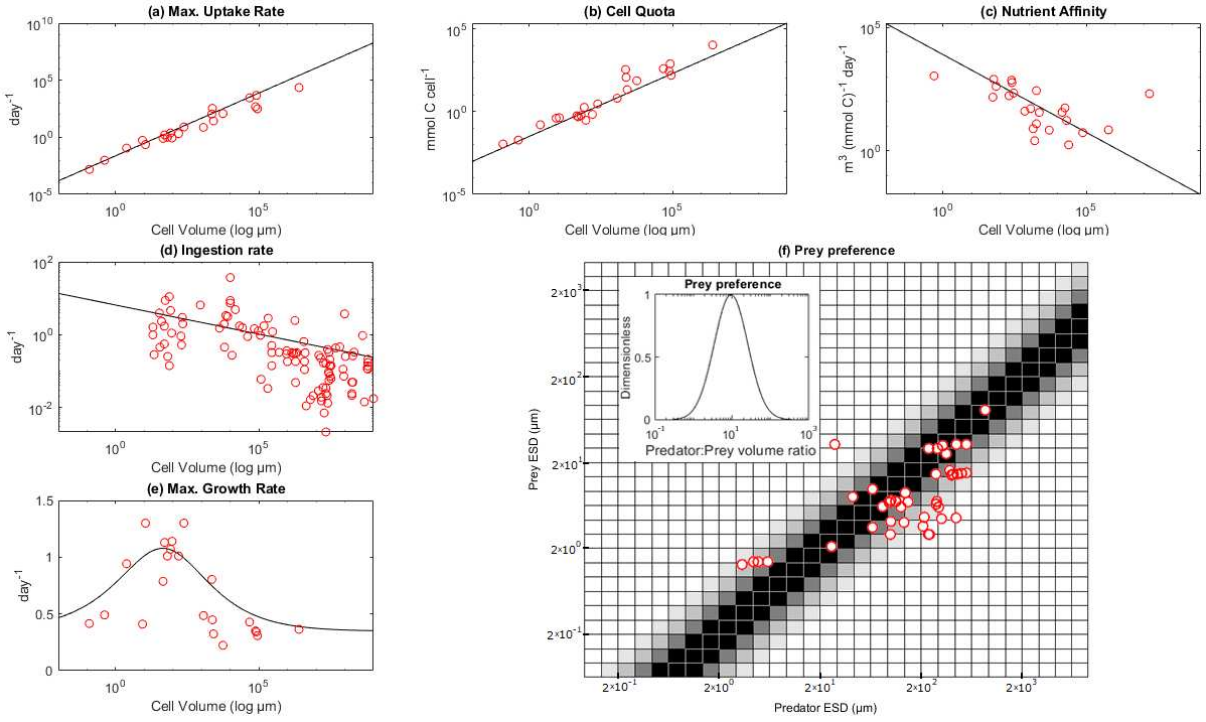

FIGURE 3.4: Relationship between size and plankton traits. Red circles: observations. Black lines: observation fitting. **(a, b)** Uptake rate and cell quota grow with size (Marañón et al., 2013). **(c, d)** Nutrient affinity and ingestion rate decrease with size (Hansen et al., 1997; Edwards et al., 2012). **(e)** Maximum growth rate is a monomodal function (Marañón et al., 2013). **(f)** Predators prefer prey 10 times smaller than their ESD, or 1,000 times smaller than their volume (Gibbs et al., 2020b).

TABLE 3.1: List of the size-dependent ecophysiological parameters. The coefficients are used in the power law equation aV^b, where V is cellular volume. This is with the exception of:

$$P_C^{max} = (a + log_{10}(V))/(b + c \cdot log_{10}(V) + log_{10}(V)^2)$$

$$\beta = a - ((a - b)/(1 + b/ESD))$$

Source: Ward et al. (2018) and references therein.

Parameter	Symbol	Size-scaling coefficients			Units
		a	b	c	
Max. P uptake rates	V_P^{max}	4.4×10^{-2}	0.06		mmol P (mmol C)$^{-1}$ d^{-1}
Max. Fe uptake rates	V_{Fe}^{max}	1.4×10^{-4}	-0.09		mmol Fe (mmol C)$^{-1}$ d^{-1}
Nutrient affinities P	α_P	1.10	-0.35		m^3 (mmol C)$^{-1}$ d^{-1}
Nutrient affinities Fe	α_{Fe}	0.175	-0.36		m^3 (mmol C)$^{-1}$ d^{-1}
Cell carbon quota	Q_c	1.45×10^{-11}	0.88		mmol C cell^{-1}
Max. prey ingestion rate	G_C^{max}	21.9	-0.16		d^{-1}
Max. photosynthetic rate	P_C^{max}	3.08	5.00	-3.80	d^{-1}
Fraction to DOM	β	0.8	0.4	100	-

TABLE 3.2: List of the other ecophysiological parameters. Source: Ward et al. (2018) (Iron quota was updated according to Section 3.8).

Parameter	Symbol	Value	Units
Minimum P:C quota	Q_P^{min}	3.3×10^{-3}	mmol P (mmol C)$^{-1}$
Maximum P:C quota	Q_P^{max}	1.1×10^{-2}	mmol P (mmol C)$^{-1}$
Minimum Fe:C quota	Q_{Fe}^{min}	3.0×10^{-6}	mmol Fe (mmol C)$^{-1}$
Maximum Fe:C quota	Q_{Fe}^{max}	6.0×10^{-6}	mmol Fe (mmol C)$^{-1}$
Reference temperature	$Tref$	20	°C
Temperature dependence	A	0.05	-
Maximum Chl*a*:phosphorus ratio	θ_P^{min}	48	mg Chl a (mmol P)$^{-1}$
Initial slope of P–I curve	α	3.83×10^{-7}	mmol C (mg Chl a)$^{-1}$ (μEin m^{-2})$^{-1}$
Cost of biosynthesis	ξ	37.28	mmol C (mmol P)$^{-1}$
Optimum predator:prey length ratio	υ_{opt}	10	-
Size standard deviation	σ_{graz}	2.0	-
Total prey half-saturation	k_C^{min}	5.0	mmol C m^{-3}
Maximum assimilation efficiency	λ^{max}	0.7	-
Grazing refuge parameter	Λ	-1	(mmol C m^{-3})$^{-1}$
Active switching parameter	s	2	-
Assimilation shape parameter	h	0.1	-
Plankton mortality	m	0.05	d^{-1}
Water light attenuation	k_w	0.04	m^{-1}
Chlorophyll light attenuation	k_{Chl}	0.03	m^{-1} (mg Chl)$^{-1}$

3.6 Configurations

EcoGEnIE can be run with an arbitrary number of plankton populations across three functional groups consisting of phytoplankton, mixotrophs and zooplankton. Three ecological configurations were tested: a "Two-Guild" configuration (containing 8 phytoplankton and 8 zooplankton populations), a "Mixotrophic" configuration (containing 8 mixotrophic populations) and a "Mixotrophic-Plus" configuration (containing 8 phytoplankton, 8 mixotroph and 8 zooplankton populations) (see Figure 3.5). In the Mixotrophic configuration the 8 mixotroph populations are assigned the full traits of both the phytoplankton and zooplankton populations from the Two-Guild configuration with no trade-off applied (see Section 3.7). In the Mixotrophic-Plus configuration, the 8 mixotroph populations are assigned the traits of the phytoplankton and zooplankton populations, but with the maximum nutrient uptake and grazing rates scaled down (according to a trade-off function in Section 3.7).

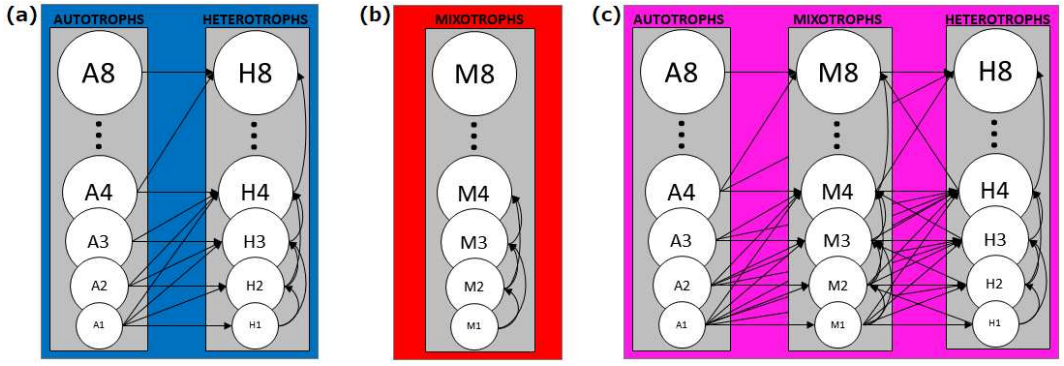

FIGURE 3.5: Schematic representation of the three configurations. Two-Guild **(a)**, Mixotrophic **(b)** and Mixotrophic-Plus **(c)**. A denotes autotrophs, H heterotrophs and M mixotrophs. The colour code will be respected throughout the rest of the thesis: blue for the Two-Guild configuration, red for the Mixotrophic configuration and magenta for the Mixotrophic-Plus configuration.

TABLE 3.3: List of the ecological configurations.

Ecosystem	**Phyto.**	**Mixo.**	**Zoo.**
Two-Guild	8	0	8
Mixotrophic	0	8	0
Mixotrophic-Plus	8	8	8

In Chapters 4 and 6 simulations using the Two-Guild configuration are compared with simulations using the Mixotrophic and the Mixotrophic-Plus configuration. The Mixotrophic configuration comparison was used to check the impact of mixotrophs on plankton communities structure and function. The Mixotrophic-Plus configuration comparison was used to put in direct competition mixotrophs and specialists, and in this way directly testing the mixotrophic trade-off.

3.7 Mixotrophic trade-off

It is often assumed that mixotrophy requires a compromise between autotrophic and heterotrophic traits (Thingstad et al., 1996; Troost et al., 2005; Våge et al., 2013; Ward and Follows, 2016). With limited resources and space inside the cell, it is also assumed to be unlikely that a mixotroph can perform both autotrophy and heterotrophy as fast or efficiently as otherwise similar specialist phytoplankton and zooplankton. While such a trade-off has been invoked primarily on a theoretical basis, there is some recent evidence that mixotrophs may incur such a penalty in the real ocean (Edwards, 2019).

The equations used to modify the maximum autotrophic growth rate (V^{max}) and the heterotrophic grazing rate (g) in mixotrophs are:

$$V^{max}(\tau) = \omega^{\tau} \cdot V^{max} \tag{3.5}$$

$$g(\tau) = (1-\omega)^{\tau} \cdot g \tag{3.6}$$

In these configuration ω is set to 1 for Phytoplankton, 0.5 for mixotrophs and 0 for zooplankton, while τ modifies the shape of the mixotrophic trade-off (Figure 3.6).

Since different penalties for the trade-off impact community structure and function, the simulations with the Mixotrophic-Plus configuration were repeated four times, each with a different value of trade-off (τ), assessing in this way the influence of the shapes of the trophic trade-off in the scenarios. In these simulations τ was set equal to 0, 0.74, 1 and 1.32, which respectively assigns to mixotrophs approximately 100% ($\mathbf{M}_{100}$), 60% ($\mathbf{M}_{60}$), 50% ($\mathbf{M}_{50}$) and 40% ($\mathbf{M}_{40}$) of the original autotrophic growth and grazing rate (Table 3.4, Figure 3.6). In the Mixotrophic configuration, τ was set to zero, such that there was no penalty for mixotrophy and plankton had 100% of the equivalent specialist rates.

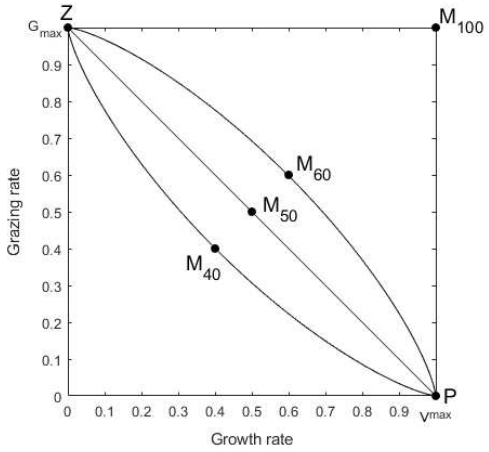

FIGURE 3.6: Schematic representation of the mixotrophic trade-off. Each dot corresponds to the photosynthetic growth and the grazing rate of each ecological configuration used with EcoGEnIE.

TABLE 3.4: Trade-off table with relative mixotrophic trait assignment. The trade-off impacts the rates of nutrient uptake, photosynthesis and grazing, and goes from 1 (100% of specialist rate) to 0 (0% of specialist rate). Only the Mixotrophic-Plus configuration have populations with efficiency not equal to 1 or 0.

Configuration	**Two-Guild**		**Mixotrophic**	**Mixotrophic-Plus**					
Population	**P**	**Z**	$\mathbf{M_{100}}$	**P**	**Z**	$\mathbf{M_{40}}$	$\mathbf{M_{50}}$	$\mathbf{M_{60}}$	$\mathbf{M_{100}}$
Photosyn. growth efficiency	1	0	1	1	0	0.4	0.5	0.6	1
Grazing efficiency	0	1	1	0	1	0.4	0.5	0.6	1

3.8 Tuning of phytoplankton iron physiology

The EcoGenie model used here and in Ward et al. (2018), differs in spatial ($36 \times 36 \times 16$) and biological resolution (8 size classes for each trophic strategy) from the model used to study the global biogeochemical effects of mixotrophy in Ward and Follows (2016) (1° horizontal resolution, 24 vertical levels and 10 size classes for each trophic strategy). As it is helpful to compare the simulations used here to those of Ward and Follows (2016), it was necessary to adjust some parameters to align the coarse level behaviour of EcoGEnIE to the simulated ecosystem analysed in Ward and Follows (2016).

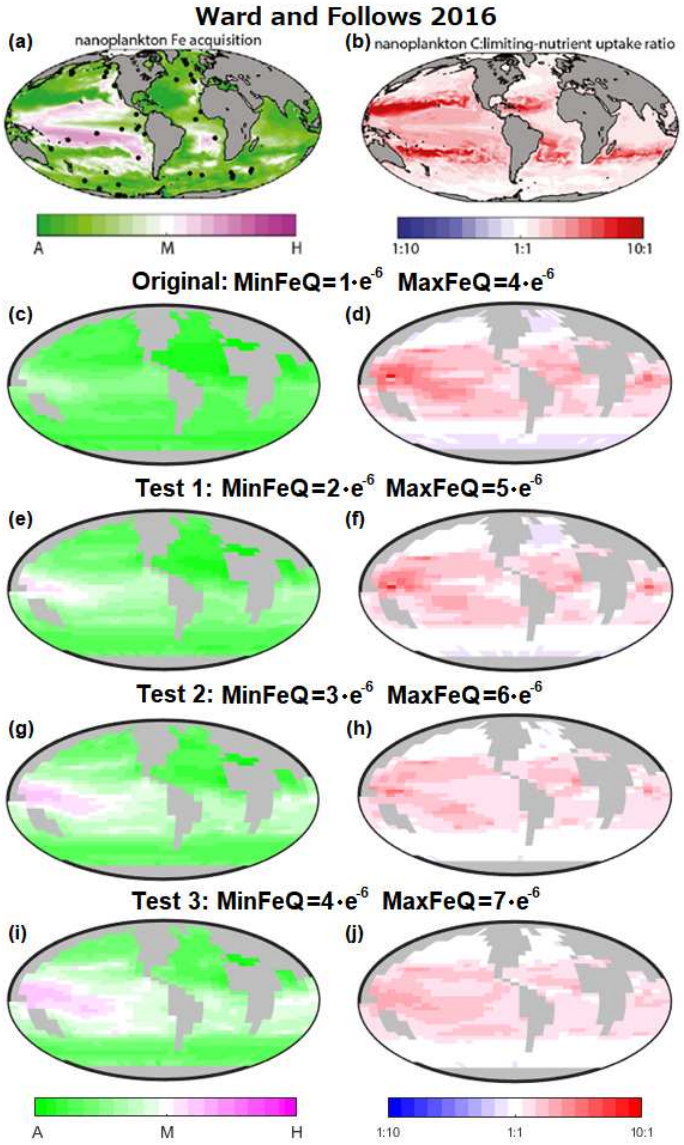

FIGURE 3.7: Comparison of the results from Ward and Follows (2016) (**a**, **b**) with the EcoGEnIE results with different minimum and maximum iron quotas (**c** to **j**).

The initial simulations with mixotrophs showed an artificially high iron autotrophic uptake in the equatorial Pacific (Figure 3.7c), and a low C:limiting nutrient ratio in the high latitudes (Figure 3.7d), in the ratio of the two nanoplankton size classes of the two configurations, if compared to the results of nanoplankton in Ward and Follows (2016) (Figure 3.7a, b, or their Fig.3i, j). This comparison showed that there was an overestimation in the rate of iron absorption made by the modelled phytoplankton if compared to the zooplankton, and in the mixotrophs' autotrophic uptake rate if compared to the mixotrophs' heterotrophic rates.

To investigate this issue, the iron quota was plotted on a map (Figure 3.8a), showing an unreliable very low nutrient limitation distribution (compare Figure 3.8a with c). To

compensate for the excessively low iron limitation, it was clearly necessary to increase minimum and maximum cellular iron-to-carbon quotas.

Three different sensitivity tests were performed (Figure 3.7e to j, Table 3.5). The quotas were steadily increased until the closest match with Ward and Follows (2016) was found. Starting from the original MinFeQ = $1.00e^{-6}$ and MaxFeQ = $4.00e^{-6}$, MinFeQ = $4.00e^{-6}$ and MaxFeQ = $7.00e^{-6}$ were reached.

TABLE 3.5: Tested minimum and maximum iron quotas.

Tests	**MinFeQ**	**MaxFeQ**
Original	$1.00e^{-6}$	$4.00e^{-6}$
Test 1	$2.00e^{-6}$	$5.00e^{-6}$
Test 2	$3.00e^{-6}$	$6.00e^{-6}$
Test 3	$4.00e^{-6}$	$7.00e^{-6}$

At MinFeQ = $2.00e^{-6}$ and MaxFeQ = $5.00e^{-6}$ (Figure 3.7e, f), the autotrophic uptake in mixotrophs is still very high, while there are still some patches of low C:limiting nutrient ratio in the high latitudes. At MinFeQ = $3.00e^{-6}$ and MaxFeQ = $6.00e^{-6}$ (Figure 3.7g, h) finally the heterotrophic uptake is visible in the Pacific Ocean, and the low C:limiting nutrient ratio has disappeared. At MinFeQ = $4.00e^{-6}$ and MaxFeQ = $7.00e^{-6}$ (Figure 3.7i, j), the heterotrophic uptake in the Pacific Ocean has growth again, even beyond the latitudinal boundaries showed in Figure 3.7a, and the high C:limiting nutrient ratio in the low latitudes has only decreased in the last tests, so it was though that the best compromise between uptake and C:limiting nutrient ratio was reached at MinFeQ = $3.00e^{-6}$ and MaxFeQ = $6.00e^{-6}$ (Figure 3.7g, h), which was used for the thesis.

Figure 3.8 further showed how by going from $1.00e^{-6}$ and $4.00e^{-6}$ (Figure 3.8a) to $3.0e^{-6}$ and $6.0e^{-6}$) Figure 3.8b, the model achieved a more realistic distribution of Fe limitation.

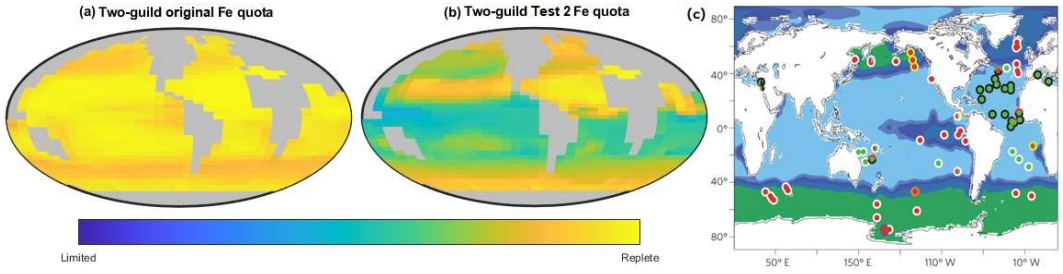

FIGURE 3.8: Comparison of iron limitation in the Two-Guild configuration with different-sized iron quotas. **(a)** The original iron quota (MinFeQ = $1.00e^{-6}$ and MaxFeQ = $4.00e^{-6}$), **(b)** The adjusted higher iron quota of Test 2 (MinFeQ = $3.00e^{-6}$ and MaxFeQ = $6.00e^{-6}$). **(c)** Global distribution of nutrient limitation from *in situ* nutrient bioassays from Moore et al. (2013). The presence of iron limitation is indicated by red circles.

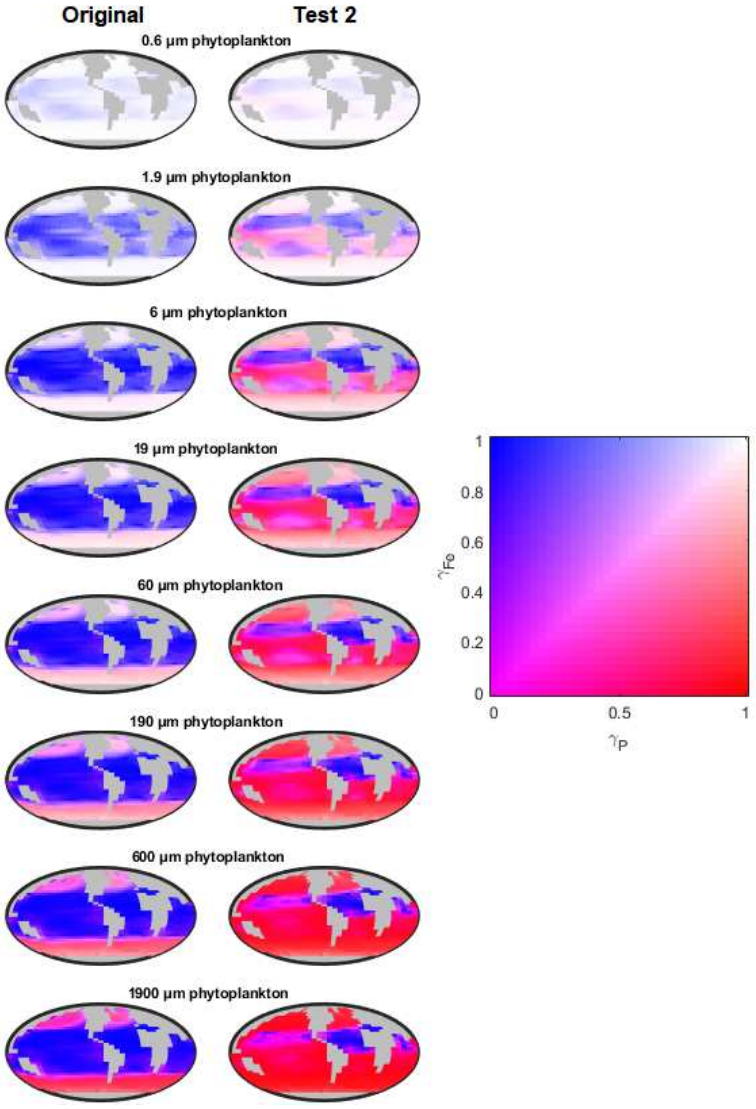

FIGURE 3.9: Co-limitations of phosphorus and iron with the original (left hand column) and Test 2 (right hand column) iron quota simulations in the different size classes of phytoplankton.

At the same time, Figure 3.9 shows how the global ocean co-limitation of the nutrients changes by going from the low to high iron quota. The switch makes most of the plankton, at low latitudes and outside the norther temperate and equatorial Atlantic Basin, going from phosphorus limitation (blue) to iron limitation (red). It also decreases phosphorous limitation in the high latitudes (from red-magenta to red). The subtropical gyres gets from being phosphorus limiting (blue) to co-limiting (magenta).

3.9 Prey switching

EcoGEnIE can be configured with different assumptions regarding how predators select their prey. Predation can be made directly proportional to the biomass of different prey

populations ("passive switching"), or it can be configured such that the more abundant prey populations are subject to a disproportionately higher degree of predation ("active switching") (Vallina et al., 2014).

In this thesis, active switching was chosen as the default mode by which predators selectively graze their prey. Active switching was chosen over passive switching because it is likely that the grazing effort for a certain prey population decreases or increases according to its relative availability ("kill-the-winner theory", Thingstad and Lignell, 1997). Thus active switching avoids the appearance of very few prey classes that dominate the community.

Vallina et al. (2014) identified that some switching formulations display an ecologically unrealistic property of "non-maximal feeding", that is, if a single population were divided into a larger number of identical sub-populations, the active switching function would lead to a decline in the integrated grazing effort.

This problem can be illustrated by considering a single homogeneous prey population B_{tot} that is divided into N equal subpopulations B_i, such that

$$B_{tot} = NB_i \tag{3.7}$$

Given that all the subpopulations are identical and equal in size, we should expect that the grazing effort should be equal, regardless of the number of subpopulations, N. In the case of non maximal feeding, the grazing effort on each prey i is defined as

$$\Phi_i = \frac{B_i^s}{(NB_i)^s} \tag{3.8}$$

Here s is the switching parameter that defines whether prey switching is passive ($s = 1$) or active ($s = 2$). We can simplify this formula by expanding the denominator and dividing by B_i^s

$$\Phi_i = \frac{B_i^s}{N^s B_i^s} = \frac{1}{N^s} \tag{3.9}$$

Thus, to find the total grazing effort we multiply previous equation by N

$$\Phi_{tot} = N\frac{1}{N^s} = \frac{1}{N^{s-1}} \tag{3.10}$$

This indicates that with active switching ($s = 2$), there would be a decrease in the total grazing effort with an increase in the number of populations. This is not ecologically plausible, and is a problem if we want to compare different configurations with different

numbers of populations (8, 16 and 24). To solve this problem, the formulation of the maximal feeding used was changed to

$$\Phi_i = \frac{B_i^s}{NB_i^s} \tag{3.11}$$

This immediately simplifies to

$$\Phi_i = \frac{1}{N} \tag{3.12}$$

With the total grazing effort again calculated by multiplying by N, we can see that the total grazing effort is independent of the number of populations, regardless of the value of the exponent s.

$$\Phi_{tot} = N\frac{1}{N} = 1 \tag{3.13}$$

However, despite the fact that active switching was used for this thesis, it was not without its flaws: it caused less competitive species to survive, which noticeably decreased surface nutrient inventory more in the Mixotrophic-Plus configuration (M_{100}) than in the Mixotrophic configuration. The aim of this analysis was to eliminate as many internal sources of perturbation as possible from the final results (i.e. to make the Mixotrophic-Plus and the Mixotrophic configuration identical in terms of top-down control and nutrient consumption). This elimination was not possible despite being important especially considering the fact that the impact of the mixotrophic trade-off on climate changes is still poorly understood. Passive switching also causes the assembly of less diverse and less stable communities, which is not ideal if we want to compare the results of different ecological configurations with an already limited number of populations (8 for each feeding strategy).

3.10 Other Minor adjustments

Another potential source of error arises because BIOGEM, and not ECOGEM, does the remineralisation of dissolved organic matter. As a consequence of this, slightly different concentrations were recorded in outputs from the two modules. In the rest of the thesis all nutrient fields were taken from the BIOGEM output files.

3.11 Modelled scenarios

Anthropogenic climate changes are caused by increasing atmospheric CO_2 concentrations, compared to the average levels of pre-industrial times. To simulate a warmer world than the average temperatures of pre-industrial times, in the model, four simulations were performed (Table 3.6): (1) a 10,000 year spin-up[1], during which the atmospheric CO_2 concentration was held at a constant "Pre-industrial" value of 277 ppm; (2) a "Historical transient" scenario from 1765 to 2010[2], during which the atmospheric CO_2 concentration was progressively increased from 277 to 388 ppm; (3) a "Control" scenario, running from 2010 to 2100, during which the atmospheric CO_2 concentration was held at a constant (2010) value of 388 ppm; (4) an "RCP8.5" scenario, during which the atmospheric CO_2 concentration was progressively increased from 388 to 936 ppm.

It is important to note that EcoGEnIE does not allow feedback from the marine ecosystem to the ocean circulation and atmospheric CO_2, so the atmospheric CO_2 concentrations, global temperature and ocean circulation are all unaffected by the ecological configurations of the model.

TABLE 3.6: Scenarios used in this research.

Scenario	**Begin**	**Stop**	**Duration**	**Start [CO_2]**	**End [CO_2]**
Pre-industrial	////	////	10,000 years	277 ppm	277 ppm
Historical transient	1765	2010	245 years	277 ppm	388 ppm
Control	2010	2100	90 years	388 ppm	388 ppm
RCP8.5	2010	2100	90 years	388 ppm	936 ppm

The end of the pre-industrial scenario (the steady state) was used to understand the differences, and long term feedback, of a model with and without mixotrophs in the long term. The control and the RCP8.5 scenarios were compared to examine the most prominent effects of global warming in simulated ecosystems with and without mixotrophs. The model did not take into account the effects of other greenhouse gasses (e.g. methane).

Finally, EcoGEnIE was already used by other researchers, with similar scenarios and ecological configurations, showing how this ecological extension can explore long term and climate change scenarios. Wilson et al. (2018) investigated a late Paleocene early Eocene boundary condition, with the use of a Two-Guild configuration with 16 size classes, as a close analogue of present climate change conditions. Reinhard et al. (2020) explored the relation between plankton size and nutrients in a late cryogenian scenario. In their case, they used one Mixotrophic configuration with 9 size classes, and two

[1]This spin-up was required to allow the modelled ocean to achieve a steady state in terms of circulation and biogeochemical cycles.

[2]The historical transient was required to shift the ocean from its pre-industrial state to one representative of 2010 conditions.

Two-Guild configurations, one with 16 size classes and one with 64 classes for a higher resolution. Grigoratou et al. (2021) also used a Two-Guild configuration with 16 size classes, but one of these was substitute with a non-spinose planktonic foraminifera, to study the impact of climate changes on calcifiers' distribution. Asselot et al. (2021) analysed a present time scenario with two Two-Guild configurations, one with 2 and one with 12 size classes, to study how phytoplankton light absorption property can also increase the temperature of the ocean.

Chapter 4

The biogeochemical impacts of mixotrophy over long timescales

4.1 Introduction

Over centuries to millennia, the balance between export production and nutrient resupply is assumed to reach steady state (Hain et al., 2014). In principle, under this assumption, nutrients supplied to the surface by vertical mixing and upwelling should balance the export of nutrients out of the surface layer. Thus, the rate of limiting nutrient supply determines the export flux, and carbon export may be determined by linking nutrient export to carbon using the Redfield ratio (Redfield, 1934).

The Redfield ratio is an established empirical observation in marine stoichiometry (Anderson and Sarmiento, 1994; Falkowski, 2000), and it is considered the global average ratio at which carbon, nitrogen and phosphorus are found in the aquatic environment. However, its constancy on a smaller scale, in time and space, has been challenged (Michael et al., 2001; Karl et al., 2001).

This deviation can impact the export of carbon at depth. Nonetheless, computer models keep using the Redfield ratio for its practicality and convenience (Bacastow and Maier-Reimer, 1990; Najjar et al., 1992; Pahlow and Riebesell, 2000). In the modelling field, to improve carbon export resolution, it is possible to go beyond the constant Redfield ratio, and adopt a more flexible stoichiometry given by resolving element quota in organisms (Caperon, 1968; Droop, 1968). Cellular quotas relies on the dynamic relationship between nutrient availability outside the cell, and the quotas filling inside the cell (Ward et al., 2018). Mixotrophs can deviate from the constant stoichiometry of the Redfield ratio because they can absorb more nutrients per unit of carbon than photoautotrophs thanks to grazing (Ward and Follows, 2016), and *vice versa*, they can absorb more carbon per unit of other elements than heterotrophs thanks to photosynthesis (Edwards, 2019).

This deviation, in models, can be achieved by assigning cellular quotas of nutrients and carbon to simulated organism.

Ward and Follows (2016) showed that mixotrophs can increase average trophic transfer efficiency, average plankton cellular size and the carbon to limiting nutrient ratio in marine microbial ecosystems (Figure 4.1). This means that with a given amount of nutrients, an ecosystem with mixotrophs will have a higher export production than an ecosystem without mixotrophs, resulting in an increase up to 35% (in absence of any trophic trade-offs; Ward and Follows, 2016). The presence of mixotrophs, therefore, implies a net increase of the strength of the BCP.

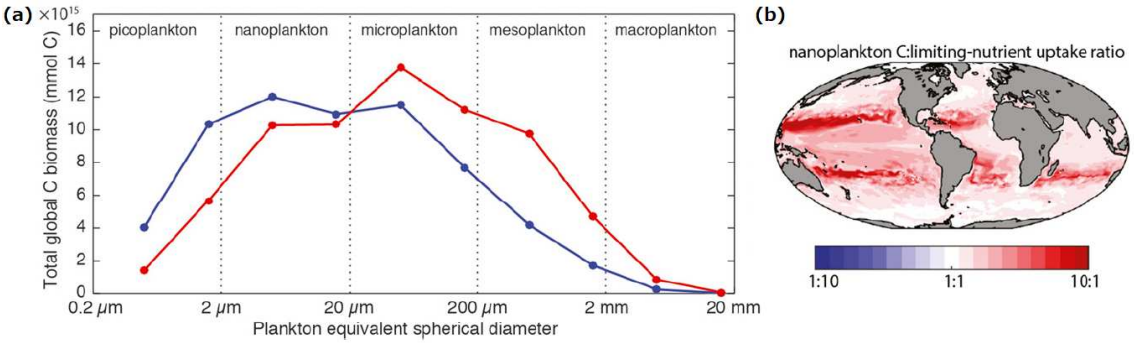

FIGURE 4.1: From Ward and Follows (2016). **(a)** Their Figure 2, showing carbon biomass distribution for each plankton size class. Blue dots/line: Two-Guild configuration. Red dots/line: Mixotrophic configuration. **(b)** Their Figure 3J, showing relative changes in the nanoplankton carbon-to-limiting-nutrient uptake ratio between the Mixotrophic and the Two-Guild configuration. Red/blue colours correspond to more/less carbon fixed in the Mixotrophic model relative to the Two-Guild model.

The original short period used by Ward and Follows (2016) was useful to observe the ecological quasi-steady state at sea surface, but it was not sufficient to resolve any feedback between ocean interior and ocean circulation. Given that carbon export happens in a time frame between 100 and 10,000 years, that mixotrophs locally change the average community stoichiometry, and that the experiment of Ward and Follows (2016) was limited to a timescale of 15 years, it may be informative to further explore the redistribution of conserved nutrients, such as phosphate, and the impact of mixotrophs on the oceanic carbon inventory over millennial timescales using a lower resolution model with a millennia time-scale.

This chapter shows the results of similar simulations to those performed by Ward and Follows (2016), using the much lower resolution EcoGEnIE model of ocean ecology, biogeochemistry and circulation (Ward et al., 2018) to resolve these long-term processes. EcoGEnIE was chosen because it uses the trait-based approach, which allows the resolution of plankton size and trophic strategy (Ward et al., 2018). Size is among the main variables that directly influence the strength of the BCP because larger plankton,

produce larger organic particles, which are less easily degraded by the microbial loop, and sink faster than smaller particles (Guidi et al., 2009).

In the experimental setting, the "Two-Guild" (ecosystem without mixotrophs) and the "Mixotrophic" configurations (ecosystem with mixotrophs) were compared after a 10,000 year simulation, showing the difference in the long term state of the two ecological configurations. The comparison also underlined how mixotrophs play a role in the long-term, by increasing the strength of the BCP at high latitude and decreasing the strength at low latitudes. The overall carbon inventory increased at all latitudes, with the exception of the North Atlantic due to the difference in seasonal bloom strength between the Two-Guild and Mixotrophic configurations.

4.2 Methods

An overview of the EcoGEnIE model is provided in Chapter 3. For a full description the reader is referred to Ward et al. (2018). EcoGEnIE is an Earth-system model of intermediate complexity (EMIC). It allows the interactions of microbial ecology, biogeochemistry and ocean circulation to be investigated at coarse resolution over multi-millennial time scales (Ward et al., 2018).

Following the experiments made by Ward and Follows (2016), two ecosystem configurations were used (Figure 3.5a, b). The first Two-Guild configuration included 8 phytoplankton and 8 zooplankton size classes, of 0.6, 1.9, 6, 19, 60, 190, 600, 1900 μm equivalent spherical diameter. The second Mixotrophic simulation used the same size classes, but with the populations of phytoplankton and zooplankton replaced with eight generic mixotrophic populations that were assigned the combined resource acquisition traits of the equivalent phytoplankton and zooplankton size classes.

Additional sensitivity tests were made with a "Mixotrophic-Plus" configuration (Figure 3.5c) that included eight size classes of phytoplankton, mixotrophs and zooplankton. As explained in Chapter 3, mixotrophs in this configuration were assigned resource acquisition traits at 100%, 60%, 50% and 40% of the values used by specialist phytoplankton and zooplankton (Table 3.4). This configuration was used to test how possible costs associated with mixotrophy might affect the presented results.

The low resolution of the model allowed the simulations to be run from uniform initial conditions, such that an equilibrium state was achieved for marine biogeochemistry in all cases.

4.2.1 C:X uptake ratio

Ward and Follows (2016) showed that mixotrophs increased the amount of carbon assimilated per mole of limiting nutrient taken up. This result required calculation of the ratio of organic carbon synthesis to uptake of the most limiting nutrient in the nanoplankton size class (Figure 4.1b). Nanoplankton were chosen because this size class has a relatively even balance of autotrophic and heterotrophic nutrition in both simulations, whereas the picoplankton and microplankton size classes were dominated by autotrophic and heterotrophic uptake, respectively (Ward and Follows, 2016).

To reproduce this metric for the simulations (Figure 4.5), the carbon, phosphorus and iron uptake fluxes in the ocean surface were integrated across two nanoplankton size classes. The net carbon uptake is defined by

$$V_{C,j} = P_{C,j} - \xi \cdot V_{N,j} \tag{4.1}$$

where P_C is the gross photosynthetic rate of the population j, ξ is the biosynthesis cost, and V_N is the net nutrient uptake of the same population. The net nutrient uptake is found through

$$V_{N,j} = V_{N,j}^{max} \frac{[R_N]}{[R_N] + k_{N,j}} Q_{N,j}^{stat} \cdot \gamma T \tag{4.2}$$

where $V_{N,j}^{max}$ is the maximum uptake rate for that nutrient, R_N is the environmental resource concentration of the nutrient, $k_{N,j}$ is the half-saturation constant for the uptake rate, $Q_{N,j}$ is the satiation quota, γT is the temperature limitation factor.

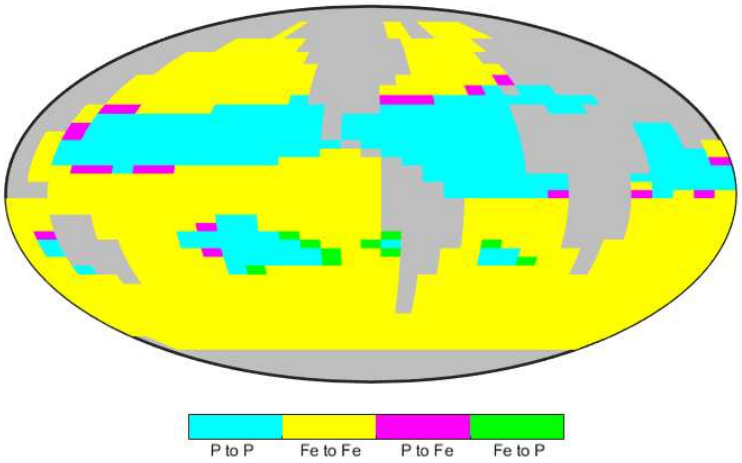

FIGURE 4.2: Nutrient limitation for nanoplankton in the two configurations. Each colour represents the identity of the most-limiting nutrient across the Two-Guild and the Mixotrophic configurations. Cyan: phosphorus limited in both configurations. Yellow: iron limited in both configurations. Magenta: phosphorus limited in the Two-Guild configuration and iron limited in the Mixotrophic configuration. Green: iron limited in the Two-Guild configuration and phosphorus limited in the Mixotrophic configuration.

To calculate the C:X uptake ratio, were X is the most-limiting nutrient between phosphorus and iron, it was necessary to identify the most limiting between these nutrients at the ocean surface in the Two-Guild model. The most limiting nutrient, in each cell of the grid, was found by comparing the biomass-weighted mean of phosphorus and iron limitation in the two nanoplankton size classes. Note that the calculation used the identity of the most-limiting nutrient from the Two-Guild model in both simulations (Figure 4.2 magenta and green squares), to avoid mismatches where the boundary between P and Fe limitation shifted between the two simulations.

From Ward and Follows (2016), this ratio is labeled the C:X uptake ratio (where X is either phosphorus or iron). The impact of mixotrophy on this ratio was obtained by dividing the C:X ratio from the Mixotrophic configuration by the C:X ratio from the Two-Guild configuration. This metric is shown in Figure 4.1b, that shows the results from Ward and Follows (2016). Values greater than one indicate regions where mixotrophy increased the amount of inorganic carbon fixed for a given amount of limiting nutrient acquired. Values less than one indicate a decline.

4.3 Results and Discussion

4.3.1 Spin up to steady state

As the goal is to asses the impact of mixotrophy in the context of long-term feedbacks between surface ecology, deep ocean biogeochemistry and ocean circulation, it is important to confirm that the simulations reach a steady state. Evidence of this is provided in Figure 4.3, where a steady state is achieved, for all variables, well before the end of the 10,000 year simulation.

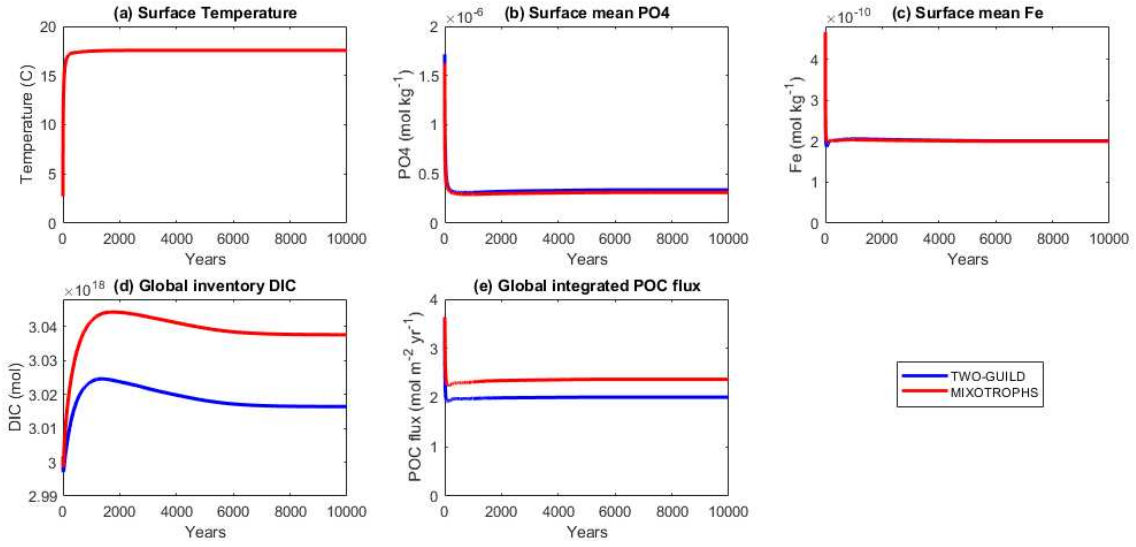

FIGURE 4.3: Behaviour of five environmental variables during the experiment. A steady state is clearly reached by the end of both simulations.

The steady state global inventory of DIC showed just a 0.7% increase from the Two-Guild to the Mixotrophic simulation (although this translates to a 0.252 gigatonnes increase in the oceanic carbon inventory in the mixotrophic simulation). The globally-integrated POC flux was 15.4% larger (0.35 mol m^{-2} $year^{-1}$) in the Mixotrophic configuration. These changes are consistent with the findings of Ward and Follows (2016), and confirm that mixotrophs can increase the strength of the BCP and the ocean's capacity to sequester carbon, even after long term feedbacks between the surface and ocean interior have been accounted for.

With the confirmation that the model reached the steady state, and that mixotrophs can increase carbon storage and export in such a system, it is possible to provide a more detailed breakdown of the simulated impacts on ecological (organism size, biomass) and biogeochemical (carbon export and inventory) factors.

In a 15 year simulation, Ward and Follows (2016) showed how average plankton size and carbon-to-limiting-nutrient uptake ratios increased in an ecosystem populated by

mixotrophs, relative to an equivalent ecosystem with a strict distinction between phytoplankton and zooplankton. The EcoGEnIE simulations over 10,000 years are broadly consistent with these ecological changes at the surface level (Figure 4.4).

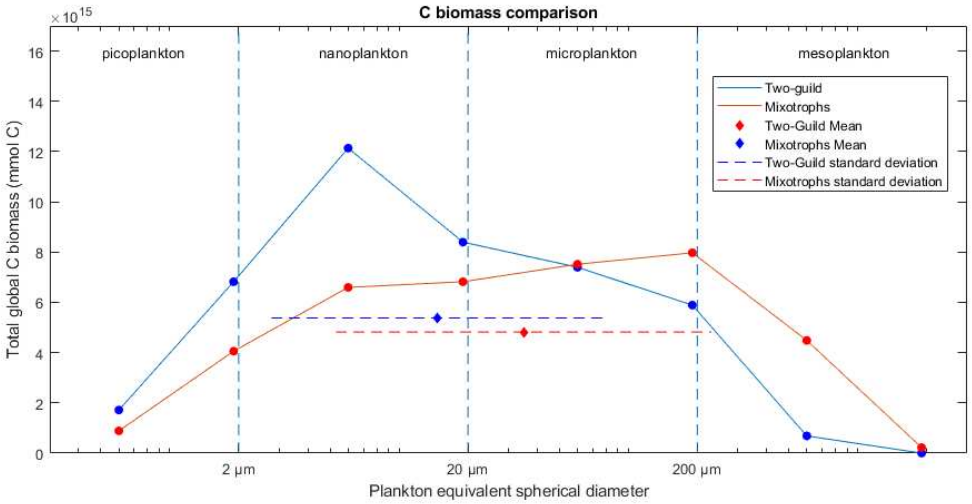

FIGURE 4.4: Biomass-weighted plankton size class distribution. Blue dots and line: Two-Guild configuration. Red dots and line: Mixotrophic configuration. Diamonds and dashed lines: biomass-weighted geometric mean and geometric standard deviation.

Figure 4.4 shows the total global carbon biomass in each EcoGEnIE plankton size class. The plot indicates, like in Figure 4.1(a), a clear increase in biomass-weighted mean plankton size in the Mixotrophic configuration. The carbon biomass-weighted geometric mean for the Two-Guild configurations is 14.66 μm ($\overset{\times}{\div}$ 5.28), while the biomass-weighted geometric mean for the Mixotrophic configuration is 34.96 μm ($\overset{\times}{\div}$ 6.58).

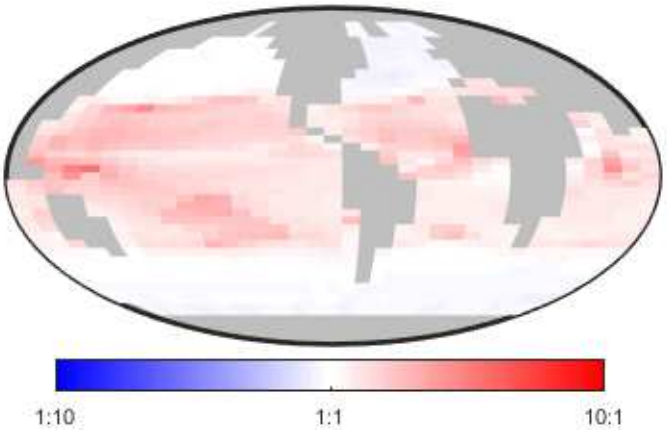

FIGURE 4.5: Relative change in nanoplankton carbon uptake to limiting nutrient uptake ratio between the Two-Guild and the Mixotrophic configuration. Blue: less carbon fixed by the Mixotrophic configuration. Red: more carbon fixed in the Mixotrophic configuration.

Figure 4.5 shows an increase in the carbon-to-limiting-nutrient uptake ratio in the lower latitudes, with no change or even a slight decline at higher latitudes. Ward and Follows (2016) likewise showed the strongest increases in this variable in the oligotrophic gyres (see Figure 4.1b). While EcoGEnIE differs from Ward and Follows (2016) in showing a weak decline in the carbon-to-limiting-nutrient uptake ratio at high latitudes, the overall trend suggests that mixotrophs can fix more carbon for the same supply of limiting nutrients, relative to phytoplankton in the Two-Guild configuration.

This section confirmed that mixotrophy allows more carbon fixation and supports an increase in global mean organism size. In the following sections, a more detailed breakdown of global scale effects of mixotrophy in the fully equilibrated system will be given.

4.3.2 Change in ecological structure and function

Table 4.1 and Figure 4.6 show, respectively, the average and the global distribution of community organism size, carbon biomass and export. In the case of size (Figure 4.6c) the switch from the Two-Guild to the Mixotrophic configuration causes an increase in all regions and latitudes. The largest increases are seen in the polar, temperate and equatorial regions, whereas the subtropical gyres and the extreme high latitudes show smaller increases. The generalized increase in size is consistent with Ward and Follows (2016), and suggests (all other things being equal) that the configuration with mixotrophs should export more carbon than the configuration with phytoplankton and zooplankton.

TABLE 4.1: Basin and latitudinal mean values. High Latitudes: 45-90°N and 45-90°S. Low Latitudes: from 45°N to 45°S

Configuration	Variable	Atlantic	Indian	Pacific	High Lat.	Low Lat.
Two-Guild	**ESD (μm)**	5.41	4.81	4.33	6.34	3.28
	C Biomass (mmol C m^{-3})	1.61	1.47	1.33	1.71	1.19
	POC (mol POC m^{-2} yr^{-1})	2.38	2.18	1.77	2.24	1.80
Mixotrophic	**ESD (μm)**	39.82	38.74	30.46	36.69	32.41
	C Biomass (mmol C m^{-3})	1.46	1.37	1.22	1.41	1.19
	POC (mol POC m^{-2} yr^{-1})	2.75	2.66	2.12	2.43	2.34
Difference	**ESD (μm)**	34.41	33.93	26.13	30.35	29.13
	C Biomass (mmol C m^{-3})	-0.15	-0.1	-0.11	-0.3	0
	POC (mol POC m^{-2} yr^{-1})	0.37	0.48	0.35	0.19	0.54

Carbon biomass (Figure 4.6f) also changes from the Two-Guild to the Mixotrophic configuration. At equatorial latitudes there is a small increase, in the subtropical regions the situation has changed very little, while in the other latitudes there is a decrease that gradually becomes more enhanced from the temperate to the polar regions.

The comparison between the two configurations, in carbon export (Figure 4.6i), shows a different outcome from size and biomass. The map shows a decrease in carbon export, in the Mixotrophic configuration, in the North Atlantic and the Southern Ocean, and an increase everywhere else. What is the cause of this trend?

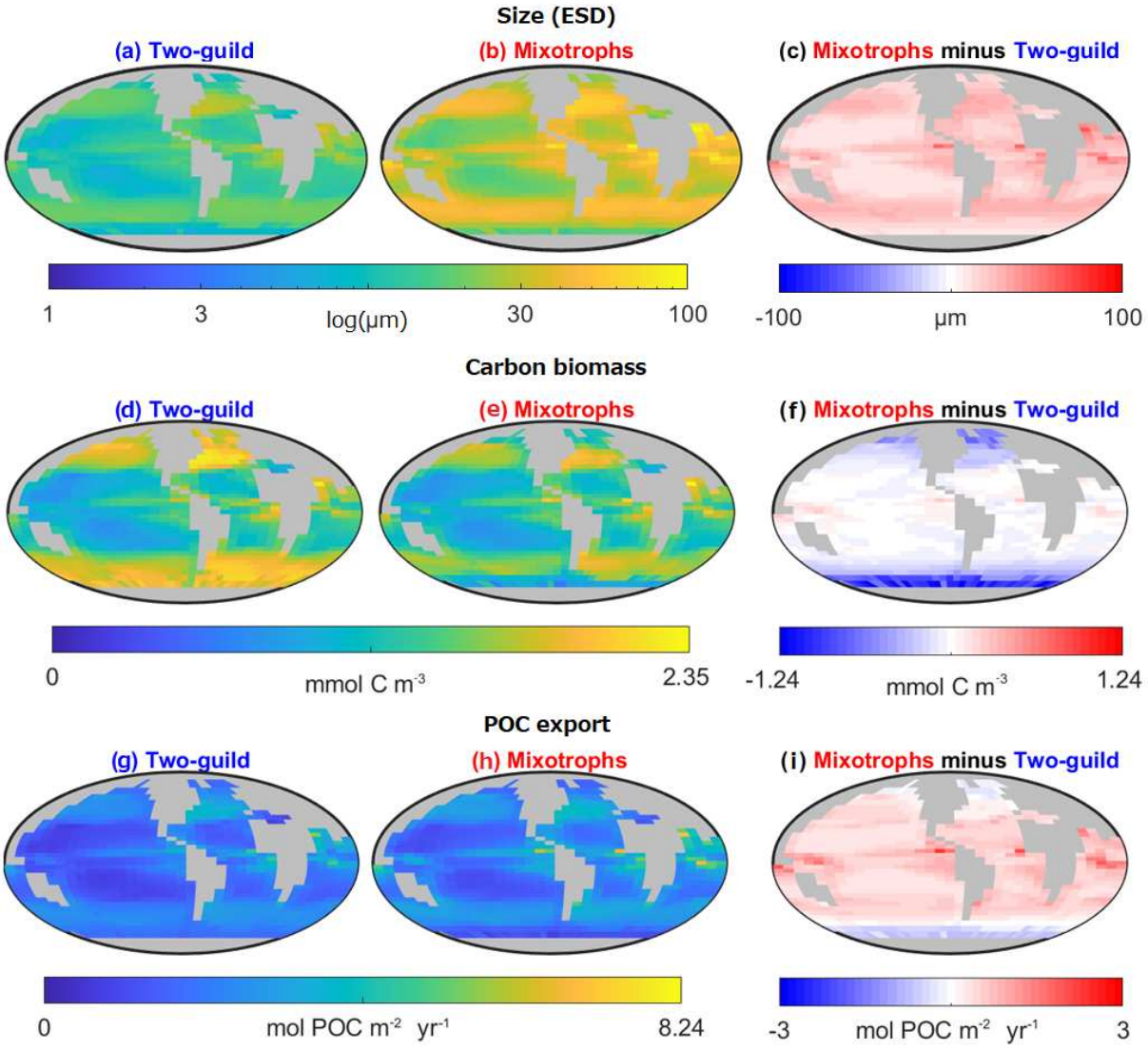

FIGURE 4.6: Geometric mean cell diameter (μm; top row), total global carbon biomass (mmol C m^{-3}; middle row) and total POC export (mol POC m^{-2} yr^{-1}; bottom row). Left hand column: Two-Guild configuration. Middle column: Mixotrophic configuration. Right hand column: difference between the two configurations, where blue means a decrease for the Mixotrophic configuration, while red means an increase for the Mixotrophic configuration.

While the changes in size are broadly consistent with the findings of Ward and Follows (2016) (i.e. increase in size due to mixotrophs trophic flexibility), the carbon export outcome is more complex to explain. The increased export at low latitudes is consistent

with the presence of mixotrophs that increase the carbon to limiting nutrient uptake ratio (Figure 4.5), the increase in size (Figure 4.6c) caused by the mixotrophic higher trophic transfer efficiency, and seemingly very little changes in carbon biomass concentration (Figure 4.6f). Additionally, in terms of the model parameterisation, the shift towards larger plankton sizes (i.e. grazers) has the implication of increasing community export through the increase of messy feeding because larger plankton produce larger amounts of uneaten biomass that in turn increases export.

However, this explanation, cannot be taken into account as showed by Figure 4.7. This picture clearly shows that despite the fact that mixotrophs increase their biomass in the larger size classes (60, 190 and 600 μm) compared to the biomass of zooplankton of the same size (Figure 4.7a, b), the mixotrophic predation rate, and the consequent sloppy feeding, is lower than the zooplankton predation rate (Figure 4.7c, d). The 60, 190 and 600 μm size classes are important because the maximum messy feeding production rate is reached in the larger size classes. This difference in the predation rate between the two configuration is due to the fact that large mixotrophs can rely also on photosynthesis, which decreases their heterotrophic feeding needs, and thus messy feeding production.

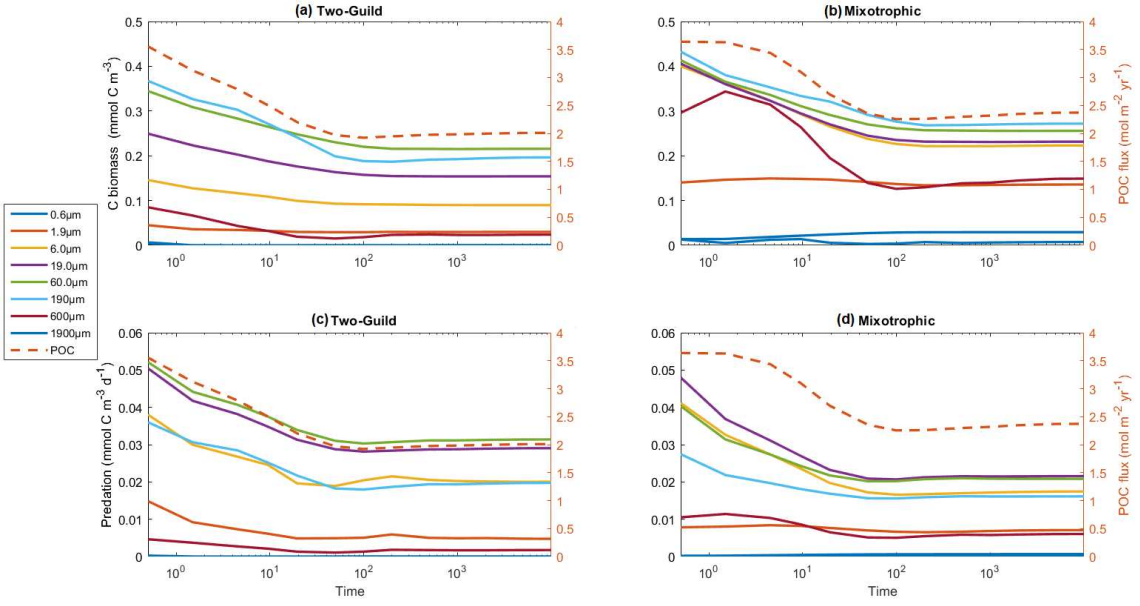

FIGURE 4.7: Comparison between zooplankton and potential mixotrophs carbon biomass and predation rate in the two configurations (left hand axis). POC export rate measured on the right hand axis.

The high latitudes show that the carbon to limiting nutrient uptake ratio (Figure 4.5) changes very little, size (Figure 4.6c) increases, while biomass (Figure 4.6f) decreases. The final outcome for carbon export (Figure 4.6i) is a decrease for the mixotrophic configuration, not an increase as it would have been expected by the increase in size, which was possibly offset by the decrease in biomass.

Figure 4.8 gives a further evidence of why carbon export does not increase at high latitudes. This picture reveals that the largest differences in size-fractionated biomass between the two configurations are concentrated in the nanoplankton size class (b). Very high levels of nanoplankton that occur at high latitudes in the Two-Guild configuration are notably absent from the Mixotrophic configuration. Nanoplankton are among the fastest growing primary producers, thus, since fast growing size classes dominate blooms, do mixotrophs decrease nanoplankton biomass through a bloom-related effect? An example to illustrate this case, is provided for the North Atlantic in the following section.

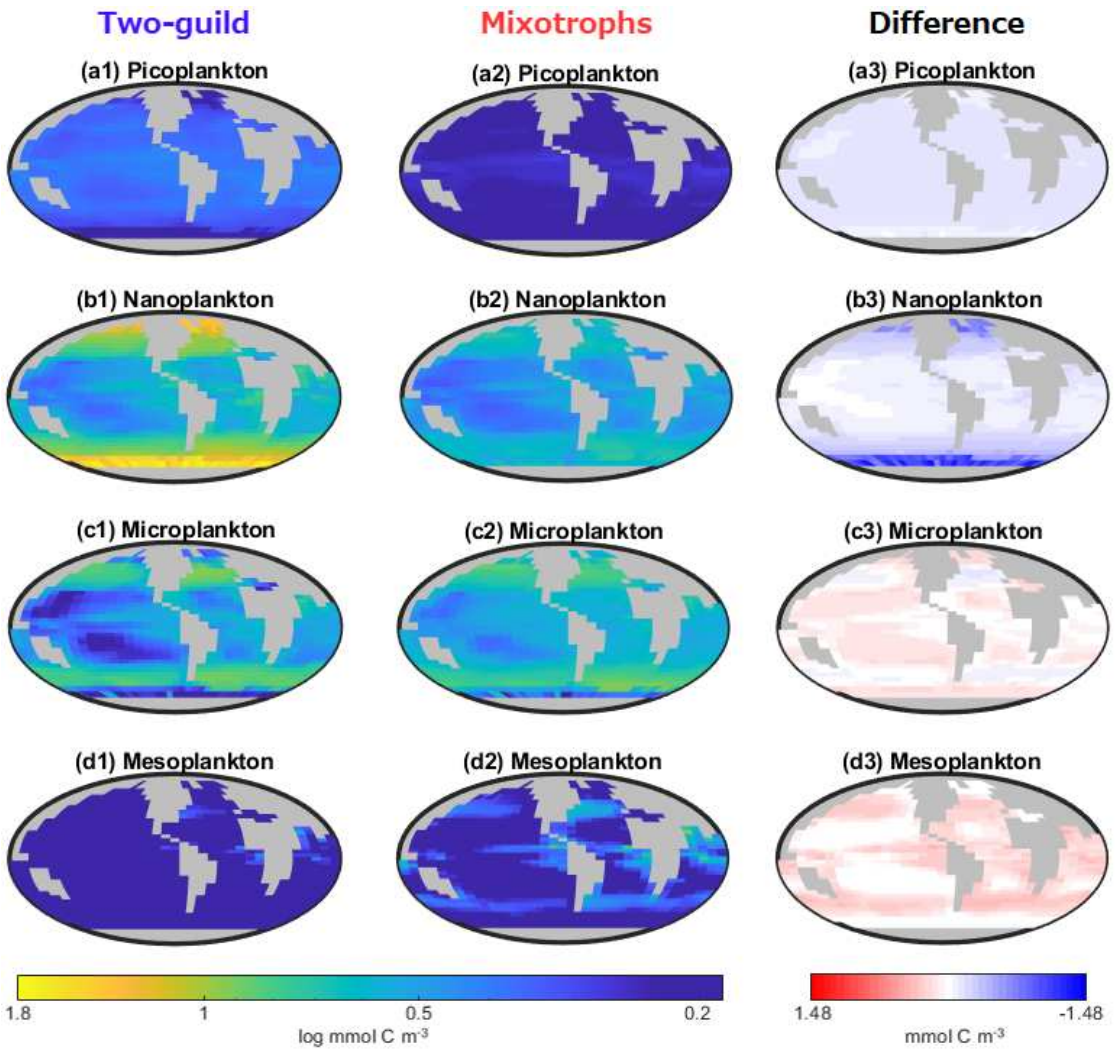

FIGURE 4.8: Total global carbon biomass for each integrated size class (log mmol C m^{-3}). **(a)** Picoplankton, **(b)** Nanoplankton **(c)** Microplankton and **(d)** Mesoplankton. **(1)** Two-Guild configuration, **(2)** Mixotrophic configuration and **(3)** difference between the two configurations. Blue: less carbon biomass in the Mixotrophic configuration. Red: more carbon biomass in the Mixotrophic configuration.

4.3.3 Decline in high latitude carbon biomass and export production

Seasonal changes in the North Atlantic are the key to understand why nanoplankton biomass and carbon export are suppressed at high latitudes in the Mixotrophic simulation. Figure 4.9 explores what happens at the North Atlantic Bloom Experiment (NABE) station (47°N -19°E) in the fully spun-up model. The black dots represent the observations in chlorophyll concentration (a) and primary production (c). The bloom occurs earlier than is observed, and it does not reach the same peak chlorophyll concentration.

This mismatch could be due to the low resolution of the model, where a single location is represented by an entire cell of the grid, and to the rapid changes of temperature and mixed layer depth that can happen in a single location, but not in the very coarse resolution model. Another possible cause is the lack, in the model, of explicitly resolving diatoms, which are the dominating taxa in the early spring blooms of the North Atlantic (Lochte et al., 1993). This absence could explain why the intensity of the simulated bloom do not reaches the same intensity of the observations.

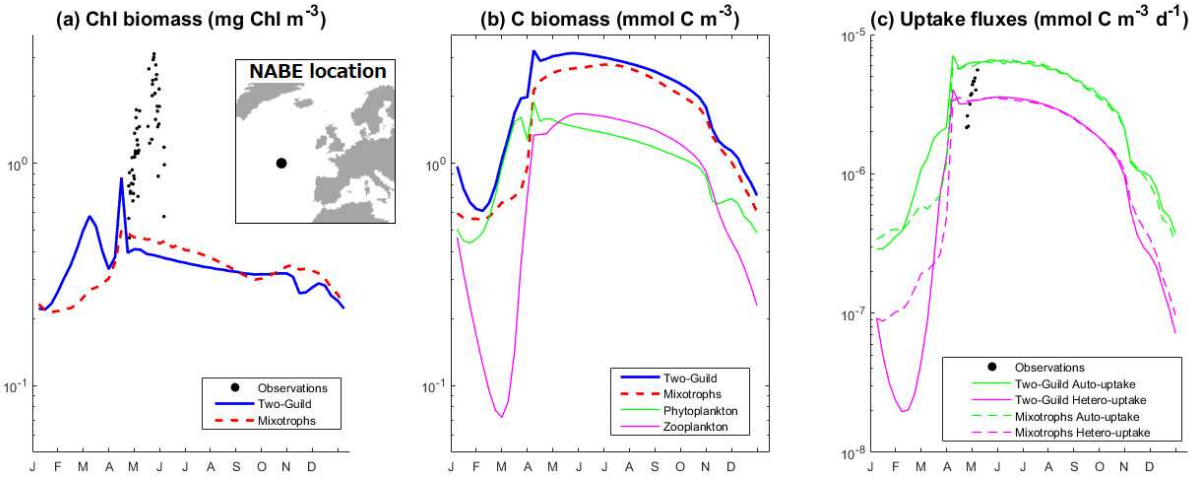

FIGURE 4.9: Carbon biomass and uptake flux in the last year of the simulation at NABE station. **(a)** Total chlorophyll biomass (mg Chl m^{-3}) **(b)** Total carbon biomass (mmol C m^{-3}). **(c)** Uptake carbon fluxes (mmol C m^{-3} d^{-1}). Black dots: observations from Kleypas (2001).

Figure 4.9 breaks down a typical high latitude plankton spring bloom. The main features here are the winter decrease in carbon biomass and the exponential growth in spring. Figure 4.9(a) shows the seasonal cycle of chlorophyll in the two simulations, and how these compare to the observations. Figure 4.9(b) shows the seasonal cycles of carbon biomass, and underlines that carbon biomass is always lower in the Mixotrophic configuration relative to the Two-Guild configuration. This difference in average quantity of

carbon biomass is consistent with the lower plankton biomass seen in the high latitudes of Figure 4.9(b), but what is the underlying cause of this difference?

Figure 4.9(b) shows that zooplankton carbon biomass in the Two-Guild simulation declines to very low levels throughout the winter. Deep winter mixing increases the mixed layer depth, such that the plankton community experiences lower average irradiance. In the Two-Guild configuration these environmental changes inhibit the growth of phytoplankton and they decline in biomass. As a consequence, zooplankton are deprived of their prey and their biomasses also decline.

At the end of winter, surface warming increases stratification and light levels increase within shallower mixed layers, allowing phytoplankton to grow exponentially. In the Two-Guild simulation, the crash of the zooplankton population over winter allows phytoplankton growth to continue unchecked by zooplankton top-down control (Tagliabue and Arrigo, 2003; Irigoien et al., 2005). Only in the late spring is this bloom finally suppressed by nutrient limitation (or by the lagging zooplankton populations).

The Mixotrophic configuration experiences the same shift in environmental conditions, however the outcome is very different. In winter, photosynthesis (Figure 4.9c, dashed lines) and biomass (Figure 4.9b dashed line) decreases, however, this time there is no decoupling between the phototrophic and heterotrophic communities. Figure 4.9(c) confirms that mixotrophs' trophic flexibility allows grazing (dashed magenta line) to decrease less than zooplankton grazing (dashed continuous line), over the winter, thus the bloom is rapidly suppressed by top-down control in spring.

Mixotrophs' ability to switch between different sources of nutrition is the reason of their success during winter, which in turn suppresses the bloom through a higher coupling between photosynthesis and grazing in the Mixotrophic simulation.

The Continuous Plankton Recorder (CPR) in the North Atlantic shows that mixotrophic dinoflagellates are typical of this region, and their average abundance peaks in August, after the end of the phytoplankton bloom (Barton et al., 2013). In a numerical experiment, Hammer and Pitchford (2005) showed that the addition of mixotrophs in a model, completely suppress the community bloom, while Wilken et al. (2014), with a chemostat experiment, suggested that mixotrophs can control cyanobacteria toxic blooms at low nutrient concentration. Likewise, the results presented in this chapter show that mixotrophic bloom suppression can also be a plausible mechanism in high-latitude spring blooms. Additionally, such suppression in the surface waters of the high latitudes, if repeated annually for a multi-millennial timescale, can potentially influence carbon storage in the ocean basin. This is explored in the next section.

4.3.4 Biogeochemical impacts of mixotrophy on the ocean interior

Ward and Follows (2016) used a global simulation to look at the carbon fluxes across the first 200 m of the water column. Further depths were beyond their initial scope because the high resolution of the system limited the simulations to no more than 15 years. Thanks to the low resolution chosen for this experiment, it was possible to describe the impact of mixotrophs, on carbon biogeochemistry, on a 10,000 year-long time scale, which affects the whole water column from surface to bottom.

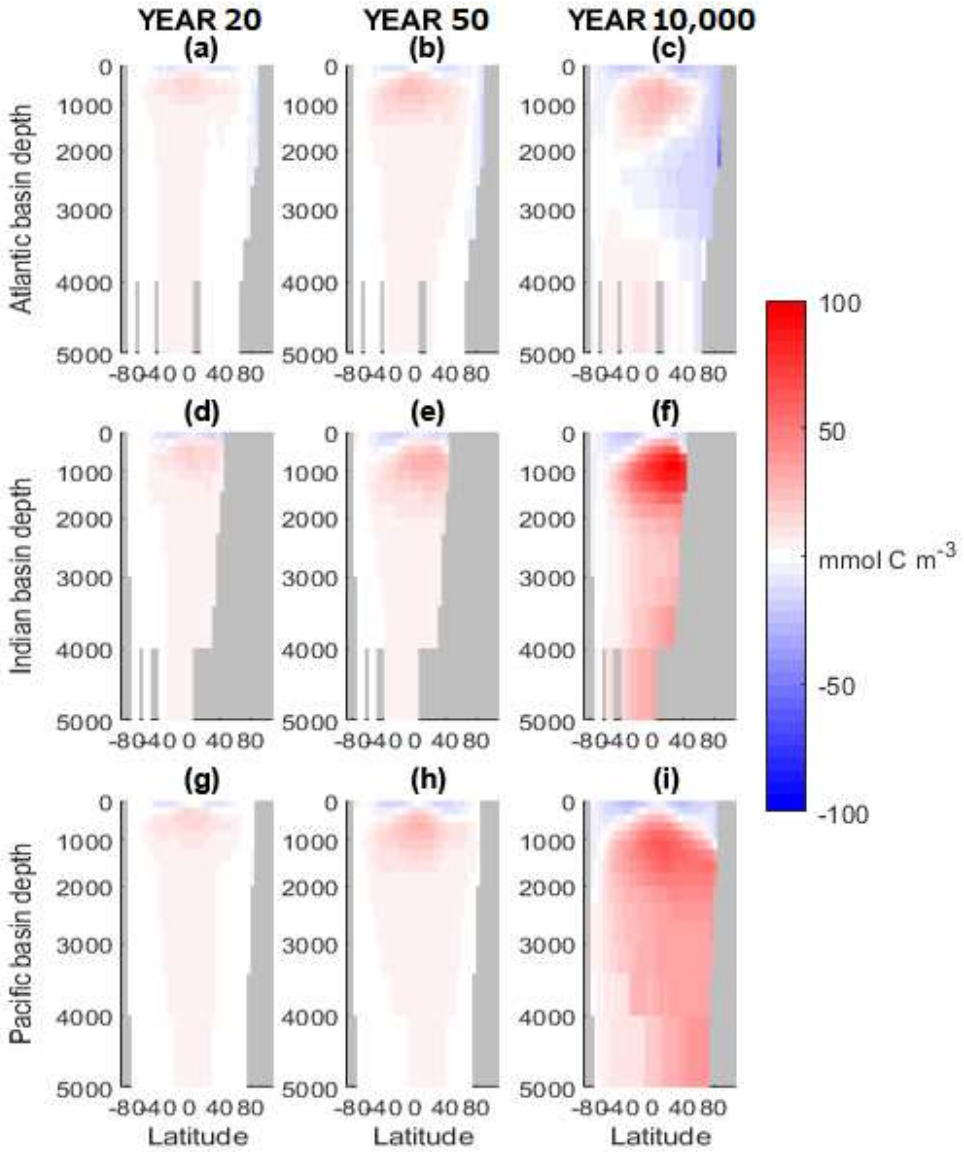

FIGURE 4.10: Time series of the difference of the meridional averaged DIC concentration in the two configurations. **(a, b, c)** Atlantic basin, **(d, e, f)** Indian basin and **(g, h, i)** Pacific basin. Blue: less DIC stored in the Mixotrophic configurations. Red: more DIC stored in the Mixotrophic configuration.

Figure 4.10 shows changes in carbon storage (DIC concentration) in the different ocean

basins between the two configurations. Only years 20, 50 and 10,000 are shown. The Indian Ocean shows the highest localised increases in stored DIC when mixotrophy is included, especially in low latitude waters at around 1,000 meters depth. The Pacific Ocean shows a similar response, but localised increases in stored DIC attributable to mixotrophy are lower. It is important to underline that the Pacific Ocean shows a higher increase in DIC inventory compared to the Indian Ocean due to their difference in size. The response in these two basins is what we would expect from the conclusions of Ward and Follows (2016), inasmuch as mixotrophy causes an increase in sequestered carbon.

The Atlantic Ocean shows a more complex pattern. With the inclusion of mixotrophy, carbon storage does increase in the low-latitude mesopelagic, but there is also a strong decrease in the waters descending from the North Atlantic into the ocean interior (i.e the North Atlantic Deep Water - NADW). The three columns in Figure 4.10 show that this decline in sequestration only occurs much later in the simulation, and is attributable to the ventilation of the ocean interior by waters formed in the North Atlantic.

The suppression of the bloom caused by mixotrophs, decreases at surface level the amount of DIC stored by the waters. This decrease is expanded at depth and in the low latitudes with the action of the NADW.

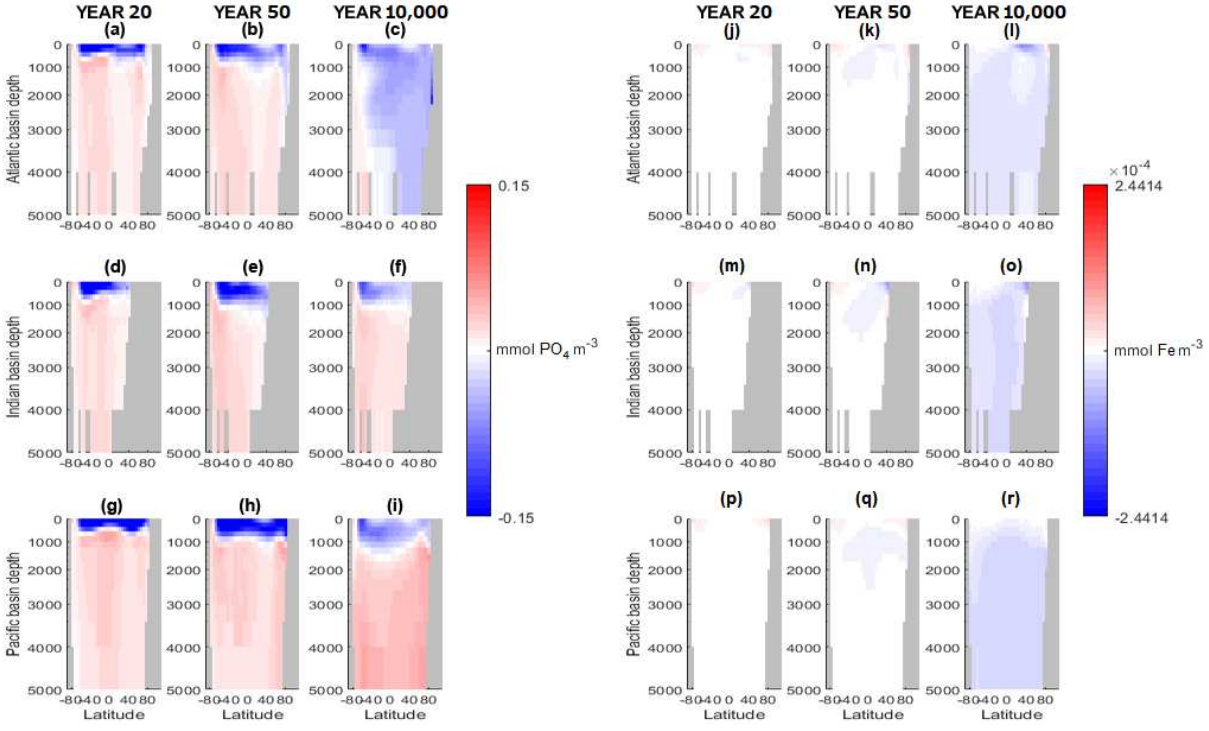

FIGURE 4.11: Time series of the difference of the meridional averaged PO_4 (a to i) and Fe (j to r) concentration in the two configurations. First row: Atlantic basin. Second row: India basin. Third row: Pacific basin. Blue: less PO_4 and Fe stored in the Mixotrophic configurations. Red: more PO_4 or Fe stored in the Mixotrophic configuration.

The nutrient concentration at basin level confirms the trend already seen in the DIC distribution (Figure 4.11). At depth (>500 m), PO_4 goes from having a higher concentration in the Mixotrophic configuration, compared to the Two-Guild configuration, in the first 50 years of the experiment. At year 50, in the Norther North Atlantic, it is already possible to see a decrease in concentration, which is fully expanded, at basin level, at year 10.000. This nutrient is clearly taken up and moved toward the bottom together with the DIC, however, since PO_4 is a limiting nutrient, mixotrophs deplete the inventory of the basin at surface more than the specialists. For the same reason, phosphate is low at surface level in the two other basins, while in the aphotic zone inventory, phosphate has a higher concentration in the Mixotrophic configuration. Kriest et al. (2012) also noted that particle flux is the dominant force that controls the phosphate gradient between North Pacific and North Atlantic.

Since iron mostly reaches the surface through wind deposition, and not through upwelling, and since it is another limiting nutrient, its concentration is lower in the Mixotrophic configuration throughout the basins. This difference is explained by the higher efficiency of mixotrophs to filter this element once it reaches the surface, if compared to the specialists of the Two-Guild.

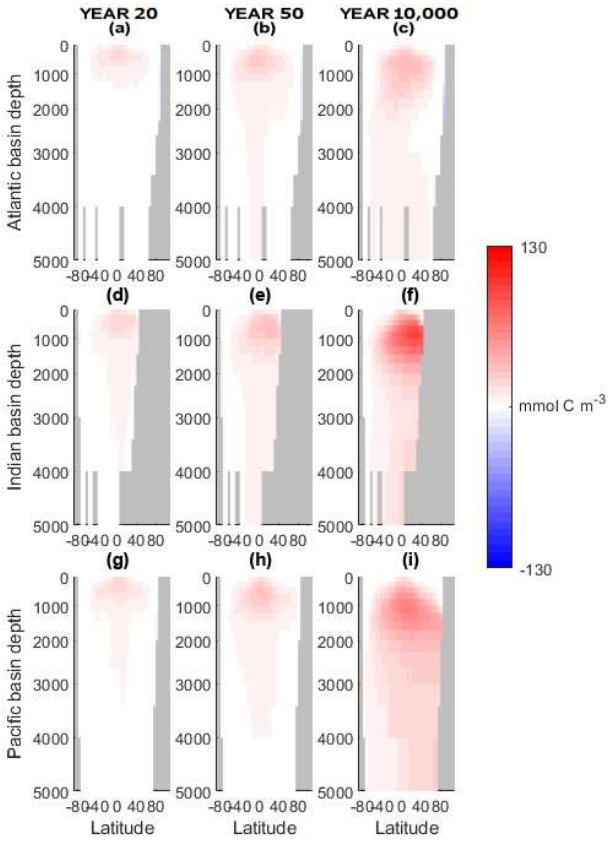

FIGURE 4.12: Time series of the difference of the meridional averaged organic carbon concentration in the two configurations. **(a, b, c)** Atlantic basin, **(d, e, f)** Indian basin and **(g, h, i)** Pacific basin. Blue: less organic carbon stored in the Mixotrophic configurations. Red: more organic carbon stored in the Mixotrophic configuration.

With EcoGEnIE it is also possible to simulate the organic carbon produced by plankton. Figure 4.12 shows how this carbon redistributes at basin level and the capacity of mixotrophs to increase carbon export at low latitudes. However, the higher latitudinal regions stay largely unchanged.

The simulations presented above agree with the conclusions of Ward and Follows (2016) on short timescales. Mixotrophs increase the global carbon inventory, but there is a clear exception where suppression of spring bloom by mixotrophs causes a decrease in the quantity of carbon exported at surface. This decline is propagated into the ocean interior over long timescales by the descending tongue of NADW. This decrease in DIC storage can be seen only in the 100-10,000 years timescale, which was precluded in the original simulations made by Ward and Follows (2016).

4.3.5 Comparison with Ward and Follows (2016)

By running the 10.000 year-long simulations for only 15 years, it was possible to obtain results analogue to the results from Ward and Follows (2016) (Figure 4.13). This further set of simulations showed how the long-term experiments enhanced the previous results.

Size does not change very much between year 15 and year 10.000 with the Two-Guild configuration (Figure 4.13a). The Mixotrophic configuration, instead, shows a net decrease in the low latitudes and a net increase in the high latitudes (Figure 4.13b). Size instead changes with both configurations, and generally decreases by going from year 10.000 to year 15 except for the Southern Ocean (Figure 4.13d, e). The same pattern is very similar for export production except for the North Atlantic and the coastal equatorial latitudes where export at year 10.000 is larger than the year 15 (Figure 4.13g, h).

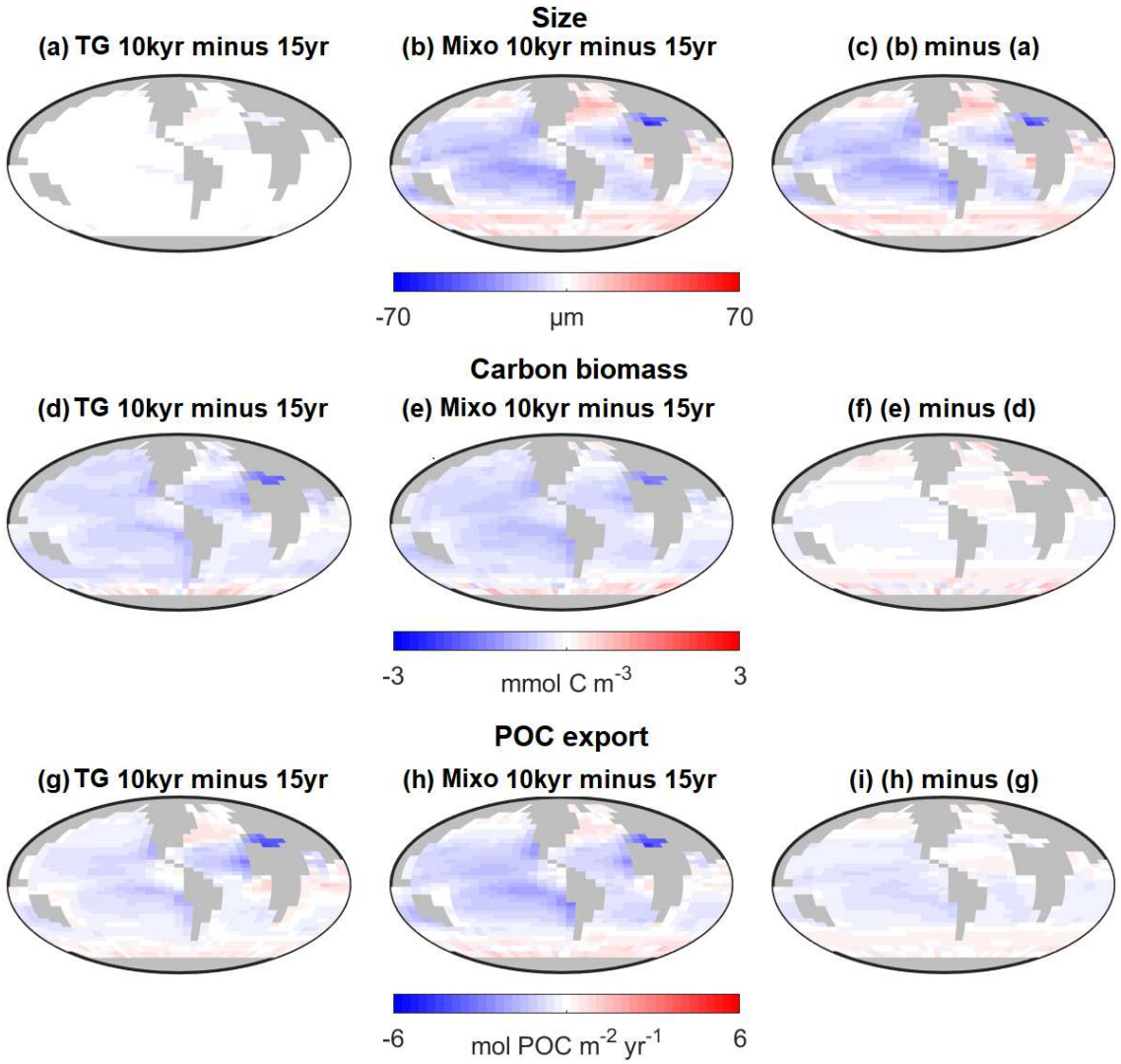

FIGURE 4.13: Difference in geometric mean cell diameter (μm; top row), total global carbon biomass (mmol C m^{-3}; middle row) and total POC export (mol POC m^{-2} yr^{-1}; bottom row) between a 10.000 year and a 15 year simulation. Left hand column: Two-Guild configuration. Middle column: Mixotrophic configuration. Right hand column: difference between the two configurations, where blue means a decrease for the Mixotrophic configuration, while red means an increase for the Mixotrophic configuration.

The final difference between Mixotrophic and Two-Guild configuration highlights a decrease at low latitudes and an increase at high latitudes for the three variables (Figure 4.13c, f and i). The only exception, in the comparison, was in the low latitudinal Atlantic Ocean that presents a slight increase. These maps clearly show how the long-term experiments was necessary to allow the full development of the plankton populations and how mixotrophs have a differential play a role in this process.

4.3.6 Sensitivity to the trophic trade-off

The mixotrophic simulations presented above assume that mixotrophs incur no physiological penalty for combining autotrophic and heterotrophic traits. In this section the Mixotrophic-Plus configuration is used to explore how potential trade-offs between trophic strategies might impact the main findings described above.

Figure 4.14 shows results from the Mixotrophic-Plus simulation, where mixotrophs were allowed to compete with specialist phytoplankton and zooplankton in each size class. Simulations were performed where the mixotrophs were assigned traits equivalent to 40, 50, 60 and 100% of the equivalent specialist values. As expected, the magnitude of the impact of mixotrophy on organism size and carbon export decreased (from 29.93 to 3.14 μm and from 0.36 to 0.03 mol m^{-2} $year^{-1}$) when mixotrophs were subject to a stronger physiological cost. In general, the simulations revealed that a weaker (i.e. more superlinear) trade-off made positive differences more positive (e.g. export production at low latitudes and organism size), and made negative differences more negative (e.g. export production at high latitudes). This pattern confirms that the results presented until now constitute only an upper limit, and the influence of the mixotrophic physiology on the carbon cycle depends on the shape of the trophic trade-off. Chapter 6 will further explore the physio-ecology of mixotrophs, in a similar way, in a climate change scenario, showing comparable results.

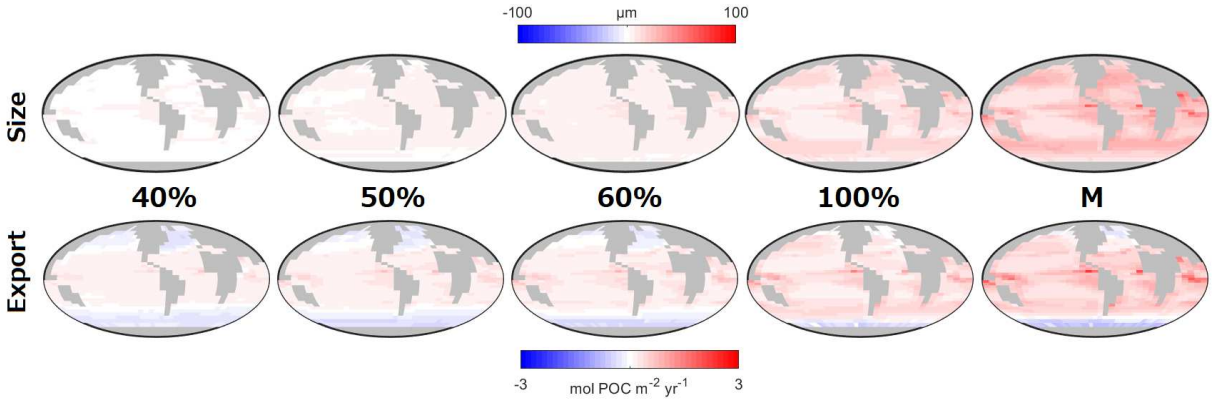

FIGURE 4.14: Impact of the trophic trade-off on size and export. The maps are the difference between the Mixotrophic configurations and the Two-Guild configuration. The percentage refers to the trait of the specialists in the Mixotrophic-Plus configuration. "M" refers to the Mixotrophic configuration used in this chapter, and which results correspond to Figure 4.6(c, i).

The Mixotrophic configuration has a higher increase in size and export than the Mixotrophic-Plus configuration because of the Active Switching turned on (read the Appendix A). This setting allowed to less competitive species to survive, and since in the Mixotrophic configuration there are only 8 populations compared to the 24 of the Mixotrophic-Plus

configuration, the Mixotrophic-Plus configuration had more small phytoplankton populations that survived than the Mixotrophic configuration. This difference implies a higher degree of decrease in nutrient concentration in the Mixotrophic-Plus configuration, which causes plankton populations to become, on average smaller, and thus causing less carbon export.

4.4 Conclusions

Over long timescales EcoGEnIE showed a similar response to the model of Ward and Follows (2016) at low latitudes. The model showed that mixotrophs increase the C:X uptake ratio, which together with the increase in organism size, increased export. However the high latitudes showed a different, more complex response.

The EcoGEnIE simulations showed that mixotrophy can suppress high latitude phytoplankton blooms because there is a tighter coupling between the phototrophic bloom and top-down grazer control. This coupling leads to a decrease in carbon export at high latitudes, which impacts the interior DIC inventory over long timescales, as the decreased export is propagated to lower latitudes via NADW subduction. The short integration time (decades) of the model used by Ward and Follows (2016) was not suited to identify this long-term accumulation of carbon caused by phytoplankton-zooplankton blooms repeated for centuries. This phenomenon was showed to be relevant when compared to the outcome of the simulation with the Mixotrophic configuration.

These results must be interpreted in light of the fact that the standard Mixotrophic configuration did not resolve any trade-offs that might be associated with mixotrophic physiology. With the Mixotorphic-Plus configuration, however, it was possible to investigate the impact of the trophic trade-off. Since a sublinear trade-off was established in Chapter 2 as the most likely shape of the mixotrophic compromise between autotrophic and heterotrophic way of feeding, the magnitude of the simulated impacts will likely be lower than the results of this chapter and the initial simulation proposed by Ward and Follows (2016).

Chapter 5

The impacts of anthropogenic climate change on a simulated global plankton community

5.1 Introduction

Climate changes will affect different aspects of the marine environment, with increased surface temperatures, increased stratification and decreased vertical mixing (Manabe et al., 1991; Steinacher et al., 2010; Tyrrell, 2011). An increase in the water column stratification will trap plankton closer to surface, exposing them to higher temperatures and irradiance, but also to less nutrients supplied by upwelling. Such a change in environmental condition, will likely impact productivity and community structure, which will impact in turn fisheries. Plankton communities play a key role in the global carbon cycle as their sinking sequesters 9-10 PG per year (Sigman and Haug, 2003; DeVries and Weber, 2017) amounts of carbon in the deep ocean away from the atmosphere (the BCP; Hain et al., 2014). Given the low confidence in understanding how the BCP will change - due to complex interactions among temperature, nutrient availability, and ocean circulation patterns influenced by climate change itself, the lack of data and modelling limitations - the magnitude and direction of the ocean carbon feedback remain uncertain (IPCC, 2023). Consequently, climate change could, potentially, create a negative feedback loop with the BCP.

Computer simulations, such as Earth System Models, are often used to assess the impacts of climate change on the oceans. For example, Bopp et al. (2001) studied export production while Sarmiento et al. (2004) studied primary production in a warmer 21^{st} century. These studies were made through coupled atmosphere-ocean models, which were then followed by the use of multiple NPZD and PFT models in the same experimental setting (Steinacher et al., 2010; Cabré et al., 2015; Fu et al., 2016). The general

result of the simulations that explicitly resolved biology in their setting was a net global decrease in primary and export production (global net decrease up to 20% according to Steinacher et al., 2010).

However, as explained in Chapter 1, many of these simulations come from models (NPZD and PFT) that include only a very limited representation of plankton diversity (le Quéré et al., 2005; Heinze and Ilyina, 2015; Hendry et al., 2018), and as such, are unable to inform us about how community size structure and the balance of trophic strategies might change in a future warmer world. It was found, that plankton traits, such as size, directly impact marine elemental cycles (Ward and Follows, 2016), even in an analogue scenario of climate changes (Wilson et al., 2018).

In this chapter, a global size-structured model (Ward et al., 2018) is applied to study how plankton community structure and carbon export might change under a scenario of extreme global warming. With EcoGEnIE it is possible to simulate a global ecosystem populated by phytoplankton and zooplankton populations with different sizes. This model setting will resolve the links between plankton community structure and key ecosystem functions including the vertical export of organic carbon (i.e. the BCP).

The questions that will be answered in this study will be: how will anthropogenic climate changes influence the size structure and function of marine plankton communities? And, conversely, how will these structural changes impact biogeochemical cycles and climate? After finding an answer to these questions, the results produced by EcoGEnIE will be compared with the results coming from literature.

In the following chapter, building on the results of this chapter, mixotrophic populations will be added to the same experimental setting and these results will be compared to find the impact of mixotrophy in a future warmer world.

5.2 Methods

The EcoGEnIE model allows the global simulation of a size-structured plankton community. This simulation resolves the oceanic biogeochemical cycles of carbon, phosphorus and iron. These elements are circulated across a 36 × 36 surface grid, with each compartment containing a local plankton community.

In this chapter, the global plankton community includes a total of 16 different plankton populations, consisting of eight phytoplankton and eight zooplankton size classes. Eight size classes were selected as a compromise between size class resolution and computational expense (1.000 years with 8 size classes run for 6 hours, while 16 size classes run for 8 hours, achieving 10.000 year in 2.5 and 3.3 days respectively). Phytoplankton can grow only through photosynthesis and the uptake of inorganic elements, while zooplankton can grow only by grazing on other plankton. As explained in Chapter 3, the

DOM/POM production ratio strongly depends on size (4:1, 1:1 and 2:3 going from the smallest, to the intermediate, and to the largest size classes respectively; Ward et al., 2018).

TABLE 5.1: List of the scenarios.

Scenario	Begin	End	Duration	Begin [CO_2]	End [CO_2]
Pre-industrial	/////	/////	10,000 years	277 ppm	277 ppm
Historical transient	1765	2010	245 years	277 ppm	388 ppm
Control	2010	2100	90 years	388 ppm	388 ppm
RCP8.5	2010	2100	90 years	388 ppm	936 ppm

This chapter examined the behaviour of the model under two scenarios: a "Control" scenario where the atmospheric CO_2 concentration was held constant at 2010 levels (388 ppm) for the remainder of the 21^{st} century, and an "RCP8.5" Representative Concentration Pathway 8.5 (Pachauri et al., 2014) scenario, where atmospheric CO_2 concentration was steadily increased to 936 ppm by 2100. These two simulations were initialised from a steady state achieved after a simulation of 10,000 years (see Chapter 4) and that was extended from the year 1765 to 2010 based on historical atmospheric CO_2 concentrations. More details of the model spin up and historical transient are provided in Chapter 3.

In the following, the simulated 2010 ecosystem is compared with observations to asses the validity of the model. Subsequently, the simulated impacts of climate change at 2100 were evaluated as the difference between the experimental RCP8.5 and the Control scenarios at 2100. It is worth nothing that, usually, a time series involving globally integrated quantities is smoothed with annual averages. GEnIE, lacking this specific capability, uses a decadal average from 2090 to 2100.

5.3 Results

5.3.1 Observations versus simulations

Figure 5.1 compares model output at the end of the simulated historical transient (2010) with contemporary observations of surface phosphate (Garcia et al., 2010) and chlorophyll (SeaWiFS) concentrations (Conkright et al., 2002; Kleypas, 2001). Figure 5.1(b) shows the difference between the simulated and observed phosphorus concentrations. Modelled surface phosphate is generally lower than observations, especially in the equatorial coasts, the North Pacific and the Southern Ocean. The only exception is a slight overestimation of PO_4 in the North Atlantic. Figure 5.1(d) shows the difference between the simulated and observed surface chlorophyll biomass (Kleypas, 2001). The model overestimates chlorophyll levels at high latitudes, and makes some large underestimations in equatorial latitudes and coastal regions.

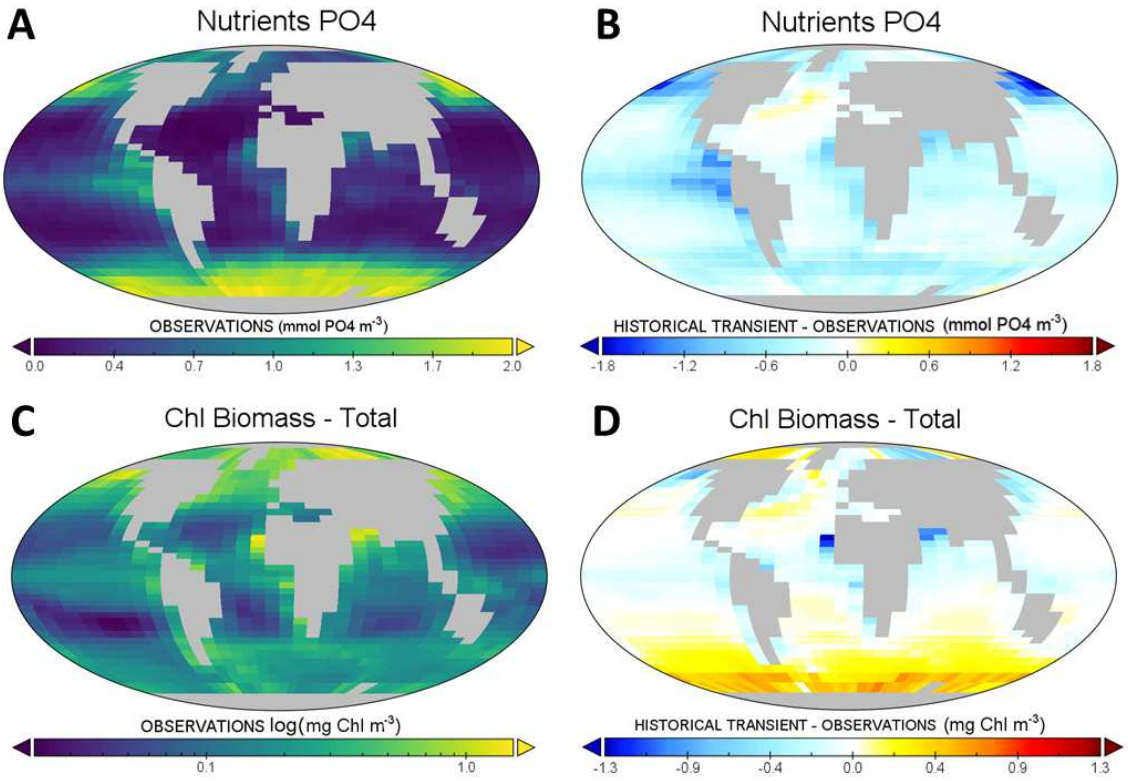

FIGURE 5.1: Phosphorus (mmol P m^{-3}) **(a, b)** and chlorophyll (mg Chl m^{-3}) **(c, d)**. **(a, c)** Observed concentrations. **(b, d)** Simulation at year 2010 minus observations.

Some of the model biases at low latitudes are attributable to a weak upwelling, due to the physic parameterisation of the GENIE framework (Marsh et al., 2011), that causes a decrease in the supply of phosphorus to the surface layer (Figure 5.1a). Other differences can be related to the coarse vertical resolution of the model grid. The model surface layer stretches from 0 to 80.8 m deep, and so the observed fields include observations within this depth range. This may introduce errors where the true surface layer is shallower, and the surface estimates therefore include values from below the mixed layer (leading to higher values of PO_4 or lower values of chlorophyll). The chlorophyll overestimation, in the Southern Ocean, could also be partly due to unrealistically low satellite observations in that region (Dierssen, 2010).

5.3.2 RCP8.5 scenario versus Control scenario

Ocean-atmosphere physics and nutrient concentration

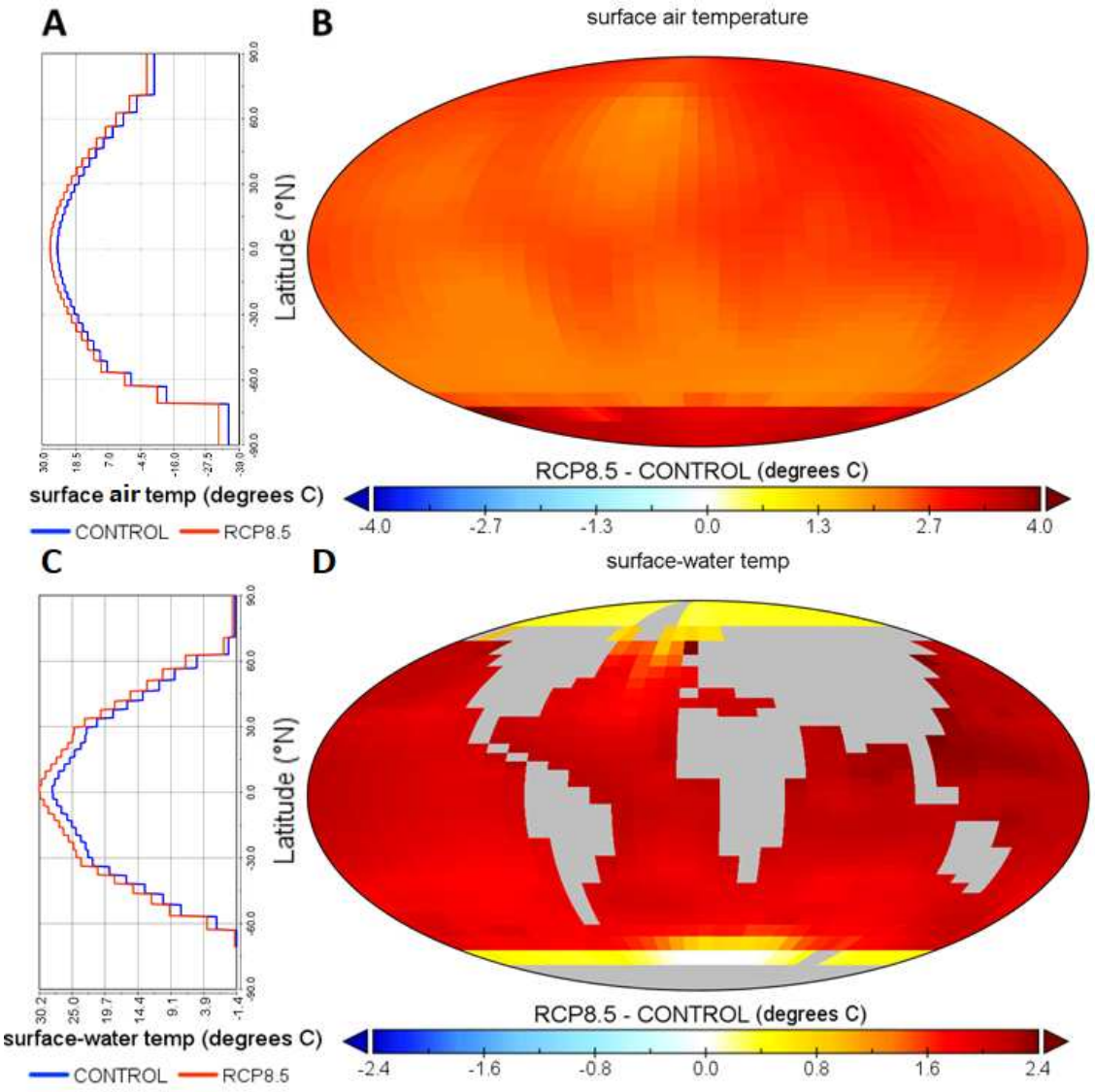

FIGURE 5.2: SST (°C). **(a, c)** Zonal average surface air temperature and SST for the Control (blue line) and RCP8.5 (red line) simulations. **(b, d)** Global distribution of surface air temperature and SST differences between the RCP8.5 and Control scenario.

Figure 5.2 shows that the RCP8.5 scenario caused a general rise of the global surface air and sea-surface temperatures (SST), relative to the Control. This increase was caused by the rise of CO_2 concentrations in the atmosphere (from 388 to 936 ppm) and the associated strengthening of the greenhouse effect. SST in Figure 5.2(d) rises more at lower latitudes (< 60°C), even though the air temperatures increase more at high latitudes in Figure 5.2(b). This reversal is attributable to the fact that, in the model (as

well in the ocean), SST cannot fall below -2°C, and thus water temperature is unaffected by changes in polar air temperatures that ranges between -30° and 0°C between winter and summer.

As a consequence of the rise in SST (Tyrrell, 2011), ocean stratification also increased under RCP8.5, with a significant shoaling of the mixed layer depth (MLD) (Figure 5.3). This change is largest in the North Atlantic and the Southern Ocean. Figure 5.3(a) shows the zonally-averaged profile of the MLD, which was always shallower under RCP8.5 relative to the Control scenario.

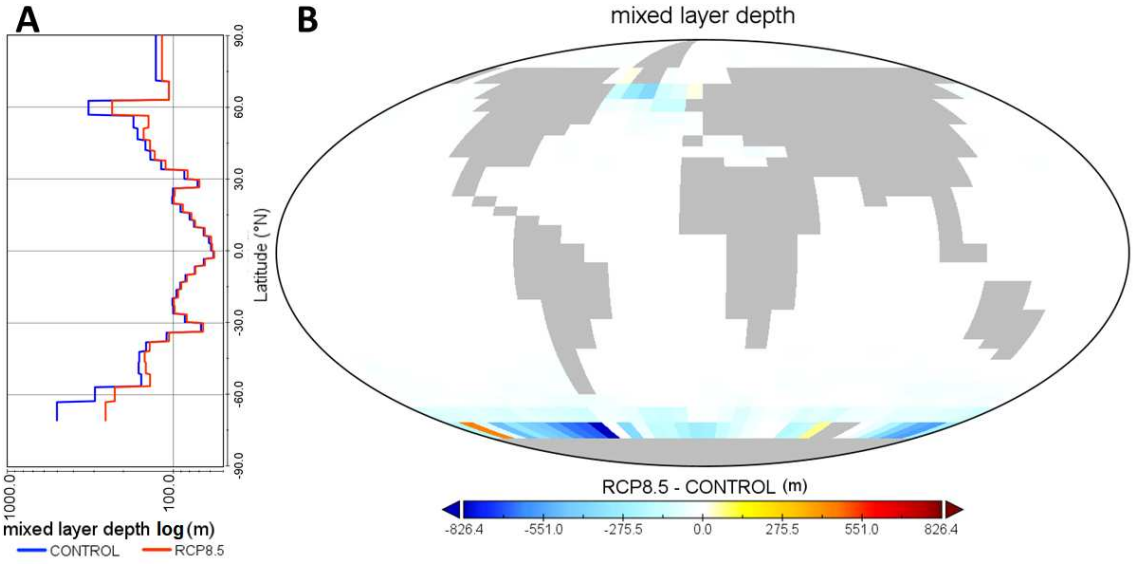

FIGURE 5.3: Mixed Layer Depth (m). **(a)** Zonal average MLD for the Control (blue line) and RCP8.5 (red line) simulations. **(b)** Global distribution of MLD differences between the RCP8.5 and Control scenario.

Figure 5.4 and 5.5 present changes in sea surface nutrient concentrations associated with RCP8.5. Figure 5.4a shows a decline in phosphorus concentration at all latitudes under RCP8.5. The maximum decrease was reached in the North Atlantic and the Southern Ocean (Figure 5.4b).

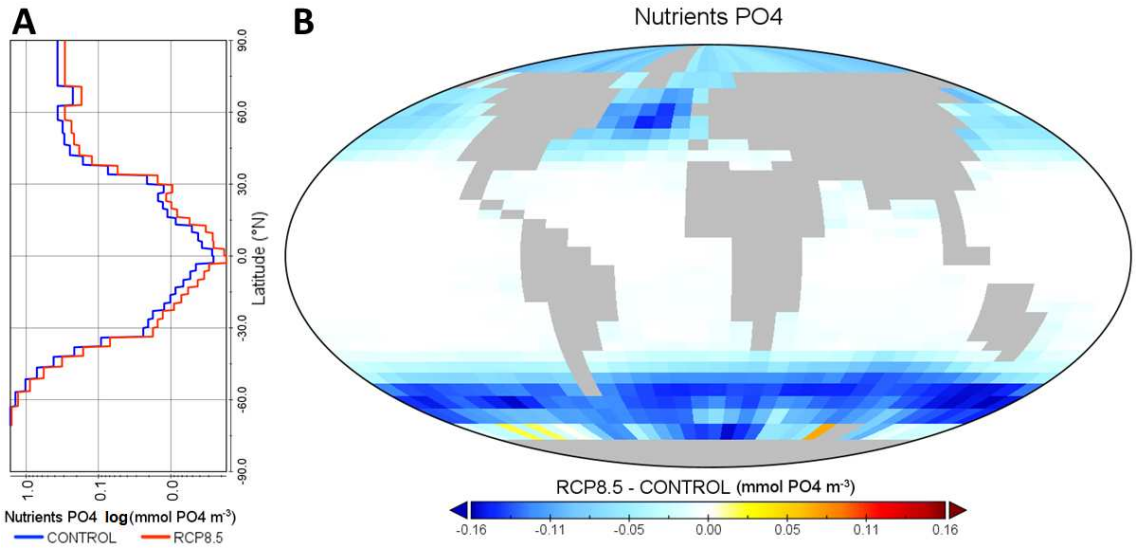

FIGURE 5.4: Surface phosphate concentrations (mmol P m^{-3}). **(a)** zonal average surface PO_4 concentration (on a logarithmic scale) for the Control (blue line) and RCP8.5 (red line) simulations. **(b)** Global distribution of surface PO_4 differences between the RCP8.5 and Control scenario.

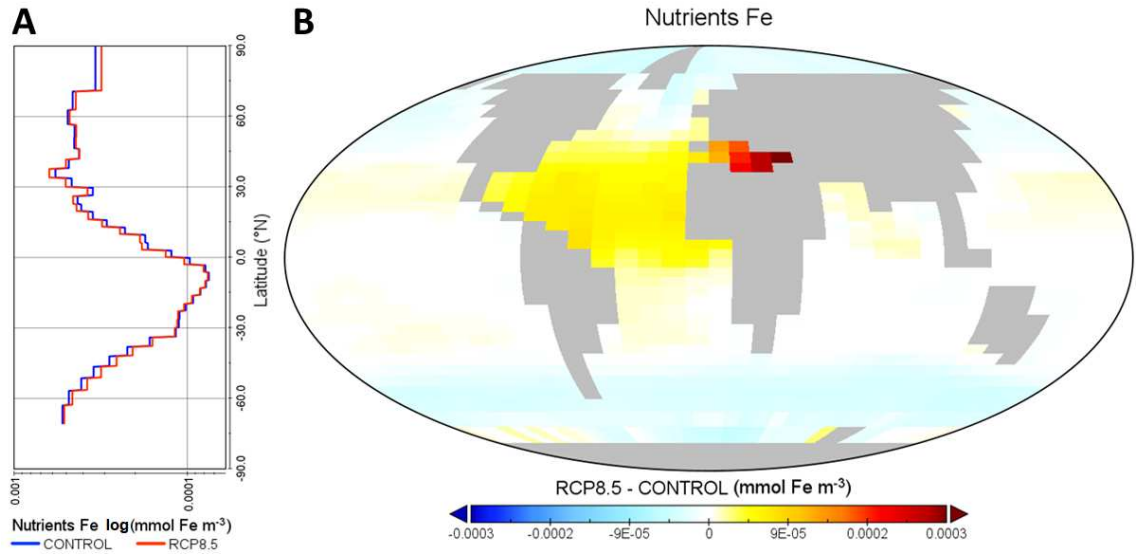

FIGURE 5.5: Surface iron concentrations (mmol Fe m^{-3}). **(a)** Zonal average surface iron concentration (on a logarithmic scale) for the Control (blue line) and RCP8.5 (red line) simulations. **(b)** Global distribution of surface iron differences between the RCP8.5 and Control scenario.

Figure 5.5(a) shows changes in surface iron concentrations from the Control to RCP8.5 scenario. Like phosphorus, iron decreases poleward of 30 degrees N/S. However, the subtropical gyres, together with the entire low-latitude Atlantic Ocean, show a net increase

in dissolved Fe (Figure 5.5b), which is related to the decrease in primary production brought by the increase in phosphorus limitation.

Biomass and community structure

Figure 5.6 shows the relative changes in chlorophyll *a* concentrations at the surface from the Control to the RCP8.5 scenario. Chlorophyll decreases across all latitudes except for the polar regions where the result is more variable. Figure 5.6(a) shows a generalized decline in chlorophyll concentration in the Southern Ocean when integrated zonally. The variable response in the polar regions is most likely caused by spatial shifts in localised regions of high and low MLD between the two scenarios, and also by the lack of biomass advection in the model.

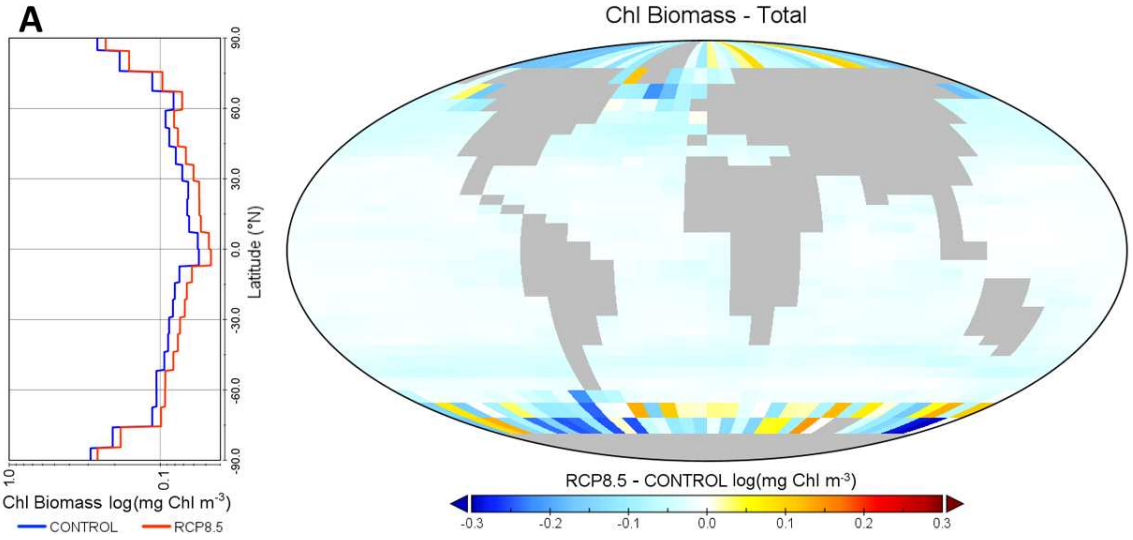

FIGURE 5.6: Total chlorophyll biomass (mg Chl m^{-3}). **(a)** Zonal average for each latitude (on a logarithmic scale). Blue line: Control. Red line: RCP8.5. **(b)** Global distribution of chlorophyll differences between the RCP8.5 and Control scenario.

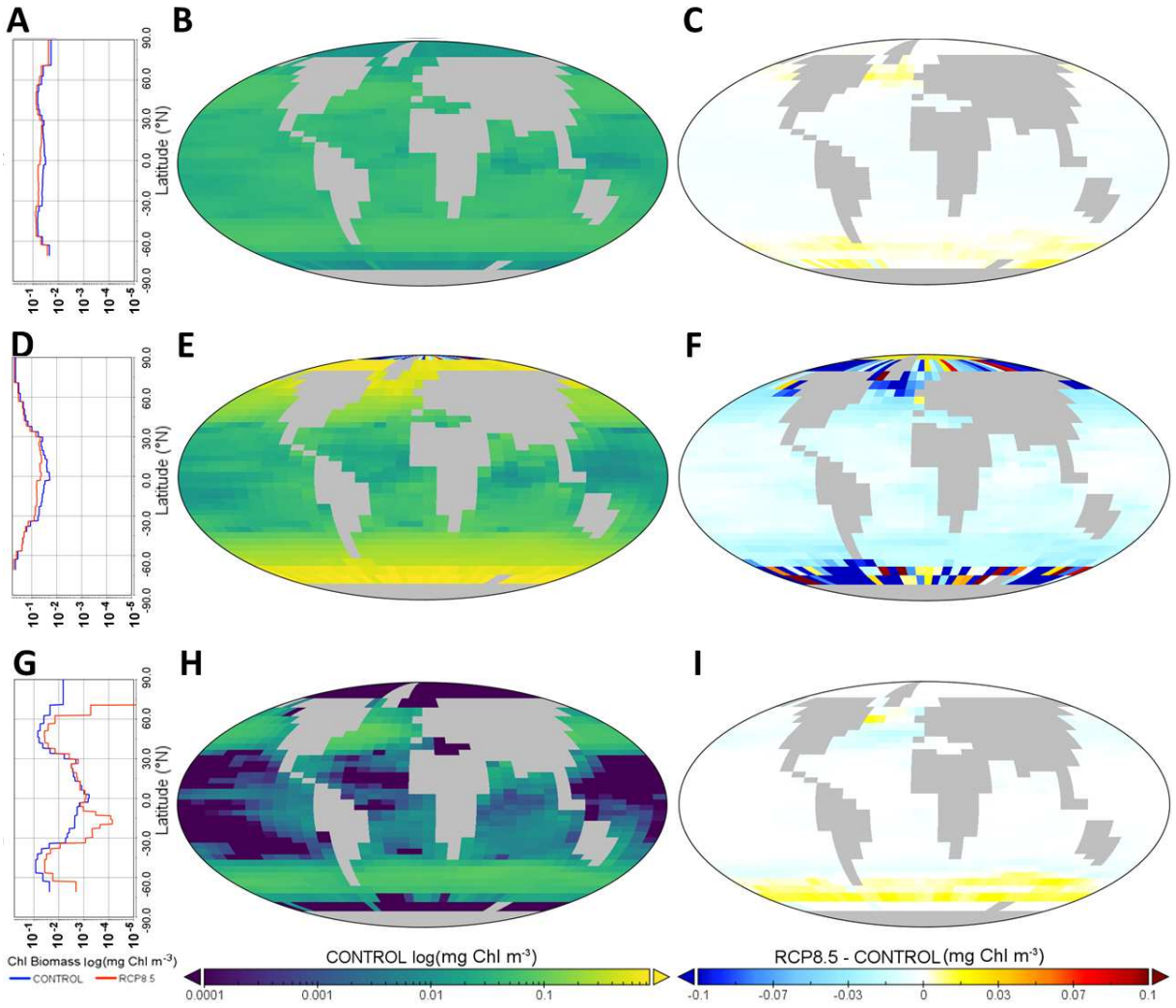

FIGURE 5.7: Chlorophyll biomass (log mg Chl m^{-3}) for different phytoplankton size classes. **(a, b, c)** Picophytoplankton (nominally 0.6 and 1.9 μm). **(d, e, f)** Nanophytoplankton (nominally 6.0 and 19.0 μm). **(g, h, i)** Microphytoplankton (nominally 60.0 and 190.0 μm). **(a, d, g)** Average for each latitude. Blue line: Control. Red line: RCP8.5. **(b, e, h)** Global distribution of chlorophyll biomass in the Control scenario. **(c, f, i)** Global distribution of chlorophyll differences between the RCP8.5 and Control scenario.

Figure 5.7 shows the partitioning of biomass among the picophytoplankton, nanophytoplankton and microphytoplankton size classes, and how these are affected by RCP8.5 conditions. In the Control scenario, picophytoplankton chlorophyll (Figure 5.7b) is slightly more concentrated in the temperate and subpolar regions, while nanophytoplankton chlorophyll (Figure 5.7e) is more abundant in the sub-polar and polar regions. In contrast, microphytoplankton chlorophyll (Figure 5.7h) is mostly distributed in the temperate regions and in the low latitudes, outside the subtropical gyres.

Figure 5.7(c, f and i) shows how the distributions of size-fractionated chlorophyll change from the Control to RCP8.5 scenario. The picophytoplankton and the microphytoplankton size classes increase in the North Atlantic and Southern Ocean, and decline at lower latitudes. Nanophytoplankton biomass shows a different response: a decline at all latitudes with some very large declines in the polar regions.

Figure 5.8 shows the climate-driven changes in the biomass-weighted geometric mean cell-diameter of the phytoplankton (a and b) and the relative change in the associated geometric standard deviation (c and d). The change in geometric mean size shows a similar pattern to the change in microphytoplankton and picoplankton chlorophyll biomass (Figure 5.7c and i): a decrease at intermediate and low latitudes, a strong decrease in the temperate North Atlantic, and an increase in the Southern Ocean and the subpolar North Atlantic. Standard deviation (Figure 5.8c, d) increases everywhere apart from few regions in the North Atlantic, the Center Pacific and the Arctic Ocean.

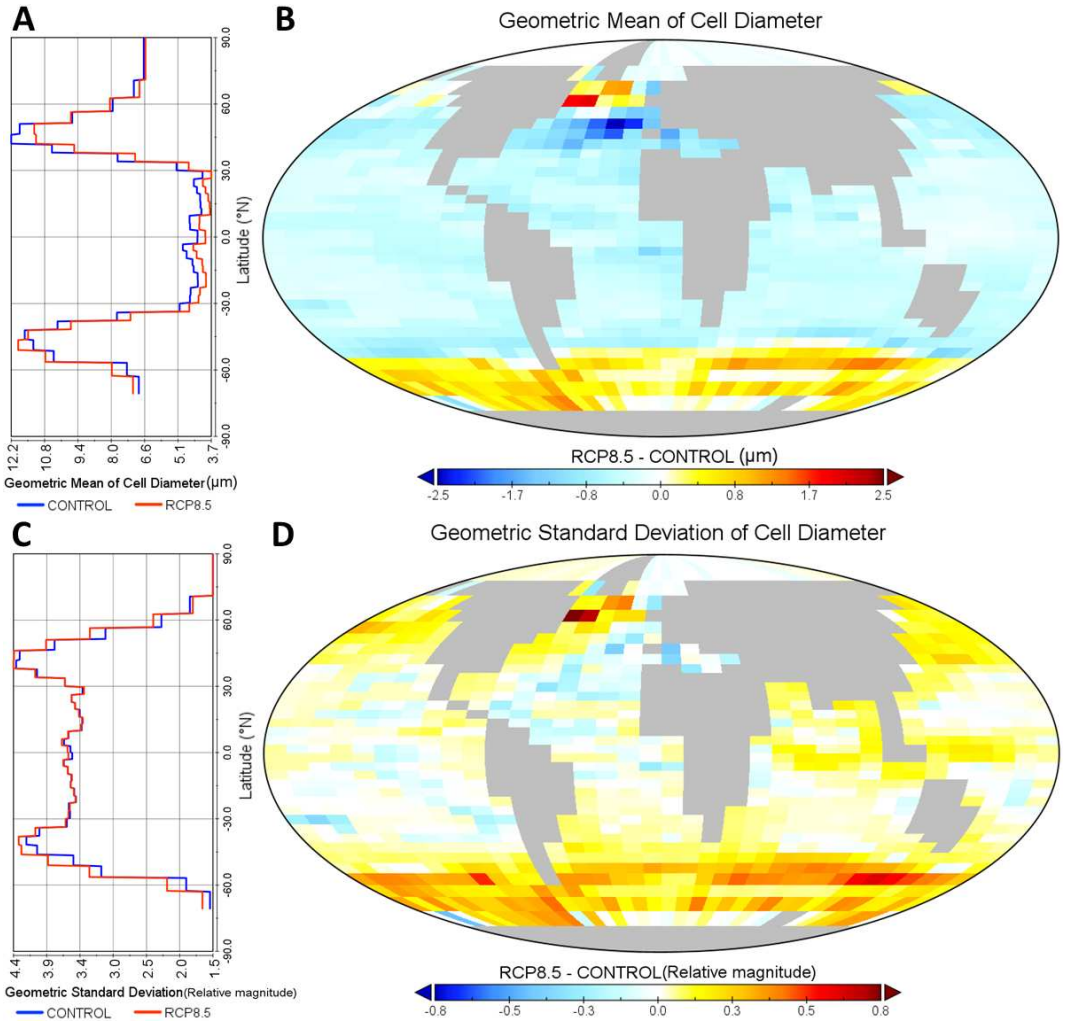

FIGURE 5.8: Geometric mean cell diameter of phytoplankton (μm) **(a, b)** and its standard deviation **(c, d)**. **(a, c)** Average for each latitude. Blue line: Control. Red line: RCP8.5. **(b, d)** Differences in the global distribution of mean cell diameter and its standard deviation between the RCP8.5 and Control scenarios.

In general, the environmental changes under RCP8.5 lead to larger mean phytoplankton size at high latitudes because the increase in microphytoplankton biomass is greater than the increase in picophytoplankton biomass (Figure 5.7c, i). A decrease in size at low latitudes is due to a generalized decrease in the chlorophyll biomass. The intermediate class nanophytoplankton is more involved in the change of the standard deviation than the mean of the size.

The change in standard deviation of phytoplankton size (Figure 5.8c, d) suggests that size is becoming more dispersed around the average, especially in the high latitudes (i.e. more picophytoplankton-microphytoplankton and less nanophytoplankton), while at low latitudes, the final outcome is a decrease for the subtropical gyres, and an increase for the rest. This difference reflects the fact that the subtropical gyres have picophytoplankton and microphytoplankton that change very little in the RCP8.5 scenario (Figure 5.7c,i), since picophytoplankton can survive in this oligotrophic environment, even with a decrease in nutrient supply, while microphytoplankton concentration is already very low in the Control scenario (Figure 5.7h).

Limiting factors

Figure 5.9 shows changes in the temperature limitation factor (γ_T) under RCP8.5. This variable describes how growth rates scale with environmental temperature (Chapter 3, Equation 3.4). Figure 5.9(b) shows the annual average global distribution of γ_T in the Control scenario. Figure 5.9(c) indicates, as expected, a general increase in γ_T under RCP8.5. As said in the previous subsection, the polar regions are less strongly affected because the changes in SST are limited by the freezing point of seawater (Figure 5.2c, d).

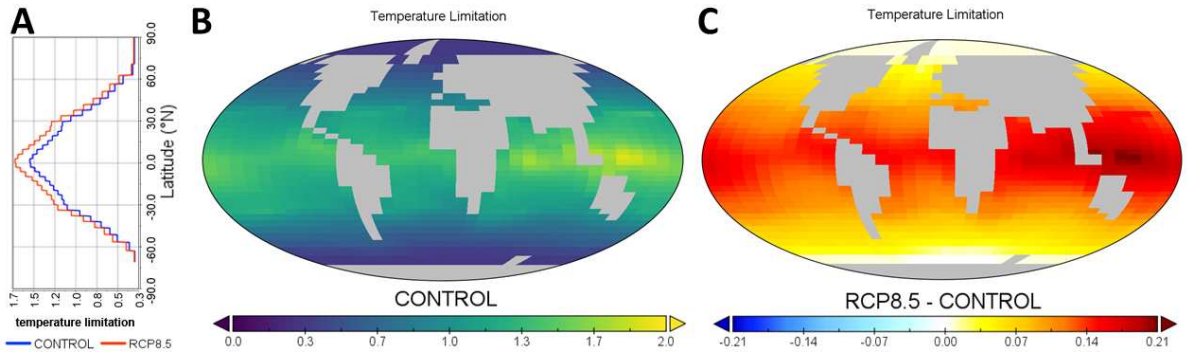

FIGURE 5.9: Temperature limitation. **(a)** Average for each latitude. Blue line: Control, Red line: RCP8.5. **(b)** Control temperature limitation. **(c)** Change in value of γ_T from Control to RCP8.5.

Figures 5.10 and 5.11 show the climate-induced changes in the simulated phosphorus and iron limitation factors. Figure 5.10 shows the phosphorus limitation in three phytoplankton size classes: 1.9 - 19.0 - 190.0 μm. Under RCP8.5 conditions (Figures 5.10b, d, f), due to the increase of temperatures, and thus to the increase in the metabolic rate of the smallest plankton, there is a general increase in the strength of phosphorus limitation. This increase in nutrient limitation is especially seen at low latitudes, for all three plankton size classes, with seemingly no change in the Southern Ocean, and low decrease in Arctic Ocean. Low latitudes have an already low concentration of phosphate (Figures 5.4a) due to weak upwelling (Figures 5.3a, where, on the log scale, the red line is always shallower than the blue line), and thus a further decrease impact more equator and subtropical regions than high latitudes, where phosphorus is more repleted (Figures 5.4a).

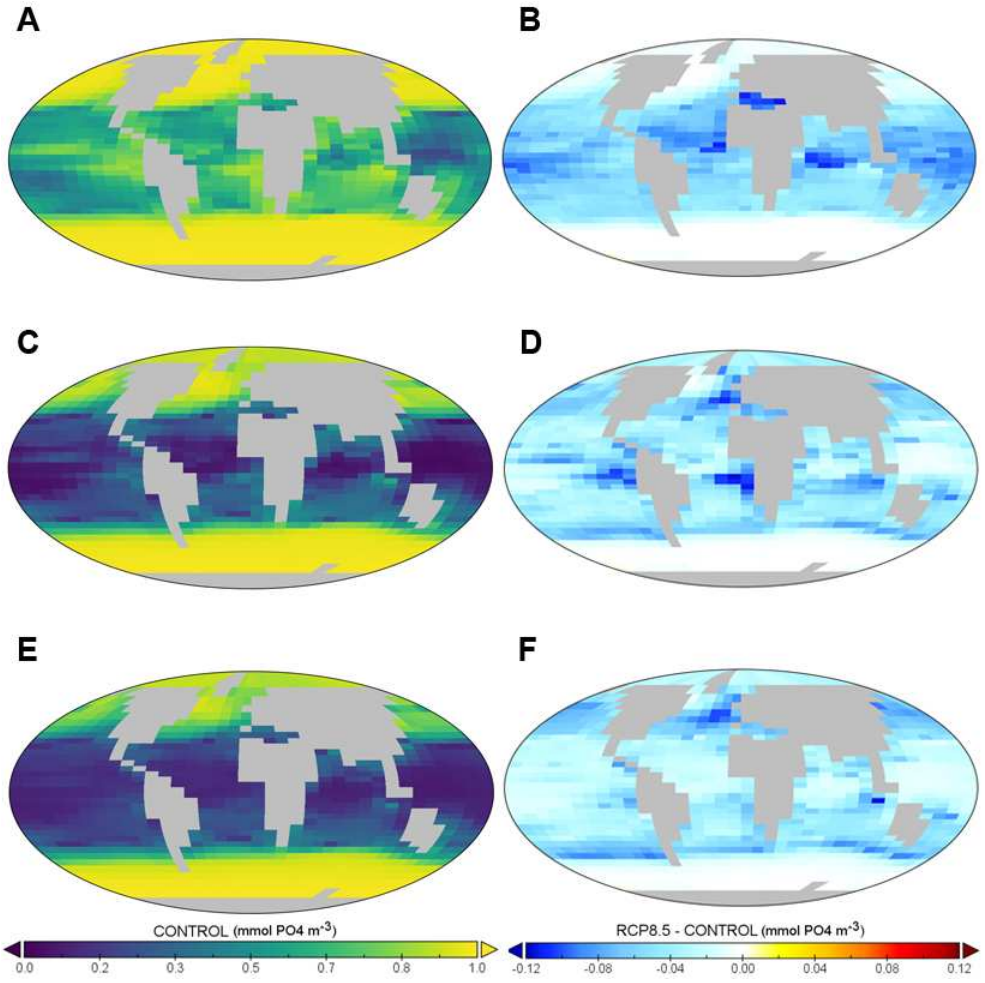

FIGURE 5.10: Phosphorus limitation (mmol P m^{-3}), blue: P limiting, yellow: P repleted. RCP8.5 minus Control. Blue/ light blue: increased limitation for the RCP8.5. **(a, b)** 1.9 μm population. **(c, d)** 19.0 μm population. **(e, f)** 190.0 μm population.

Figures 5.11(b, d, f) conversely shows weaker iron limitation under RCP8.5 at low latitudes, with stronger limitation occurring in the Southern Ocean. In the model, this

weakening happens because iron wind deposition is mostly independent from circulation and upwelling, and since phosphate become more limiting, we see in the RCP8.5 scenario a higher accumulation of the non-limiting iron (Figures 5.5b).

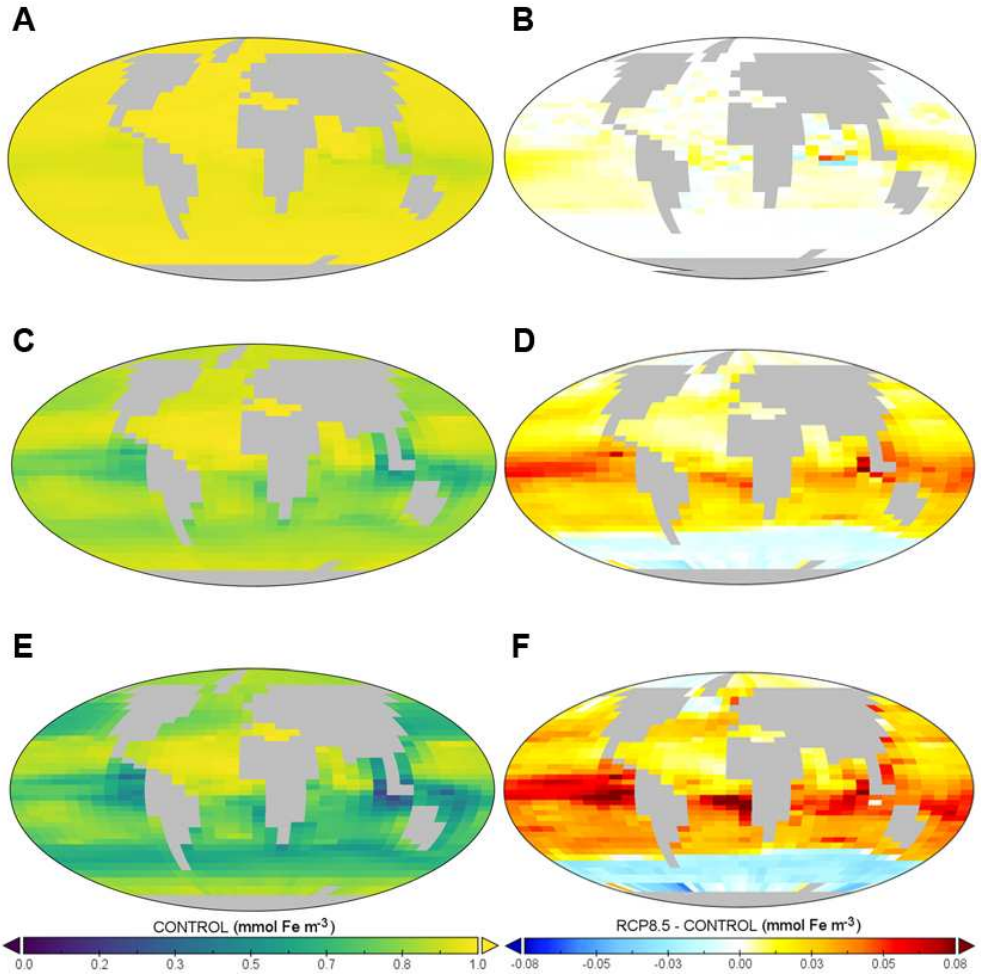

FIGURE 5.11: Iron limitation (mmol Fe m^{-3}), blue: Fe limiting, yellow: Fe repleted. RCP8.5 minus Control. Red/yellow: decreased limitation for the RCP8.5. Blue/ light blue: increased limitation for the RCP8.5. **(a, b)** 1.9 μm population. **(c, d)** 19.0 μm population. **(e, f)** 190.0 μm population.

Primary Production and Export

Figure 5.12 shows the difference in primary production between RCP8.5 and the Control scenario. The increased stratification under RCP8.5 generally causes a net decrease across most of the ocean, but also leads to increased primary production in the Southern Ocean and some high latitude regions in the northern hemisphere.

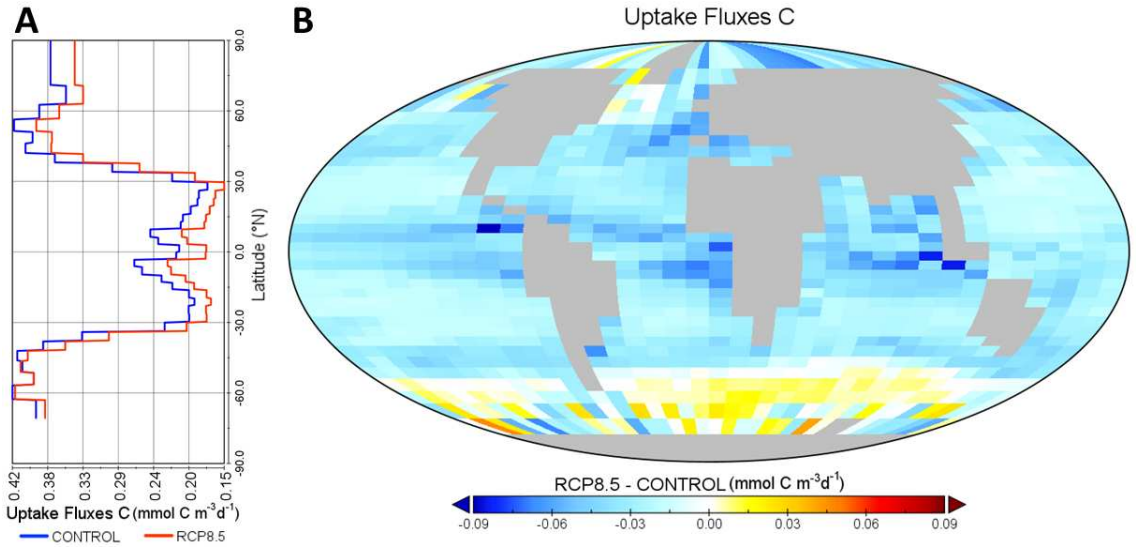

FIGURE 5.12: Simulated effect on primary production (mmol C m^{-3} d^{-1}). **(a)** Average for each latitude. Blue line: Control. Red line: RCP8.5. **(b)** Global distribution of primary production differences between the RCP8.5 and Control scenario.

Figure 5.13 shows a general decrease in vertical carbon export in the RCP8.5 scenario, especially at low latitudes, with an increase in the Southern Ocean and the North Atlantic. It is worth noting that these changes are qualitatively very similar to the changes in primary production (Figure 5.12b) and mean organism size (Figure 5.8b).

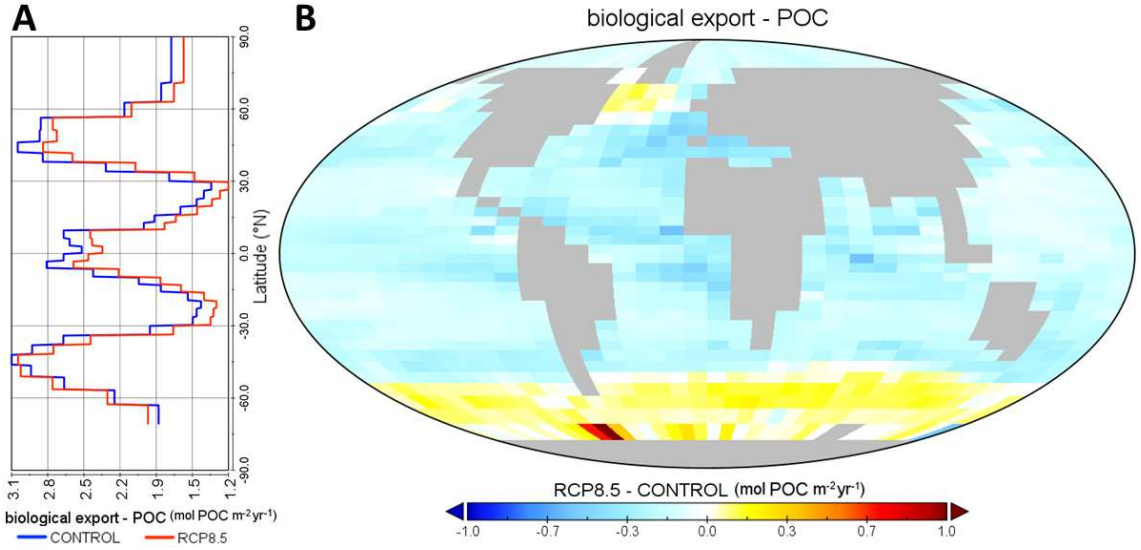

FIGURE 5.13: Export production (mol POC m^{-2} yr^{-1}). **(a)** Average for each latitude. Blue line: Control. Red line: RCP8.5. **(b)** Global distribution of export production differences between the RCP8.5 and Control scenario.

5.4 Discussion

The results presented in this chapter demonstrated that EcoGEnIE matched previously predicted environmental changes (Bopp et al., 2001; Steinacher et al., 2010; Cabré et al., 2015; Moore et al., 2018) under RCP8.5, caused by the increase of SST and a shallowing of MLD (Tyrrell, 2011). SST and MLD did not change uniformly at global scale. The major differences were between low and high latitudes. At low latitudes initially shallow mixed layers shoaled by a few metres, while SSTs universally increased by up to 2.4°C. At high latitudes initially deep mixed layers shoaled by up to several hundred meters (even between 40°S and 35°S as showed by Figure 5.3a, which explains the decline in phosphorus concentration in the higher latitudes of the Southern Ocean), while SSTs increased by far less than in the rest of the oceans.

These two environmental regimes correspond to two distinct regional ecosystem responses, which are discussed in the next two sections. This difference is driven at low latitudes by an increase in chemical limitation (i.e. decrease in nutrients supply) and at high latitudes by a decrease in physical limitation (i.e. increase in light irradiance and temperature).

It is important to note that the main changes in nutrient supply regarded phosphorus, which is completely dependent on circulation, while iron is also supplied through winds. In the model, the pattern of aeolian iron deposition was fixed across both Control and RCP8.5 scenarios (Figure 5.14). This setting, however, does not mean that iron concentrations did not change between scenarios, since, in plankton, iron utilization is linked to carbon and phosphorus acquisition.

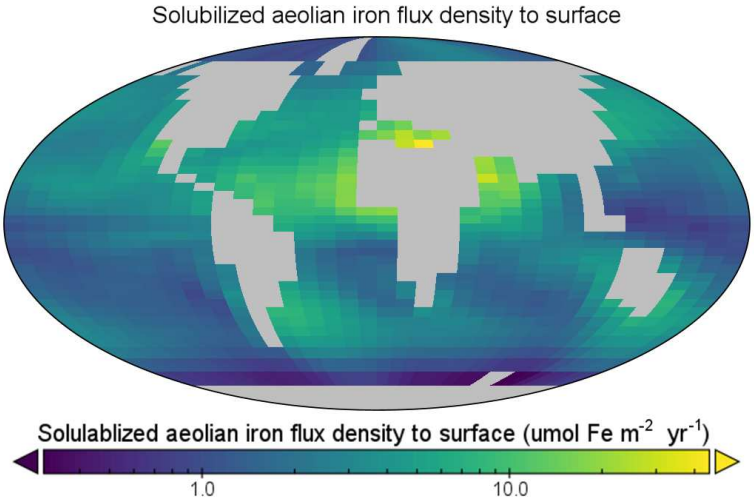

FIGURE 5.14: Aeolian iron deposition map. Soluble Fe is deposited in the ocean through the transport of dusts from the continental masses, especially from the driest regions like the Sahara desert.

The next sections will discuss the different impact of climate changes, on marine communities, at low and high latitudes.

5.4.1 Low latitudes

At low latitudes, increasing radiative forcing under RCP8.5 increases SST (Figure 5.2c, d). This in turn causes the sea surface to become more stratified (Figure 5.3a). The increased stratification suppresses the vertical supply of nutrients from depth (Figure 5.4) (Bopp et al., 2001), even at intermediate latitudes, as shown by the log-plot of Figure 5.3a. In the phosphorus-limited regions of the low latitudes (Figure 5.10b, d, f), the decrease in vertical supply of phosphorus limits primary production (Figure 5.12).

The decreased supply of limiting nutrients to the surface ocean under RCP8.5 serves to suppress primary production, which in turns yields a lower total biomass and a smaller average plankton size. The shift towards smaller cells (Figure 5.8a, b) occurs as larger phytoplankton are outcompeted for increasingly scarce nutrients by smaller and more competitive size classes (Figure 5.7c). The shift towards smaller cells (Figure 5.8a, b) limits the production of larger and faster sinking organic matter, which consequently drives a decrease in export production (Figure 5.13).

In the same phosphorus-limited regions, surface iron concentrations are seen to increase (Figure 5.5). This occurs as the lower primary production, brought about by phosphorus limitation, limits the draw down of non-limiting Fe.

While the lower nutrient supply, phytoplankton size, productivity and export are attributable to increased stratification, the lower surface concentrations of limiting nutrients in the warmer climate can be attributed to temperature-mediated changes in plankton physiology (Wilson et al., 2018). Plankton metabolic rates are accelerated by higher temperatures (Brown et al., 2004), allowing phytoplankton to draw limiting nutrients down to lower levels.

5.4.2 High latitudes

Due to similar physical parameters (deep MLD, low SST, low light availability, high seasonal nutrient concentrations), the North Atlantic and Southern Ocean experience similar changes in ecosystem structure and function. In these regions, high winds and strong surface cooling can drive very deep mixing in the late winter. In a warmer world (Figure 5.2), these forcings will be weakened, leading to a significant shoaling of the MLD (Figure 5.3a), within which circulating plankton will stay closer to the surface and experience higher irradiance. This alleviation of light limitation at high latitudes allows picophytoplankton to draw down phosphorus (Figure 5.4) and iron concentrations (Figure 5.5) to lower levels than in the Control scenario.

Furthermore, the optimal environmental conditions for microphytoplankton undergo a poleward expansion. This is clearly shown in Figure 5.7(g), where microphytoplankton chlorophyll levels expands from temperate to polar regions. By looking at Figure 5.7(d), it is possible to see this expansion also for picophytoplankton. This expansion of the habitats of microphytoplankton (Figure 5.7i) in the higher latitudes, increases the phytoplankton mean cell size, while the combined expansion of picophytoplankton and microphytoplankton (Figure 5.7c, i) increases the standard deviation (Figure 5.8). Overall, the alleviation of light and (to a lesser extent) temperature limitation at high latitudes leads to higher biomass, larger cells and an increase in export production.

5.4.3 Conclusions

The model showed two different responses to climate warming at low and high latitudes. When integrated globally, however, these changes resulted in a net global decline, in the climate changes scenario, in surface phosphorus concentration (12.6%), carbon biomass (6.1%), average cell size (1.9%), primary production (7.5%) and export production (5.1%). Thus, given these results, it is possible to hypothesis that a decrease in primary production will be reflected also into a decrease of production at all levels of the ocean food chains, which will impact average fisheries annual yield. Most importantly, it is possible that climate changes will establish a positive-feedback cycle, where warmer temperatures will cause a waning of the strength of the BCP that will allow the sequestration of increasingly smaller quantities of carbon dioxide. The CO_2 will accumulate at a higher rate than before, in the atmosphere, which will accelerate the rate of increase of the global average temperatures.

Despite its simplicity, EcoGEnIE yields climate change predictions that are largely consistent with other higher resolution but ecologically less complex ocean and ecosystem models. Bopp et al. (2001), Cabré et al. (2015) and Kwiatkowski et al. (2020) found a global net decrease in nutrient concentration. Steinacher et al. (2010) compared 4 different models, while Fu et al. (2016) compared 11 models, and both found that in all simulations there was a net global decrease of nutrients, primary and export production, which was caused by increase stratification of sea surface. Bopp et al. (2001) and Steinacher et al. (2010) described a net decrease in production in the low latitudes. Bopp et al. (2001) and Steinacher et al. (2010) also found a strong increase in primary and export production in the Southern Ocean by the year 2100. According to statistical analysis of present observations, high temperature/oligotrophic environment favour the development of communities dominated (>50%) by the smallest size classes (picophytoplankton) (Agawin et al., 2000).

Bopp et al. (2013), through the use of 10 CMIP5 models, and by making a comparison between 1990s and 2090s in an RCP8.5 scenario, found an average decrease at low latitudes, and an average increase at high latitudes of primary and export production

(Figures 5.15b). The main difference between these results and the results of this thesis (Figure 5.12 and Figure 5.13) are in the Arctic Ocean, especially in the North Atlantic that shows a decrease rather than an increase. This difference may be due to the difference in the number of plankton groups used in my research (16 in total) and the number of plankton groups used by Bopp et al. (2013) (4 or 5 for most models). This smaller number causes the absence of the formation of the larger plankton (Figure 5.7 e and h) that thrive in the high latitudes of the simulations.

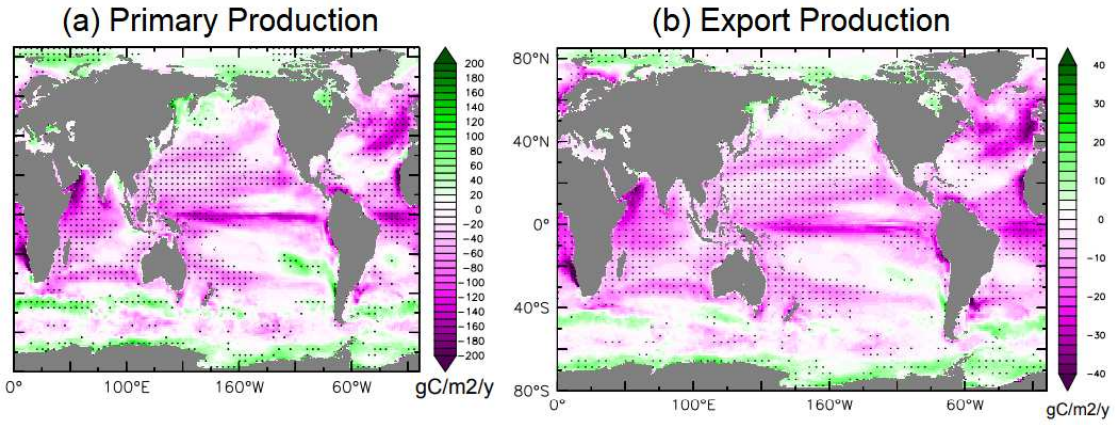

FIGURE 5.15: Change in primary production (a) and export production (b) from Bopp et al. (2013). Purple: decrease. Green: increase.

These agreements suggest that EcoGEnIE can provide reasonable climate change predictions, despite the coarse resolution of the global ocean grid. These results give strength to the results that will be presented in the next Chapter, which is the last research chapter, where mixotrophs will be added to the ocean, and the sensitivity tests will regard the trophic trade-off and the metabolic temperature dependence in plankton.

Chapter 6

The biogeochemical impacts of mixotrophy in a future warmer world

6.1 Introduction

A warmer ocean will decrease ocean mixing and increase stratification (Hays et al., 2005), will change algal bloom intensity and timing (Hallegraeff, 2010), and will decrease phytoplankton primary production (Bopp et al., 2001) and export production (Fu et al., 2016). Chapter 5 explored this scenario and its impact on plankton community structure and ocean biogeochemistry. Under a climate change scenario, the EcoGEnIE simulations showed there will be a decrease in plankton biomass, average size and carbon export at low latitudes, while at high latitudes, specifically in the Southern Ocean and the North Atlantic, there will be an increase of the same variables.

In general, the "Two-Guild" configuration of EcoGEnIE suggests that climate change selects for smaller phytoplankton and zooplankton at low latitudes and larger at high latitudes. A missing element from this scenario is the fact that most microbial life in the ocean has some degree of mixotrophic capability (Flynn et al., 2013), which can globally increase plankton average size and carbon export (Ward and Follows, 2016)(Chapter 4). Thus, a question rises naturally: how will mixotrophy affect the response of community function and biochemical cycles in a climate change scenario?

In models, both in a 0D environment (Mitra et al., 2014) and in an Earth System Model (Ward and Follows, 2016), prior research showed that simulations with mixotrophs can increase primary production, water net DOC production, carbon transfer efficiency and export if compared to simulations with the same environmental condition and with only specialists. These increases are due to mixotrophs' feeding flexibility that allows more

more nutrients and carbon to be absorbed by multiple trophic levels in the plankton community. Chapter 4 likewise showed that mixotrophy impacts ecosystem function and the marine carbon cycle. A system populated by mixotrophs can increase average plankton size and fixed carbon-to-limiting-nutrient uptake ratio. These increases translated to an increase in exported carbon and deep ocean carbon inventory, with the exception of the North Atlantic, where mixotrophs suppressed the magnitude of the spring bloom and its associated ability to export carbon into the ocean interior.

This chapter explores how the inclusion of mixotrophy in an Earth system model modifies the simulated response to predicted climate changes in the 21^{st} century. Again, this chapter uses the EcoGEnIE model with and without a representation of mixotrophy under two climate scenarios. In the first case (the Control scenario) atmospheric carbon concentrations are held fixed at 2010 concentrations. In the second case (the "worst case" RCP8.5 scenario) atmospheric carbon concentrations are progressively increased to 934 ppm by 2100 (Schwalm et al., 2020).

Different strengths of the assumed trade-off between autotrophic and heterotrophic traits were explored in the sensitivity tests. The trophic trade-off is the compromise between autotrophic and heterotrophic trophic strategy in the same mixotrophic organism. Again, superlinear, sublinear and linear trade-off change how mixotrophs affect community structure and biogeochemical cycles (Figure 3.6).

The main hypothesis proposed by this chapter are as follows: (1) the presence of mixotrophs decreases the impact of climate changes when compared to their absence (Chapter 5); (2) moving from a superlinear to a sublinear trade-off will decrease the resistance to changes in biological export and plankton community structure and function.

6.2 Method

The EcoGEnIE model presented in Chapter 3 will be again the tool used to explore plankton ecology. The Two-Guild configuration (eight phytoplankton, eight zooplankton), already seen in the previous two chapters, will run in parallel with the "Mixotrophic" (eight mixotrophs) and the "Mixotrophic-Plus" (eight phytoplankton, eight mixotrophs, eight zooplankton) configuration used for the sensitivity tests in Chapter 4 (Figure 3.5). All model simulations will resolve eight size classes for each trophic strategy. The Mixotrophic configuration will be also used in the sensitivity tests together with the Mixotrophic-Plus configuration.

TABLE 6.1: List of the ecological configurations.

Ecosystem	**Phyto.**	**Mixo.**	**Zoo.**
Two-Guild	8	0	8
Mixotrophic	0	8	0
Mixotrophic-Plus	8	8	8

The Mixotrophic-Plus configuration was repeated four times with different mixotrophic trade-offs. This was done to assess the impact of the trade-off in the climate changes scenario. The trade-off value (τ) modifies the maximum phototrophic growth rate (μ_{max}) and the heterotrophic grazing rate (g_{max}) according to the equations

$$V^{max}(\tau) = \omega^{\tau} \cdot V^{max} \tag{6.1}$$

$$g(\tau) = (1-\omega)^{\tau} \cdot g \tag{6.2}$$

where $V^{max}(\tau)$ and $g(\tau)$ are the modified maximum photopsynthetic and grazing rates used by the mixotrophic populations, while ω is the balance between autotrophic and heterotrophic traits. In all simulations $\omega = 1$ for strict phytoplankton, $\omega = 0$ for strict zooplankton, and $\omega = 0.5$ for mixotrophs. τ is the value that changes the shape of the trade-off. It can be 1 (linear trade-off), <1 (superlinear trade-off), or >1 (sublinear trade-off).

In the sensitivity experiments τ was set equal to 0, 0.74, 1 and 1.32, which represent mixotrophs with 100% ($\mathbf{M}_{100}$), 60% ($\mathbf{M}_{60}$), 50% ($\mathbf{M}_{50}$) and 40% ($\mathbf{M}_{40}$) of the feeding efficiency if compared to the specialists. Table 6.2 and Figure 3.6 show the different values of $V^{max}(\tau)$ and $g(\tau)$ and how these change the autotrophic and heterotrophic growth rate in the mixotrophic populations.

TABLE 6.2: Trade-off value list. Each number is a value of μ_{max} and g_{max} that impact mixotrophic feeding.

Configuration	**Two-Guild**		**Mixotrophic**	**Mixotrophic plus**					
Population	**P**	**Z**	$\mathbf{M}_{100}$	**P**	**Z**	$\mathbf{M}_{40}$	$\mathbf{M}_{50}$	$\mathbf{M}_{60}$	$\mathbf{M}_{100}$
Photosyn. growth efficiency	1	0	1	1	0	0.4	0.5	0.6	1
Grazing efficiency	0	1	1	0	1	0.4	0.5	0.6	1

As in Chapter 4, each configuration was run through a 10,000 year spin up and the 245 year historical transient. Following this, the configurations were run from 2010 to 2100 under the Control and RCP8.5 CO_2 forcings (see Table 6.3).

TABLE 6.3: List of the scenarios.

Scenario	**Begin**	**End**	**Duration**	**Begin [CO_2]**	**End [CO_2]**
Pre-industrial	/////	/////	10,000 years	277 ppm	277 ppm
Historical transient	1765	2010	245 years	277 ppm	388 ppm
Control	2010	2100	90 years	388 ppm	388 ppm
RCP8.5	2010	2100	90 years	388 ppm	936 ppm

6.3 Results and Discussion

Figure 6.1 shows the ecological and biogeochemical differences between the RCP8.5 scenario, Control scenario and the difference between Two-Guild and Mixotrophic configuration. Figure 6.1 d and g show respectively the same result from Figure 5.8b and 5.13b.

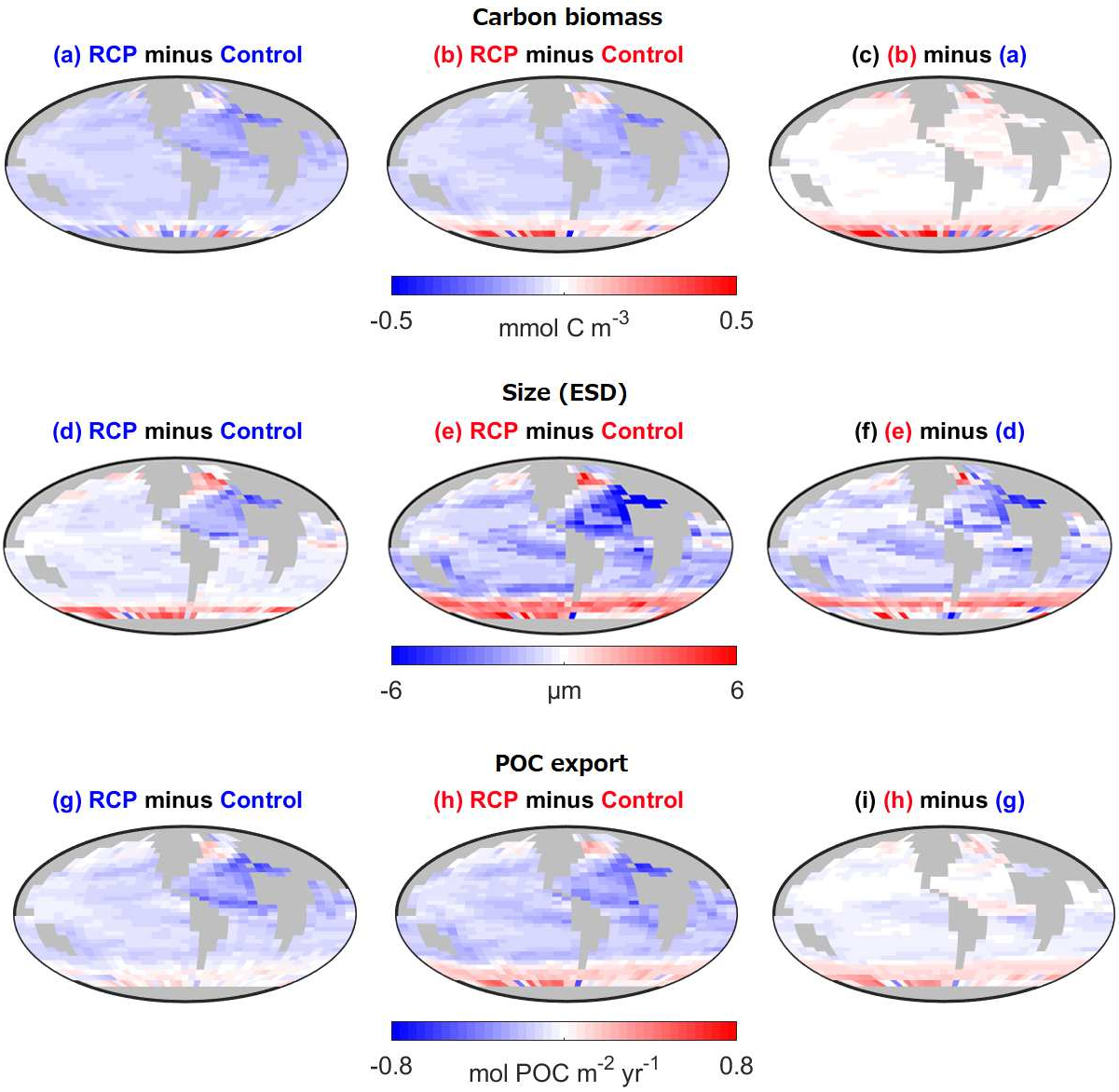

FIGURE 6.1: Total global carbon biomass (mmol C m^{-3}; upper row), geometric mean cell diameter (μm; middle row), and export production (mol POC m^{-2} yr^{-1}; lower row). Differences between RCP8.5 and Control scenarios are shown for the Two-Guild configuration (left-hand column) and the Mixotrophic configuration (middle column), and differences between the two configurations (right-hand column).

The left-hand column of Figure 6.1 shows the relative change in carbon biomass (top row), mean organism size (middle row) and vertical POC export (bottom row) from the Control to the RCP8.5 scenario in the Two-Guild configuration (these results are the same from Chapter 5 but with a different color scale). At low and temperate latitudes there is a general decrease in these three variables, while at higher latitudes there is a more variable response with some regions showing increases and others decreases. At

higher latitudes there is an increase in carbon export but almost no change in organism size.

The centre column of Figure 6.1 shows the relative change of the same three ecosystem variables from the Control to the RCP8.5 scenario in the Mixotrophic configuration. In comparison to the Two-Guild configuration there is the same pattern of increases and decreases in different regions, but the changes in either direction are generally larger in the Mixotrophic configuration than the Two-Guild configuration.

To understand how the inclusion of mixotrophy changes the model's response to projected climate changes, the right-hand column of Figure 6.1 shows the differences between the changes in the Two-Guild and Mixotrophic configurations. These maps emphasise that changes from the Two-Guild to the Mixotrophic configuration lead to larger increases in carbon biomass, organism size and POC flux at high latitudes, and larger decreases in organism size and POC flux at low latitudes. Predicted changes in carbon biomass were very similar between the configurations at low latitudes. The only exceptions are the high latitudes of the carbon biomass map, which increase, rather than having a mixed behavior, in the Mixotrophic configuration.

6.3.1 Mixotrophy enhances climate-driven changes in ecosystem structure and function

In general, mixotrophs enhance the projected ecological and biogeochemical responses to climate change that were seen in the Two-Guild configuration. In the low latitudes, there was an enhancement of the decreases, while in the high latitudes there was an enhancement of the increases. These two patterns can be explained using the same general rules and considering the different conditions of the low and high latitudes.

To understand the differential latitudinal trend, it is necessary to look at Chapter 4, which showed that for any given level of productivity, the mixotrophic simulations supported larger plankton and higher export fluxes. Thus, the gradient of these variables with respect to productivity will be steeper, and so any given increase in productivity will lead to bigger increases in plankton size and export, while any given decrease in productivity will lead to correspondingly bigger decreases in the same variables.

At high latitudes, warmer temperatures and increased stratification under RCP8.5 alleviate temperature and light limitation, leading to higher productivity. This is true for both Two-Guild and Mixotrophic configuration, however because the mixotrophic community is more efficiently converting the productivity to large and fast sinking organic matter, the increases under RCP8.5 are larger.

At low latitudes, there is also increased stratification in the RCP8.5 scenario, however here the changes are mostly driven by a suppression of the limited vertical nutrient

supply, such that productivity at year 2100 is lower. Again, this is true in both scenarios, but because the gradients of plankton size and export as a function of productivity are steeper in the mixotrophic simulations, the decreases are larger when mixotrophy is included.

Since the presence of mixotrophy leads to climate-driven responses of opposing sign at different latitudes, the globally-integrated changes underlines how the projected changes affect the system at the global scale.

6.3.2 Global-integrated alterations

When integrated globally, climate changes caused a net increase in global stratification, which led to a decrease in surface phosphorus supply in both configurations and to a decrease in phosphorus concentrations (Figure 6.2b). The difference between the Two-Guild and Mixotrophic configurations was driven by mixotrophs at the end of the pre-industrial scenario, where phosphorus concentrations were lower with the mixotrophic configuration because mixotrophs can draw nutrients down at a lower level. The same logic applies to iron (Figure 6.2c).

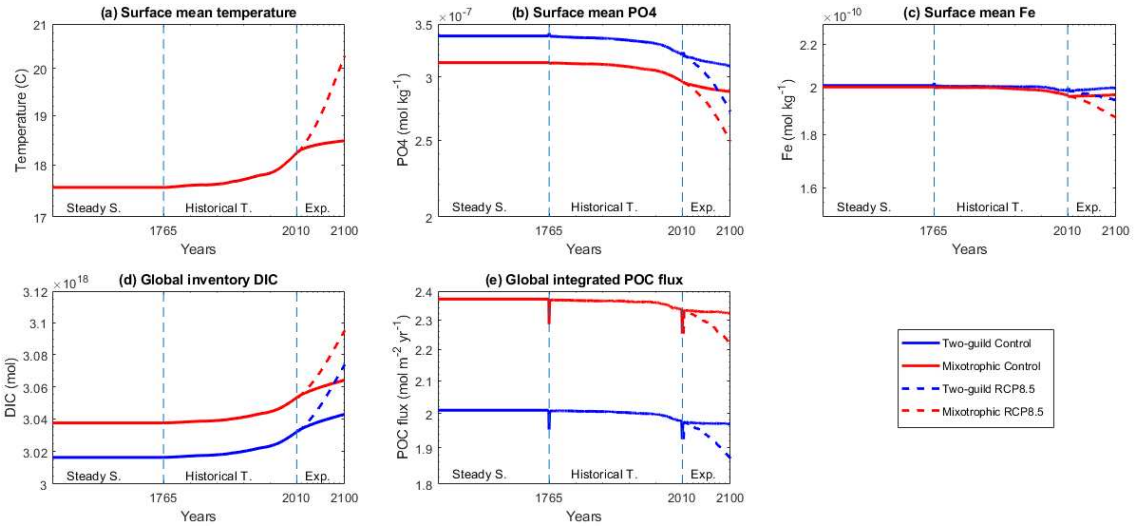

FIGURE 6.2: Time series of the main biogeochemical variables, from the steady state after the spin up (-1765), through the historical transient (1765-2010) and the experiment (2010-2100).

The dissolved inorganic carbon (DIC) global inventory (Figure 6.2d) increased in both configurations, driven by rising atmospheric CO_2 concentrations under RCP8.5. However, the DIC inventory increased more in the Mixotrophic configuration. This difference is explained by the increased vertical carbon export attributable to mixotrophy (Figure 6.2e, the downward spikes between simulations are caused by the restart of the run

since ECOGEM does not load the previous biomass state). These changes in the carbon cycle and storage confirm that, potentially, mixotrophs can decrease the atmospheric carbon concentration in a climate changes scenario.

To estimate the feedback of the BCP on the atmosphere, according to Koeve et al. (2020), it is possible to use, as approximation, the global true oxygen utilization (TOU). To calculate the TOU I turned on the Csof variable of the EcoGEnIE simulations, and then I divide the variable by the C:O Redfield ratio (which is equal to 1.4). The result is showed in Figure 6.3, which suggests that both configurations have, on the atmospheric concentration of CO_2, a negative feedback.

By comparing the Control versus the RCP8.5 scenario in the same configuration, it is possible to see that the Two-Guild configuration goes from 7.05 $\cdot 10^{-5}$ to 7.17 $\cdot 10^{-5}$ O_2 mol Kg^{-1} (with a difference of 1.27 $\cdot 10^{-6}$ O_2 mol Kg^{-1}) while going from the Control to RCP8.5 scenario. The Mixotrophic configuration goes from 8.3 $\cdot 10^{-5}$ to 8.45 $\cdot 10^{-5}$ O_2 mol Kg^{-1} (with a difference of 1.51 $\cdot 10^{-6}$ O_2 mol Kg^{-1}). Thus the Mixotrophic configuration causes a stronger negative feedback on the atmosphere than the Two-Guild configuration in the case of climate warming.

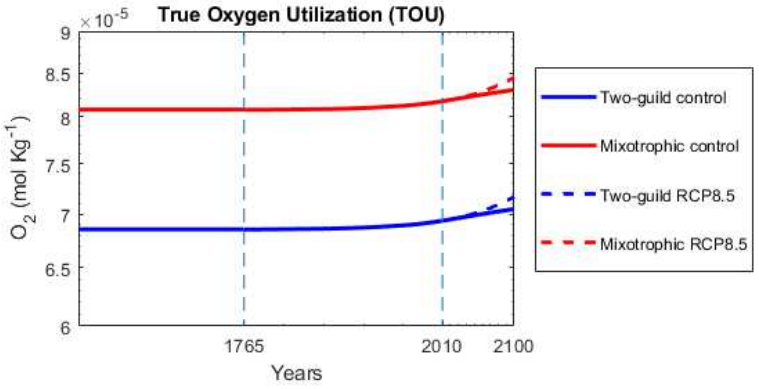

FIGURE 6.3: Time series of total oxygen utilization (TOU) in the two configurations.

To better highlight the difference between the two configuration in a climate change scenario, it is possible to make the Mixotrophic configuration start from the last step of the Two-Guild spin up (Figure 6.4). The final results hardly change, and the time series resemble closely the results from Figure 6.2. The quick change in POC flux Figure 6.2e is caused by the instantaneous switch from the Two-Guild to the Mixotrophic configuration, and because it is not cumulative as the other variables.

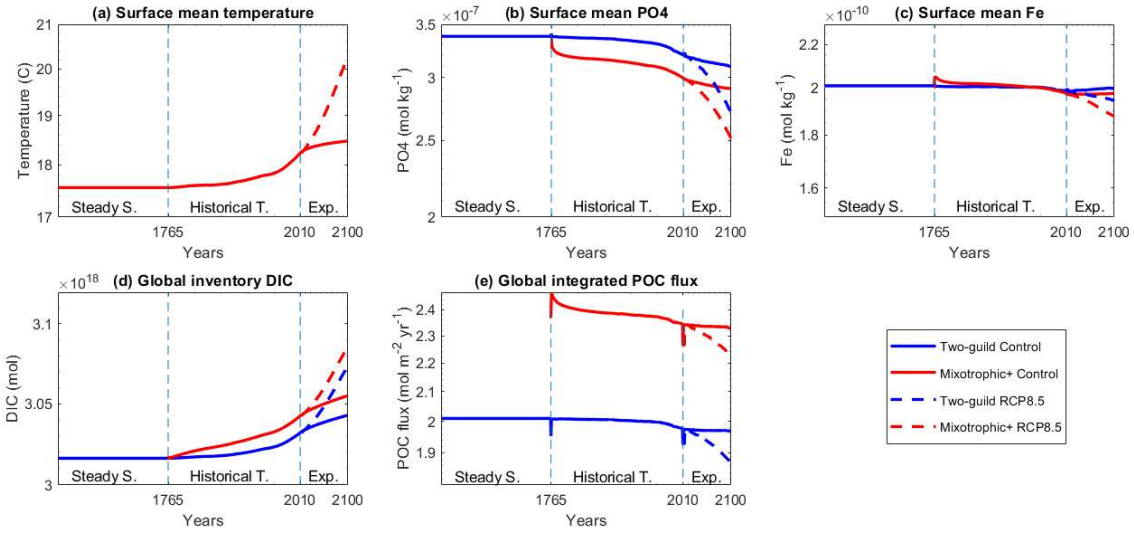

FIGURE 6.4: Time series where the Mixotrophic configuration started from the last step of the spin up of the Two-Guild simulation.

6.3.3 Sensitivity to the trophic trade-off

The results above are based on a mixotrophic configuration in which mixotrophs are able to photosynthesise, absorb nutrients and catch prey with no cost, and without competition with phytoplankton and zooplankton specialists. This setting maximises the differences directly attributable to mixotrophy. Mixotrophy is, however, likely to have physiological costs driven by limited cellular space and energy consumption (Stoecker, 1998). To assess the possible impact of potential mixotrophic trophic trade-offs, on future ecosystems, the following sensitivity tests used the Mixotrophic-Plus configuration. Since mixotrophic trade-offs are still poorly constrained, different shaped trade-offs (Figure 3.6) were applied to explore their potential impacts.

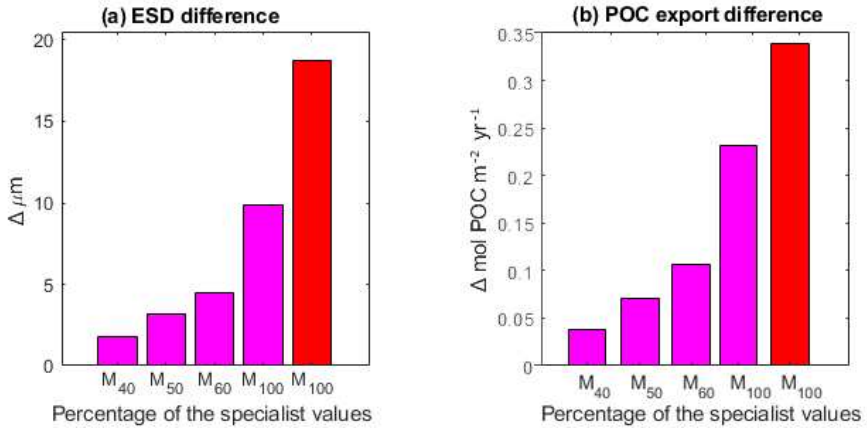

FIGURE 6.5: Differences between Mixotrophic configurations and Two-Guild configuration variables in the RCP8.5 scenario. Each bar is the difference between mixotrophic and Two-Guild configuration in the RCP8.5 scenario. In magenta the Mixotrophic-Plus configurations with different trade-offs, in red the Mixotrophic configuration.

Figure 6.5 shows how much community average ESD and the vertical POC flux change relative to the Two-Guild simulation under different assumed trade-offs.

The bars correspond to the difference between a Mixotrophic configuration with a specific trade-off and the Two-Guild configuration. The M_{100} bars (Mixotrophic and Mixotrophic-Plus configurations) indicate mixotrophs capable of doing autotrophy and heterotrophy with same rate of a strict autotroph and strict heterotroph, while the M_{40}, M_{50} and M_{60} bars (only Mixotrophic-Plus configuration) indicate mixotrophs capable of doing autotrophy and heterotrophy with 40, 50 and 60%, respectively, of the efficiency of a pure specialist. The Mixotrophic configuration is higher than the M_{100} because the active switching setting in the latter configuration allowed some less competitive specialist populations to survive (while these are *a priori* completely absent from the Mixotrophic configuration). This difference decreased the average surface nutrient concentration in the M_{100} more than in the Mixotrophic configuration, causing in turn a average decrease in plankton size and thus export.

As expected, with the increase of the penalty of the trade-off (going from 100 to 40%), climate-driven changes in size and carbon export decline relative to each other and to the Two-Guild configuration. However, even the simulations with the highest penalty for mixotrophy see an enhancement of ESD and carbon export, relative to the Two-Guild configuration. These results reflect the findings of Ward and Follows (2016), and confirm that mixotrophy is likely to be an important factor in an ocean where mixotrophs are demonstrably prevalent. This is relevant to our understanding of possible future global warming scenario since mixotrophy seems to be ubiquitous and composing most of the microbial life in world's oceans (Stoecker, 1998; Flynn et al., 2013). Since Chapter 2 suggest that the trophic trade-off is sublinear (M_{40} in this model), then the final enhancement should be lower than the original M_{100} result.

6.4 Conclusion

As was the case for the Two-guild configuration (Chapter 5), the net global impact of climate change in the Mixotrophic configuration, was a decrease in phosphorus concentration (13.8%), carbon biomass (5.1%), average cell size (2.4%), primary production (5.6%) and export production (4.5%). These results are perhaps only slightly different from the results of Chapter 5 (phosphorus concentration 12.6%, C biomass 6.1%, size 1.9%, primary production 7.5%, export production 5.1%), nonetheless, they show often a more contained outcome, in a warmer planet, for plankton communities and carbon cycle.

This result supports the initial hypothesis that mixotrophs increase the ecological and biogeochemical resistance to changes in a climate changes scenario. Mixotrophs, again, increase average plankton size and carbon export even in the year 2100. However this is the net result. The latitudinal response is more complex. At low latitudes, mixotrophs decrease plankton mean size and the strength of the BCP, and conversely, at high latitudes mixotrophs increase size and carbon export. These changes are already present in the simulation with the Two-guild configuration, although the presence of mixotrophs enhances this response.

The first part of this chapter showed only the upper limit of the possible outcomes. The main simulation assigned no trophic trade-off to mixotrophic plankton. With the addition of a trade-off the magnitude of the simulated effects declined. This difference suggests that moving from an idealized situation with no trade-off at all, to a more realistic sublinear/superlinear trade-off, there is a decrease in the strength of the BCP, and thus an enhancement of the impact of climate changes.

While it was not possible to find other papers about the role of mixotrophs in a climate change simulation, given the limited time frame in which ocean climate change simulations have been performed (Bopp et al., 2001) and the recently discovered importance/distribution of mixotrophs (Stoecker et al., 2017), a larger body of research supports the fact that mixotrophs become more heterotrophic with increasing temperatures (Wilken et al., 2013, 2018; Chan et al., 2019; González-Olalla et al., 2019). The model here presented shows that mixotrophs, in the Mixotrophic Plus configuration, decrease their uptake rate (from 0.134 to 0.126 mmol C m^{-3} d^{-1}) more then their predation rate (from 0.074 to 0.069 mmol C m^{-3} d^{-1}) at global level. Albeit small, the decreases were respectively 6.82% for uptake and 6.75% predation, which indicate a tendency of the mixotrophs to switch from the autotrophic to the heterotrophic feeding strategy.

In conclusion, mixotrophs play a biogeochemical role in a climate change scenario, thus, future research and modelling should keep into account these organisms to increase the accuracy of their predictions.

Chapter 7

Discussion

7.1 Research questions

In mixotrophs, the main trade-off arises in the acquisition and allocation of resources coming from two different trophic systems. This compromise occurs between two different kinds of cross-membrane transporters that share a finite cell surface (Ward et al., 2011) and the cellular biomass and energy allocation system that must satisfies two internal trophic systems (Edwards, 2019). This competition inevitably impacts growth, competitiveness with the specialists (Våge et al., 2013), and ecological function such as the relation between community average cellular size and export production (Ward and Follows, 2016).

This thesis started with the intention of studying the rules that guide plankton community assembly and what is the role of mixotrophs in this process. It was argued (Mitra et al., 2023) that the analysis of mixotrophic trade-offs is only meaningful among organisms with a close evolutionary history (Garland, 2014). While it is true that the study of the trade-offs in sufficiently similar lineages is a potential approach to understand physiological compromises within a monophyletic group, it should also be noted that polyphyletic groups can show convergent evolution under similar selective pressure, allowing a comparison in their traits (Leander, 2008). Furthermore, some physiological mechanisms, such as oxygenic photosynthesis (Fischer et al., 2016) and phagocytosis (Yutin et al., 2009), originated so deep in the tree of life that they should be comparable even among polyphyletic groups.

In Chapter 2, emphasis was put on two questions: what is the impact of temperature on plankton community structure? Is the balance between the costs and benefits of the mixotrophic strategy a net disadvantage or advantage for mixotrophs, when compared to the specialist strategies?

The following chapters studied the relation between environmental condition and plankton community structure, with the specific goal of establishing the spatial and temporal impact of plankton, with particular attention on mixotrophs, in the global carbon cycle. The questions were: what is the impact of mixotrophs on the carbon cycle in the long term? What is the impact of climate changes on plankton and global biogeochemical cycles? What is the global impact of mixotrophy in a climate change scenario? The sensitivity tests also took into account the possibility of different trophic trade-offs in mixotrophs.

In the next sections, answers will be given to these questions and the findings of each chapter will be summarised and put in relation with each other. The next step will be that of analysing the ecological implications of the mixotrophic trade-offs in nature, and the consequences of mixotrophy in future warmer oceans, with reference to previous research. After this analysis, the limitation of the used models and possible future works will be listed.

7.2 Summary of chapters

7.2.1 Chapter 2: A trait-based model of a plankton food web for the Gulf of Naples

Ecological interactions do matter at different temperatures

A highly abstracted model showed that an increase in environmental temperatures drove a shift in community structure. By going from 0° to 30°C, there is a shift in the balance of the populations with different trophic strategy in the ecosystem. At low temperatures strict autotrophic plankton dominate the community, but with increasing temperature, the balance moves toward more heterotrophic populations.

This shift was achieved without assigning differential temperature sensitivities for phototrophic and kinetic metabolism, as suggested by Gillooly et al. (2001), Allen et al. (2005), Rose and Caron (2007) and Wilken et al. (2013).

These results shows that both ecology and physiology play a role in defining how temperature affects plankton community assembly. The model suggests that temperature pushes the balance of the community towards more heterotrophic populations. This dominance was true not only for the specialists, but also for the mixotrophs. To explain this relation, it is important to underline that communities were dominated by phytoplankton at low temperatures. This dominance may depend on the low growth rate of phytoplankton at these temperatures, which in turn causes phytoplankton to produce such a low amount of biomass that the heterotrophic strategy is not viable.

Mixotrophs arises before the strictly heterotrophic zooplankton with the increase of the temperature. The success of mixotrophs is based on the fact that they can outcompete zooplankton at low prey concentration, since they can also take up nutrients together with prey (Edwards, 2019). However, the degree of the success of mixotrophs depends also on the trade-off (i.e. superlinear trade-offs increase the success over sublinear trade-off). Finally, when temperatures are high enough to allow phytoplankton to have a high growth rate, zooplankton takes over mixotrophs.

Modelling and *in vitro* experiments should take into account the possibility that physiology is not enough to define the success of a population at different temperatures. If the metabolic rate and its response to different temperatures are at the base of ecological patterns such as growth rate and mortality rate (Brown et al., 2004), it is important to consider that also ecological interactions play as well an important role in the success of organisms with different trophic strategies. However, the mixotrophic success in a community depends also on the trophic trade-off as showed in the next section.

Mixotrophy is a viable strategy even with sublinear trade-offs

The same model from the previous section also showed that the best fit between observations from the GoN and simulations indicated a slightly sublinear shape of the trophic trade-off for the mixotrophic populations. A sublinear trade-off underlines that the trophic strategy of mixotrophs is less efficient than the trophic strategy of phytoplankton and zooplankton. This trade-off is relevant for both ocean ecology and biogeochemistry and it is also shown by observations. For example, Tang (1995) showed that flagellates are less efficient than diatoms in nutrient uptake, while Pérez et al. (1997) showed that mixotrophic ciliates grow slower than copepods.

A potential sublinear trade-off partially explains why we do not see that every plankton organism is a mixotroph. If the mixotrophic strategy is not as efficient, or it is even less efficient, than the trophic strategy of the specialist, then the physiological costs partially play a role in weather or not mixotrophs are present in the ecosystem and how their population changes in time.

Despite these costs, however, we still see that the mixotrophic strategy is globally ubiquitous (Stoecker, 1998). How is it possible to solve this apparent contradiction between model and observations? According to Våge et al. (2013), if the trade-off in mixotrophs is sublinear, the costs must be surpassed by the benefits in some other way, and these benefits can be used to justify the capacity of mixotrophs to coexist with phytoplankton and zooplankton. For example, Ward et al. (2011) assumed that autotrophic uptake rate and heterotrophic grazing rate were limited by cell surface area, showed that mixotrophs can outcompete phytoplankton and zooplankton when resource encounters (nutrients

and prey) are low. Mixotrophs success is achieved because cell surface area loses its importance when the resource-encounter rate is diffusion limited.

Edwards (2019) proposed that the co-limitation between inorganic nutrients and carbon in specialists, can favour mixotrophs. Phytoplankton growth is limited by the acquisition of nutrients while being carbon replete thanks to photosynthesis. Zooplankton are limited by carbon, while being nutrient replete due to predation. Mixotrophs can flexibly balance both resources at the same time, and in case of environmental depletion of nutrients and/or carbon, they can use the two strategies to grow better than the limited phytoplankton and zooplankton.

A sublinear trade-off implies that the mixotrophic potential positive impact on carbon export is not around a 35% increase in sinking POC, as suggested in the no-trade-off case of Ward and Follows (2016), but more below 10%. Further implications for a similar model at steady state and climate changes will be listed in section 7.2.2 and 7.2.4

7.2.2 Chapter 4: The biogeochemical impacts of mixotrophy over long timescales

Latitudinal response to mixotrophy

Using a global ocean circulation model with one-degree resolution, Ward and Follows (2016) showed that mixotrophs have the capacity to increase average plankton size and export production. A potential unresolved question of this research was what would have happened to community structure and carbon cycle if the model was run until feedbacks between the surface ecology and the ocean interior reached a steady state. To answer this question it is possible to use the lower resolution EcoGEnIE model to simulate the system over the ten-thousand year timescales required to reach equilibrium.

Chapter 4 showed that the global scale biogeochemical response was more complex than the simple and universal increase in oceanic carbon sequestration that might be concluded from Ward and Follows (2016). EcoGEnIE confirmed that mixotrophy frequently increases plankton size and carbon export, but also revealed that mixotrophs do not necessary increase carbon sequestration at all latitudes. Low and high latitude regions showed a different response when comparing model configurations with and without mixotrophs.

At low latitudes, the inclusion of mixotrophy increased size and carbon export, as expected from the results of Ward and Follows (2016). However, at high latitudes adding mixotrophs only increased size while, counterintuitively, export production declined because the addition of mixotrophs to the model led to the suppression of seasonal plankton blooms at high latitudes. This difference was caused by the high resilience of mixotrophs, during the unproductive winter season: zooplankton biomass crashed during the cold

season due to the lack prey, while mixotrophs survived by supplementing their diet with photosynthesis. Thus, mixotrophs flexibility created a tighter coupling between production and grazing in the early spring, which suppressed a part of the growth during the blooming phase. However it is important to notice that the model lacks diatoms, which dominate high latitudinal blooms (Alvain et al., 2013), and which presence account for 40% of total marine primary production (Field et al., 1998) and 40% of POC export (Jin et al., 2006). Due to these differences, real oceans might be much more productive than the modelled ocean, and they might also export more carbon at depth. Mixotrophs can feed on diatoms blooms (do Rosário Gomes et al., 2014), which can imply that in the model there was a lower growth for the mixotrophic strategy, which can then decrease the overall carbon export.

As in Ward and Follows (2016), the magnitude of the differences between Two-Guild and Mixotrophic configuration represented an upper limit, and since in Chapter 2 it was showed that mixotrophs may have a sublinear trade-off, the final differences in size and export, between a model with and without mixotrophs, are smaller than showed in this chapter (Table 7.1).

TABLE 7.1: Summary of the global average increases between Mixotrophic configurations in the pre-industrial scenario and the Two-guild configuration in the same scenario. PP=Primary production (mmol C m^{-3} d^{-1}), ESD=size (μm) EP=Export production (POC mol m^{-2} yr^{-1}).

Configuration	**PP**	**ESD**	**EP**
Mixotrophic	0.019	19.5	0.35
Mixotrophic-Plus$_{100}$	0.013	10.4	0.26
Mixotrophic-Plus$_{60}$	0.009	4.6	0.10
Mixotrophic-Plus$_{50}$	0.007	3.2	0.06
Mixotrophic-Plus$_{40}$	0.005	1.7	0.02

North Atlantic Deep Waters

The NADW is a dense water mass (due to low temperature and high salinity) that originates in the subpolar regions of the North Atlantic (Dickson and Brown, 1994). With its sinking, the NADW is one of the main locations of carbon sequestration in the global ocean (Baker et al., 2022). The coupling between autotrophs and mixotrophs in the Mixotrophic configuration, in the North Atlantic, leads to a decrease in carbon export. The DIC inventory at depth, over 10,000 years, decreases as the the combined action of NADW subduction and waning strength of the BCP occur in the North Atlantic.

A low DIC concentration in the NADW was already showed in the Two-Guild configuration cGenie and Ecogenie from (Ward et al., 2018, Figure 9), and also in the observations coming from the Global Ocean Data Analysis Project version 2 (GLODAPv2; Olsen et al., 2016). The presence of mixotrophs decreased the surface concentration of

DIC in the North Atlantic at surface due to their capacity of suppressing phytoplankton bloom, and in this way they amplified the decrease in the amount of carbon in the deep waters.

This is relevant to the study of climate changes because it was suggested, by models and observations (Collins et al., 2019), that the strength of the North Atlantic thermohaline circulation could decrease due to global warming. If the capacity of increasing the strength of the BCP in mixotrophs (Ward and Follows, 2016), in the North Atlantic, is also due to this downward flux of waters, then mixotrophs could lose a part of their capacity of decreasing the impact of climate changes (Table 7.2).

The presence of mixotrophs in a global model, at steady state, showed how the final outcome depends on long term phenomena such as the repeated suppression of blooms over millennial time scales and the slow transfer of carbon to depth via the global circulation system. Thus, it is important for future models that study mixotrophs to keep into account these long-term processes since the final picture is more complex than the initial increase in size and export suggested Ward and Follows (2016) and because there is a lasting impact on ocean biogeochemistry, which feedbacks on marine communities and also climate changes.

7.2.3 Chapter 5: Plankton latitudinal response to climate changes: ecological and geochemical implications

Numerous models have underlined the decrease in primary production and biomass caused by climate changes (Bopp et al., 2001; Cabré et al., 2015; Steinacher et al., 2010; Fu et al., 2016; Kwiatkowski et al., 2020). This impact is important to study because plankton also impact the carbon cycle which feedbacks on climate changes themselves. Mixotrophs can amplify the strength of the BCP, thus a possible hypothesis is that mixotrophs will increase ecosystem resistance to global warming. To test this idea, the EcoGEnIE model was used to compare the RCP8.5 scenario in a global ocean without (Chapter 5) and with (Chapter 6) mixotrophs.

The experimental setting prescribed in EcoGEnIE an increase in atmospheric carbon concentration, increasing in this way the global atmospheric average temperature which led to a net global shoaling of the mixed layer depth in world's oceans. The increased stratification caused a generalized decline in the quantity of nutrients supplied to the surface layer at all latitudes. These changes caused plankton to face new environmental conditions which forced a rearrangement of their community structure.

Two major latitudinal regimes, in terms of their response to climate changes, were generated by a warmer 21^{st} century: a low latitudinal regime where a decrease in nutrient supply caused a decrease in average cell diameter, primary and export production; and a high latitudinal regime, where a decrease in mainly light limitation, but also temperature

limitation, typical of the polar regions, caused plankton to grow faster than before, and which increased average size, primary production and carbon export.

Plankton populations of different sizes changed their environmental boundaries: picophytoplankton, usually found mostly in the equatorial subtropical regions, expanded toward the temperate and subpolar latitudes because the global increase in stratification also caused a global decrease in phosphorus supply, and thus phosphorus concentration, creating oligotrophic conditions to the detriment of the largest photoautotrophs; nanophytoplankton, usually dominant in the subpolar and extreme high latitudes, decreased in concentration because they were outcompeted by picophytoplankton in terms of nutrient requirement; microphytoplankton, mostly found in the temperate regions, expanded poleward because the higher temperatures and the increase in shoaling of the mixed layer moved plankton closer to surface in the high latitudes, increasing light availability.

These results are largely within the boundary of previous research: it was predicted a decrease in most environmental and ecological variables, from nutrient concentration (Bopp et al., 2001; Cabré et al., 2015; Kwiatkowski et al., 2020), to primary and export production (Steinacher et al., 2010; Fu et al., 2016), and a differential regional regime, causing a decrease at low latitude (Bopp et al., 2001; Steinacher et al., 2010) and an increase in the Southern Ocean (Steinacher et al., 2010) in term of productivity and carbon export.

The overall change, however, was a net global decrease in biomass, size, primary production and export production. These changes can be summarised as an overall detrimental effect on plankton communities and the carbon export. A decreased export production can exacerbate climate changes because the strength of the BCP decreases, generating a positive feedback loop that could enhance the impact of climate warming (Cabré et al., 2015). The poleward expansion of subtropical and temperate condition caused many populations to change their geographical distribution.

Given thee presented and other experimental results mentioned above, it is possible to conclude that climate changes have serious effect on community structure and carbon cycle, which could lead to larger changes if positive feedback are established. However, all these experiments lacked mixotrophs and their capacity to increase the strength of the BCP, which have the potential of limiting the impact of climate changes on plankton communities and the carbon cycle by increasing community resistance. This addition can alter the overall outcome of our predictions, improving our understanding of climate changes, and can also justify the inclusion of mixotrophs in the simulation summarized in the next section.

7.2.4 Chapter 6: The biogeochemical impacts of mixotrophy in a future warmer world

Similarly to the previous chapter, the Control and the RCP8.5 scenario were compared to see the impact of climate changes on plankton community and biogeochemical cycles. However, this time, the Mixotrophic configuration was tested with the Two-Guild configuration to asses the impact of mixotrophs in a warmer 21^{st} century. As explained in previous section, mixotrophs can increase the strength of the BCP, thus there is the possibility for mixotrophs to enhance the resistance of community function in a climate change scenario.

The experiments performed with EcoGEnIE suggested that mixotrophs enhance the climate impacts already seen with the Two-Guild configuration. Both increasing and decreasing trends were exacerbated: size and export declined even more at low latitudes, and increased even more at high latitudes. However, despite the fact that the final global net result saw again an overall decrease in nutrient concentration, biomass, average cell size, production and export as in models without mixotrophs (Bopp et al., 2001; Steinacher et al., 2010; Cabré et al., 2015; Fu et al., 2016; Moore et al., 2018; Kwiatkowski et al., 2020), mixotrophs were capable of decreasing the magnitude of the impacts in terms of carbon biomass, primary production and export production (Table 7.2).

TABLE 7.2: Summary of the net global average changes caused by the RCP8.5 scenario in each ecological configuration. PP=Primary production, EP=Export production.

Configuration	**[PO4]**	**C biomass**	**ESD**	**PP**	**EP**
Two-Guild	-12.6%	-6.1%	-1.9%	-7.5%	-5.1%
Mixotrophic	-13.8%	-5.1%	-2.4%	-5.6%	-4.5%
Mixotrophic-Plus$_{100}$	-14.0%	-5.4%	-2.6%	-6.5%	-4.9%

By accounting for the difference between Two-Guild and the mixotrophic configurations in the RCP8.5 scenario (Table 7.3), it is also possible to see how much mixotrophs increase the resistance of the system to climate warming.

TABLE 7.3: Summary of the global average increases between Mixotrophic configurations in RCP8.5 scenario and the Two-guild configuration in the same scenario. PP=Primary production (mmol C m^{-3} d^{-1}), ESD=size (μm) EP=Export production (POC mol m^{-2} yr^{-1}).

Configuration	**PP**	**ESD**	**EP**
Mixotrophic	0.021	18.7	0.34
Mixotrophic-Plus$_{100}$	0.013	9.8	0.23

The results from Table 7.3 confirm that mixotrophs do indeed decrease the impact of climate changes if compared to a system without mixotrophs, however, according to Table 7.2, they do not seem to be able to stop the potential positive feedback loop between waning BCP and increasing CO_2 atmospheric concentrations. This conclusion becomes even more relevant if we consider that this result was obtained by using mixotrophs without any trophic trade-off, which is an unlikely scenario. For this reason, further sensitivity test were produced to establish the impact of the mixotrophic compromise between autotrophic and heterotrophic way of feeding.

Trophic trade-off and climate changes

Together with the Two-Guild and the Mixotrophic configuration, four other experiments were performed, but with the Mixotrophic-Plus configuration with different values of trade-off (sublinear, linear, superlinear and no trade-off at all). These settings were tested again within the Control and the RCP8.5 scenarios. These tests shed light on the impact of the trophic trade-off on community structure and the global carbon cycle. By going from the idealized condition of no trade-off at all in mixotrophs, to a sublinear condition, it was possible to establish that the enhancement seen in the comparison between Two-Guild and Mixotrophic configuration were decreased (Table 7.4). In other words, the higher the costs for the trophic trade-off is, the smaller the difference between the two configurations becomes.

TABLE 7.4: Summary of the global average increases between Mixotrophic configurations with different trophic trade-offs in RCP8.5 scenario and the Two-guild configuration in the same scenario. PP=Primary production (mmol C m^{-3} d^{-1}), ESD=size (μm) EP=Export production (POC mol m^{-2} yr^{-1}).

Configuration	**PP**	**ESD**	**EP**
Mixotrophic	0.021	18.7	0.34
Mixotrophic-Plus$_{100}$	0.013	9.8	0.23
Mixotrophic-Plus$_{60}$	0.012	4.5	0.11
Mixotrophic-Plus$_{50}$	0.011	3.1	0.07
Mixotrophic-Plus$_{40}$	0.009	1.8	0.04

This cost is relevant because in Chapter 2 it was shown that mixotrophs may have a sublinear trade-off which would erode the capacity of mixotrophs to decrease the impact of climate changes.

7.3 Study limitations

The presented models from Gibbs et al. (2020a) and Ward et al. (2018) are simplified representations of plankton communities and biogeochemical cycles, with simplifies ecology. They are unable to make accurate predictions or to fully reproduce modern day observations. Due to this inaccuracy, they were applied in this thesis only with the purpose of exploring the impact of eco-physiological observations (size, trophic strategy) on a small and on a global scale. This level of abstraction allowed the simulation to run within a useful time-frame, but also to infer what role each single element plays in determining how plankton self-assemble their communities.

The EcoGEnIE model was limited by a crude representation of the microbial loop, which is an important step in the carbon cycle. The models were designed to show what are the implications of the presence or absence of mixotrophs in a simulated plankton community. How mixotrophs and the microbial loop, or any other non-simulated property of marine system, interact when they are coupled together in the same environment remain to be seen. The level of ecological complexity of the models was high enough to permit the assessment of properties such as size and trophic strategy, but not enough to take into account, for example, different shapes of plankton bodies or different kinds of mixotrophic functional groups (i.e. phytoplankton that eat or photosynthetic zooplankton Stoecker, 1999) which limits the study of phenomena such as the kleptoplasty and mixotrophic symbiosis.

Temperature sensitivity changes in plankton with different metabolisms (Wilken et al., 2013) (more in the next section) and it is only one of the many factors that impact marine community structures and that were not tested in the model. Example of these factors are water pH or UV irradiance, which will change in a climate change scenario. UV exposure in particular will increases because, on average, plankton will get closer to the surface with the shoaling of the MLD. González-Olalla et al. (2019) suggested that "stratification traps" (shallow mixed layer with high temperatures and ultraviolet irradiance) can cause mixotrophs to become more autotrophic to dissipate the excessive light into heat and protect themselves from the photodamage (Halac et al., 2014).

7.4 Future directions

Rising temperatures impact more the grazing metabolism than the photoautotrophic metabolism. This is due to the dissimilar activation energy of cellular respiration and photosynthesis, and to the carbon fixation activity of RuBisCO which decreases with increasing temperatures in favour of the photorespiration activity. In summary, by going from 0° to 40°C, there is a 4-fold increase of plankton photosynthesis and a 16-fold increase in the kinetic metabolism (Wilken et al., 2013).

Future oceans will become warmer and generally more oligotrophic. Therefore, future scenarios could see a physiological shift in plankton communities toward a more mixotrophic-heterotrophic-based ecology. This outcome in turn could change total biomass distribution in plankton communities, and modify the strength of the BCP. By using again the EcoGEnIE model, and fitting the temperature dependence of the autotrophic an the heterotrophic growth rate, it will be possible to see changes in a future warmer world, ocean nutrient and chlorophyll concentrations, average plankton size, primary production and export production. These changes then will be compared to a model with grazing and phototropic metabolism with the same dependence for temperatures, and what is the impact of a mixotrophs shifting toward the more heterotrophic portion of the trophic spectrum. The main hypothesis is that mixotrophs decrease their nutrient uptake in favor of their grazing activity, which will cause a decrease in the strength of the BCP.

Another possible starting point for future investigations would be the study of the Paleocene–Eocene Thermal Maximum (PETM). This 4-5°C increase in the average global temperatures, that lasted 100,000 years, occurred 55 million years ago. The fossil record, associated to this time frame, shows an increase in the mixotrophic percentage (*Apectodinium*) in the community composition (Sarkar et al., 2022).

Such shift in environmental conditions is an analogue of present climate changes. Changes in plankton community structure and strength of the BCP due to increasing temperature can be related to present times, offering insight in future oceans. The experimental setting can be done by replicating the experiment performed by Wilson et al. (2018), which used EcoGEnIE, and by adding the Mixotrophic and Mixotrophic-Plus configuration. As in the original research, the simulations will involve a global setting with a Paleocene early–Eocene scenario (continental masses, temperatures, current pattern etc.). In this way, it will be possible to replicate similar condition to the PETM, and to resolve what is the role of mixotrophs in such scenario.

A long-term objective would be that of replicating again the experiment from Gibbs et al. (2020a) with the use of EcoGEnIE.

The original 0D model, used in that research, captured the evolutionary pattern by allowing plankton to move from one point to the other of the trait-space through mutations. These mutations corresponded to the invasion of plankton biomass in the adjacent cells of the grid with each new generation. Then, through natural selection (i.e. environmental conditions) only the most fitted populations were allowed to survive. In this context, phytoplankton became larger and passed across different stages of mixotrophy, from the more autotrophic mixotrophs to the more heterotrophic mixotrophs.

The fossil record shows that after the K–Pg boundary, autotrophs increased in size and became more heterotrophic in a 2 million year time frame, which was correctly simulated by Gibbs et al. (2020a). However, due to the lack of spatial resolution in the model, the

results did not show the lagging recovery of the North Atlantic mixotrophs compared to faster recovery rate of the the mixotrophs of the South Atlantic and the Pacific Ocean.

In order to explore this difference, the generic mixotrophic populations associated to the presented Mixotrophic-Plus configuration of EcoGEnIE should be increased in number, and assigned different values for the mixotrophic balance between autotrophy and heterotrophy. In this way the full mixotrophic spectrum should be obtained for each of the elements of the grid in the global simulated ocean. With this improvement, it should be possible to document the physiological differences between different ocean basins. To resolve evolution, a mutation matrix should be added to the system and the "everything is everywhere" option should be turned off since it does not allow plankton extinction.

Overall, the next big questions that should be investigated lie in the understanding of the real shape of the mixotrophic trade-off, since the shape presented in this research is just a tentative and very simplified step in a much more complex physiological framework. Additionally, my research did not take into account the existence of possible different kinds of mixotrophs (i.e. phagocytic "algae" and photosynthetic "protozoa", Stickney et al., 2000), and the difference between constitutive and non-constitutive mixotrophy, which have an unrelated phylogenetic history and which are unlikely to impact marine communities in a similar manner. Further analyses should carefully weight the importance of these kinds of mixotrophs on the biogeochemical cycle, especially on the carbon cycle.

Broader, deeper questions, regard the role and the place of mixotrophs in the tree of life: given that mixotrophy is not the exception, but rather the rule among unicellular organisms, why don't we see the same rule applied also to multicellular organisms (i.e. classic dichotomy of land plants - embryophyta - versus animals - metazoa)? Is there a metabolic or physiological barrier that prevents mixotrophs to achieve multicellular forms? Is this barrier linked to the shape of the trade-off? And if it is linked to the trade-off, is this "metabolic burden" another proof of the inefficiency of the mixotrophic strategy compared to the trophic strategies of the specialists? According to Millette et al. (2023), our knowledge about mixotrophs lags behind our knowledge about autotrophs and heterotrophs. Given the global geographical and phylogenetical distribution of the mixotrophic strategy in the oceans, it seems that the analysis of these organisms have still a lot to tell about the past, the present and the future of marine communities, and their relation with their ever-changing environment.

7.5 Conclusion

The experimental setting in this thesis showed the potential of using the trait-based approach, and how the resolution of the mixotrophic trade-off, together with size, allowed the analysis of the eco-physiology of mixotrophs. Trade-offs helps us to constrain

plankton growth in our models, and improve out knowledge of the biological world. This thesis further shows that mixotrophs not only impact community structure and the biogeochemical cycle in the present, but they will keep impacting them in a future warmer world.

The trophic trade-off defines the life of what seems to be an ubiquitous strategy in our oceans, therefore its inclusion must be kept into account if we want to understand the impact of these organisms on the rest of the community. Trait-based modelling gives us the possibility of studying mixotrophs by leaving behind assumptions linked to taxonomical and functional classification.

This work is a step toward a much longer research needed to understand the complex phenomenon of mixotrophy. Additional experimental work (modelling, *in vitro* and *in situ*) and observations, are necessary before drawing more conclusive understandings on the trophic trade-off and its impact on communities. Further experiments are also necessary to better constrain plankton traits and their eco-physiological trade-offs to make more accurate predictions about the role of mixotrophy in present and future plankton communities. In this thesis, it was showed that mixotrophs play a role in defining community structure, plankton function and biogeochemical cycles. Thus future experiments must take into account mixotrophs and their eco-physiology, witch particular attention to their trophic trade-off. Furthermore, temperature sensitivity experiments will need to take into account ecology together with physiology if they want to correctly interpret their results.

Appendix A

Ecological feedback

Initial experiments with the Mixotrophic-Plus configuration of the model revealed some unexpected behaviours. It was expected that an increase in the mixotrophic penalty given by the trade-off (i.e. going from a superlinear to a sublinear trade-off) would lead to increasing concentrations of dissolved phosphorus. This consideration came from the fact that it is assumed that less efficient mixotrophs (with a sublinear trade-off) are less able to deplete nutrients in the water column (Ward et al., 2018). However, this assumption was shown to be incorrect for simulations with a value for the trade-off parameter, τ less than 0.25. Below this threshold there was a decrease in ocean average phosphorus concentration (Figure A.1a).

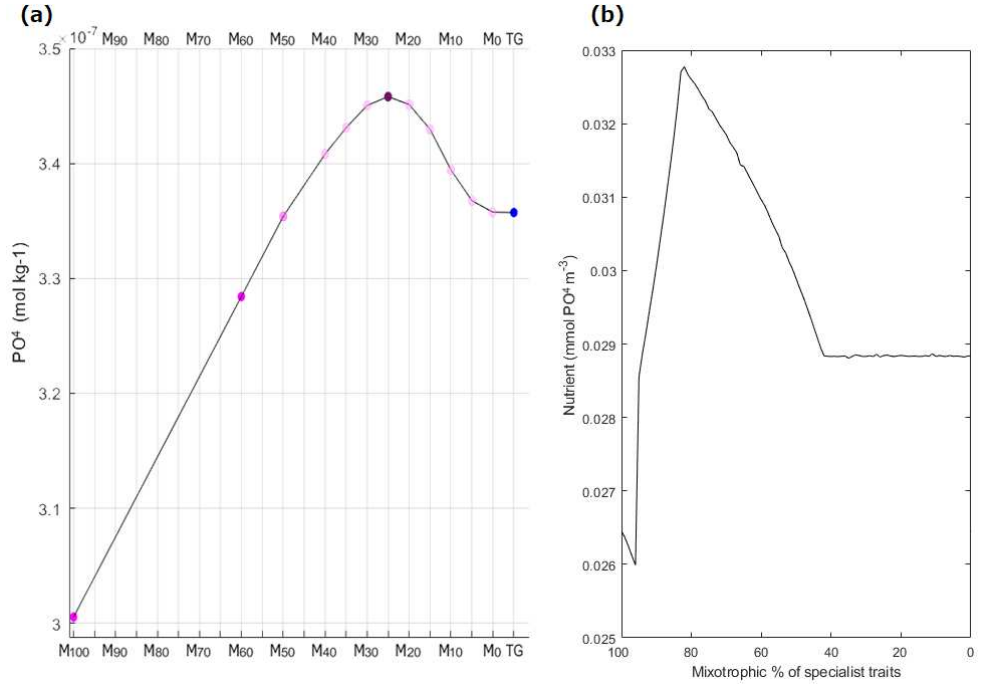

FIGURE A.1: Impact of the mixotrophic trade-off on nutrient concentration. **(a)** Change in global average surface phosphate concentration during the historical transient simulations in EcoGEnIE. **(b)** Nutrient concentration in the idealised model.

It was not clear from the simulations whether this response was attributable to ecological interactions, ocean circulation, spatial effects or seasonal dynamics. To address this uncertainty, a simplified version of the EcoGEnIE ecosystem was set up in a non-spatial environment. This simplified model had no spatial structure and could be run to equilibrium without the influence of spatial structure, ocean circulation or seasonality. The new model included the same 24 populations (8 size classes and 3 trophic classes) as the full simulation. The physiological parameters and differential equations were the same as in Chapter 2.

This new model was run for 100 years to equilibrium across a range of values for the mixotrophic trade-off parameter τ. Figure A.1(b) shows the nutrient concentration in the idealised model. This simulation produced the same qualitative pattern as EcoGEnIE, with nutrient concentrations declining as the trade-off value increases.

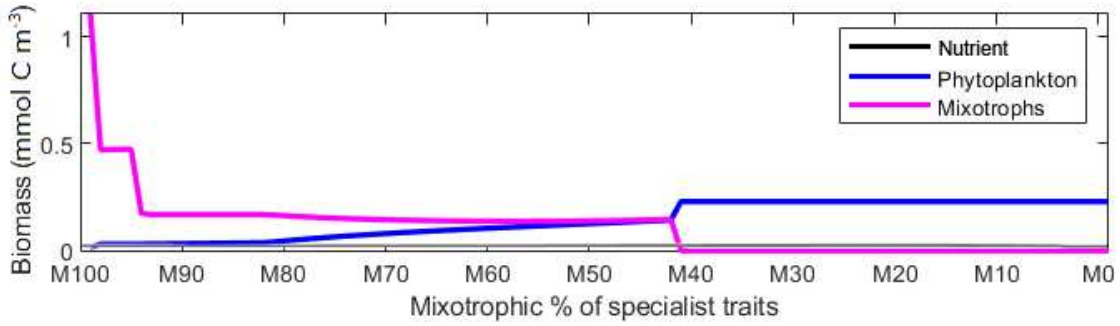

FIGURE A.2: Impact of the mixotrophic physiology and phytoplankton uptake efficiency on plankton biomass.

Figures A.2 shows the same simulation from Figure A.1(b), but this time together with nutrient concentration, it also shows plankton biomass of phytoplankton and mixotrophs. Below the 0.4 trade-off (M_{40}), there is no mixotrophic population. Mixotrophs associated with this strongly sub-linear trade-off are outcompeted by phytoplankton, thus their impact on phosphorus concentration does not follow the expected pattern, which is a function of phytoplankton uptake rate and zooplankton grazing.

Bibliography

Agawin, N. S., Duarte, C. M., and Agustí, S. Nutrient and temperature control of the contribution of picoplankton to phytoplankton biomass and production. *Limnology and oceanography*, 45(3):591–600, 2000.

Allen, A., Gillooly, J., and Brown, J. Linking the global carbon cycle to individual metabolism. *Functional Ecology*, 19(2):202–213, 2005.

Alvain, S., Le Quéré, C., Bopp, L., Racault, M.-F., Beaugrand, G., Dessailly, D., and Buitenhuis, E. T. Rapid climatic driven shifts of diatoms at high latitudes. *Remote Sensing of Environment*, 132:195–201, 2013.

Andersen, K. H., Aksnes, D. L., Berge, T., Fiksen, , and Visser, A. Modelling emergent trophic strategies in plankton. *Journal of Plankton Research*, 37(5):862–868, 08 2015. ISSN 0142-7873.

Anderson, L. A. and Sarmiento, J. L. Redfield ratios of remineralization determined by nutrient data analysis. *Global biogeochemical cycles*, 8(1):65–80, 1994.

Anderson, T. R. Plankton functional type modelling: running before we can walk? *Journal of Plankton Research*, 27(11):1073–1081, 2005.

Archer, D. and Johnson, K. A model of the iron cycle in the ocean. *Global Biogeochemical Cycles*, 14(1):269–279, 2000.

Armstrong, R. A. Grazing limitation and nutrient limitation in marine ecosystems: steady state solutions of an ecosystem model with multiple food chains. *Limnology and Oceanography*, 39(3):597–608, 1994.

Armstrong, R. A. Nutrient uptake rate as a function of cell size and surface transporter density: A michaelis-like approximation to the model of pasciak and gavis. *Deep Sea Research Part I: Oceanographic Research Papers*, 55(10):1311–1317, 2008.

Armstrong, R. A., Lee, C., Hedges, J. I., Honjo, S., and Wakeham, S. G. A new, mechanistic model for organic carbon fluxes in the ocean based on the quantitative association of poc with ballast minerals. *Deep Sea Research Part II: Topical Studies in Oceanography*, 49(1-3):219–236, 2001.

Asselot, R., Lunkeit, F., Holden, P. B., and Hense, I. The relative importance of phytoplankton light absorption and ecosystem complexity in an earth system model. *Journal of Advances in Modeling Earth Systems*, 13(5):e2020MS002110, 2021.

Azam, F., Fenchel, T., Field, J. G., Gray, J. S., Meyer-Reil, L.-A., and Thingstad, F. The ecological role of water-column microbes in the sea. *Marine ecology progress series*, pages 257–263, 1983.

Baas-Becking, L. G. M. *Geobiologie of inleiding tot de milieukunde*. Number 18-19. WP Van Stockum & Zoon, 1934.

Bacastow, R. and Maier-Reimer, E. Ocean-circulation model of the carbon cycle. *Climate dynamics*, 4:95–125, 1990.

Baird, M. E. and Suthers, I. M. A size-resolved pelagic ecosystem model. *Ecological Modelling*, 203(3):185–203, 2007.

Baker, C. A., Martin, A. P., Yool, A., and Popova, E. Biological carbon pump sequestration efficiency in the north atlantic: a leaky or a long-term sink? *Global biogeochemical cycles*, 36(6):e2021GB007286, 2022.

Banas, N. S. Adding complex trophic interactions to a size-spectral plankton model: Emergent diversity patterns and limits on predictability. *Ecological Modelling*, 222 (15):2663–2675, 2011. ISSN 0304-3800.

Baretta-Bekker, J., Baretta, J., Hansen, A., and Riemann, B. An improved model of carbon and nutrient dynamics in the microbial food web in marine enclosures. *Aquatic microbial ecology*, 14(1):91–108, 1998.

Barton, A. D., Finkel, Z. V., Ward, B. A., Johns, D. G., and Follows, M. J. On the roles of cell size and trophic strategy in north atlantic diatom and dinoflagellate communities. *Limnology and Oceanography*, 58(1):254–266, 2013.

Benndorf, J., Böing, W., Koop, J., and Neubauer, I. Top-down control of phytoplankton: the role of time scale, lake depth and trophic state. *Freshwater biology*, 47(12):2282–2295, 2002.

Bopp, L., Monfray, P., Aumont, O., Dufresne, J.-L., Le Treut, H., Madec, G., Terray, L., and Orr, J. C. Potential impact of climate change on marine export production. *Global Biogeochemical Cycles*, 15(1):81–99, 2001.

Bopp, L., Resplandy, L., Orr, J. C., Doney, S. C., Dunne, J. P., Gehlen, M., Halloran, P., Heinze, C., Ilyina, T., Seferian, R., et al. Multiple stressors of ocean ecosystems in the 21st century: projections with cmip5 models. *Biogeosciences*, 10(10):6225–6245, 2013.

Brown, J. H., Gillooly, J. F., Allen, A. P., Savage, V. M., and West, G. B. Toward a metabolic theory of ecology. *Ecology*, 85(7):1771–1789, 2004.

Cabré, A., Marinov, I., and Leung, S. Consistent global responses of marine ecosystems to future climate change across the ipcc ar5 earth system models. *Climate dynamics*, 45:1253–1280, 2015.

Caperon, J. Population growth response of isochrysis galbana to nitrate variation at limiting concentrations. *Ecology*, 49(5):866–872, 1968.

Carr, M.-E., Friedrichs, M. A., Schmeltz, M., Aita, M. N., Antoine, D., Arrigo, K. R., Asanuma, I., Aumont, O., Barber, R., Behrenfeld, M., et al. A comparison of global estimates of marine primary production from ocean color. *Deep Sea Research Part II: Topical Studies in Oceanography*, 53(5-7):741–770, 2006.

Castellani, M., Våge, S., Strand, E., Thingstad, F., and Giske, J. The scaled subspaces method: a new trait-based approach to model communities of populations with largely inhomogeneous density. *Ecological Modelling*, 251:173–186, 2012.

Chan, Y.-F., Chiang, K.-P., Ku, Y., and Gong, G.-C. Abiotic and biotic factors affecting the ingestion rates of mixotrophic nanoflagellates (haptophyta). *Microbial ecology*, 77: 607–615, 2019.

Cheung, W. W. L., Dunne, J., Sarmiento, J. L., and Pauly, D. Integrating ecophysiology and plankton dynamics into projected maximum fisheries catch potential under climate change in the Northeast Atlantic. *ICES Journal of Marine Science*, 68(6): 1008–1018, 04 2011. ISSN 1054-3139.

Chisholm, S. W. Phytoplankton size. *Primary productivity and biogeochemical cycles in the sea*, pages 213–237, 1992.

Christensen, V. and Pauly, D. Ecopath ii—a software for balancing steady-state ecosystem models and calculating network characteristics. *Ecological modelling*, 61(3-4): 169–185, 1992.

Claussen, M., Mysak, L., Weaver, A., Crucifix, M., Fichefet, T., Loutre, M.-F., Weber, S., Alcamo, J., Alexeev, V., Berger, A., et al. Earth system models of intermediate complexity: closing the gap in the spectrum of climate system models. *Climate dynamics*, 18:579–586, 2002.

Coale, K. H., Johnson, K. S., Fitzwater, S. E., Gordon, R. M., Tanner, S., Chavez, F. P., Ferioli, L., Sakamoto, C., Rogers, P., Millero, F., et al. A massive phytoplankton bloom induced by an ecosystem-scale iron fertilization experiment in the equatorial pacific ocean. *Nature*, 383(6600):495–501, 1996.

Collins, M., Sutherland, M., Bouwer, L., Cheong, S.-M., Frolicher, T., DesCombes, H. J., Roxy, M. K., Losada, I., McInnes, K., Ratter, B., et al. Extremes, abrupt changes and managing risk. 2019.

Conkright, M. E., Locarnini, R. A., Garcia, H. E., O'Brien, T. D., Boyer, T. P., Stephens, C., and Antonov, J. I. World ocean atlas 2001: Objective analyses, data statistics, and figures: Cd-rom documentation. 2002.

D'Alelio, D., Mazzocchi, M. G., Montresor, M., Sarno, D., Zingone, A., Di Capua, I., Franzè, G., Margiotta, F., Saggiomo, V., and Ribera d'Alcalà, M. The green–blue swing: plasticity of plankton food-webs in response to coastal oceanographic dynamics. *Marine Ecology*, 36(4):1155–1170, 2015.

Dawson, S. K., Carmona, C. P., González-Suárez, M., Jönsson, M., Chichorro, F., Mallen-Cooper, M., Melero, Y., Moor, H., Simaika, J. P., and Duthie, A. B. The traits of "trait ecologists": An analysis of the use of trait and functional trait terminology. *Ecology and Evolution*, 11(23):16434–16445, 2021.

De Vargas, C., Audic, S., Henry, N., Decelle, J., Mahé, F., Logares, R., Lara, E., Berney, C., Le Bescot, N., Probert, I., et al. Eukaryotic plankton diversity in the sunlit ocean. *Science*, 348(6237):1261605, 2015.

Denman, K. L. Modelling planktonic ecosystems: parameterizing complexity. *Progress in Oceanography*, 57(3-4):429–452, 2003.

DeVries, T., Primeau, F., and Deutsch, C. The sequestration efficiency of the biological pump. *Geophysical Research Letters*, 39(13), 2012.

DeVries, T. and Weber, T. The export and fate of organic matter in the ocean: New constraints from combining satellite and oceanographic tracer observations. *Global Biogeochemical Cycles*, 31(3):535–555, 2017.

Dickson, R. R. and Brown, J. The production of north atlantic deep water: sources, rates, and pathways. *Journal of Geophysical Research: Oceans*, 99(C6):12319–12341, 1994.

Dierssen, H. M. Perspectives on empirical approaches for ocean color remote sensing of chlorophyll in a changing climate. *Proceedings of the National Academy of Sciences*, 107(40):17073–17078, 2010.

do Rosário Gomes, H., Goes, J. I., Matondkar, S. P., Buskey, E. J., Basu, S., Parab, S., and Thoppil, P. Massive outbreaks of noctiluca scintillans blooms in the arabian sea due to spread of hypoxia. *Nature Communications*, 5(1):4862, 2014.

Droop, M. R. Vitamin b12 and marine ecology. iv. the kinetics of uptake, growth and inhibition in monochrysis lutheri. *Journal of the Marine Biological Association of the United Kingdom*, 48(3):689–733, 1968.

Ducklow, H. W., Steinberg, D. K., and Buesseler, K. O. Upper ocean carbon export and the biological pump. *Oceanography*, 14(4):50–58, 2001.

Dutkiewicz, S., Ward, B. A., Monteiro, F., and Follows, M. J. Interconnection of nitrogen fixers and iron in the pacific ocean: Theory and numerical simulations. *Global Biogeochemical Cycles*, 26(1), 2012.

D'Alelio, D., Libralato, S., Wyatt, T., and d'Alcalà, M. R. Ecological-network models link diversity, structure and function in the plankton food-web. *Scientific Reports*, 6, 2016a.

D'Alelio, D., Libralato, S., Wyatt, T., and d'Alcalà, M. R. Supplementary information: Ecological-network models link diversity, structure and function in the plankton food-web. *Scientific Reports*, 6, 2016b.

Edwards, K. F. Mixotrophy in nanoflagellates across environmental gradients in the ocean. *Proceedings of the National Academy of Sciences*, 116(13):6211–6220, 2019. ISSN 0027-8424.

Edwards, K. F., Thomas, M. K., Klausmeier, C. A., and Litchman, E. Allometric scaling and taxonomic variation in nutrient utilization traits and maximum growth rate of phytoplankton. *Limnology and Oceanography*, 57(2):554–566, 2012.

Edwards, N. and Shepherd, J. Bifurcations of the thermohaline circulation in a simplified three-dimensional model of the world ocean and the effects of inter-basin connectivity. *Climate dynamics*, 19:31–42, 2002.

Edwards, N. R. and Marsh, R. Uncertainties due to transport-parameter sensitivity in an efficient 3-d ocean-climate model. *Climate dynamics*, 24:415–433, 2005.

Edwards, N. R., Willmott, A. J., and Killworth, P. D. On the role of topography and wind stress on the stability of the thermohaline circulation. *Journal of physical oceanography*, 28(5):756–778, 1998.

Emerson, S. Annual net community production and the biological carbon flux in the ocean. *Global Biogeochemical Cycles*, 28(1):14–28, 2014.

Eppley, R. W. and Peterson, B. J. Particulate organic matter flux and planktonic new production in the deep ocean. *Nature*, 282(5740):677–680, 1979.

Falkowski, P. G. Evolution of the nitrogen cycle and its influence on the biological sequestration of co2 in the ocean. *Nature*, 387(6630):272–275, 1997.

Falkowski, P. G. Rationalizing elemental ratios in unicellular algae. *Journal of Phycology*, 36(1):3–6, 2000.

Falkowski, P. G., Laws, E. A., Barber, R. T., and Murray, J. W. Phytoplankton and their role in primary, new, and export production. *Ocean biogeochemistry: The role of the ocean carbon cycle in global change*, pages 99–121, 2003.

Fiechter, J., Moore, A. M., Edwards, C. A., Bruland, K. W., Di Lorenzo, E., Lewis, C. V., Powell, T. M., Curchitser, E. N., and Hedstrom, K. Modeling iron limitation of primary production in the coastal gulf of alaska. *Deep Sea Research Part II: Topical Studies in Oceanography*, 56(24):2503–2519, 2009.

Field, C. B., Behrenfeld, M. J., Randerson, J. T., and Falkowski, P. Primary production of the biosphere: integrating terrestrial and oceanic components. *science*, 281(5374): 237–240, 1998.

Fischer, R., Giebel, H.-A., Hillebrand, H., and Ptacnik, R. Importance of mixotrophic bacterivory can be predicted by light and loss rates. *Oikos*, 126(5):713–722, 2017.

Fischer, W. W., Hemp, J., and Johnson, J. E. Evolution of oxygenic photosynthesis. *Annual Review of Earth and Planetary Sciences*, 44:647–683, 2016.

Flynn, K. J., Stoecker, D. K., Mitra, A., Raven, J. A., Glibert, P. M., Patricia, M., Hansen, P. J., Granéli, E., and Burkholder, J. M. Misuse of the phytoplankton–zooplankton dichotomy: the need to assign organisms as mixotrophs within plankton functional types. *Journal of Plankton Research*, 35(1):3–11, 2013.

Follows, M. J., Dutkiewicz, S., Grant, S., and Chisholm, S. W. Emergent biogeography of microbial communities in a model ocean. *Science*, 315, 2007.

Fu, W., Randerson, J. T., and Moore, J. K. Climate change impacts on net primary production (npp) and export production (ep) regulated by increasing stratification and phytoplankton community structure in the cmip5 models. *Biogeosciences*, 13 (18):5151–5170, 2016.

Garcia, H., Locarnini, R., Boyer, T., Antonov, J., Zweng, M., Baranova, O., and Johnson, D. Volume 4: Nutrients (phosphate, nitrate, silicate), world ocean atlas 2009, s. *Levitus, Ed., NOAA Atlas NESDIS*, 71, 2010.

Garland, T. Trade-offs. *Current Biology*, 24(2):R60–R61, 2014.

Geider, R. J. and La Roche, J. Redfield revisited: variability of c [ratio] n [ratio] p in marine microalgae and its biochemical basis. *European Journal of Phycology*, 37(1): 1–17, 2002.

Geider, R. J., Maclntyre, H. L., and Kana, T. M. A dynamic regulatory model of phytoplanktonic acclimation to light, nutrients, and temperature. *Limnology and oceanography*, 43(4):679–694, 1998.

Gentleman, W. and Neuheimer, A. Functional responses and ecosystem dynamics: how clearance rates explain the influence of satiation, food-limitation and acclimation. *Journal of Plankton Research*, 30(11):1215–1231, 2008.

Gibbs, S. J., Bown, R., Ward, B. A., Alvarez, A., Kim, H., Archontikis, O. A., Sauterey, B., Poulton, A., Wilson, J., and Ridgwell, A. Algal plankton turn to hunting to survive and recover from end-cretaceous impact darkness. *Science Advances*, 6(44), 2020a.

Gibbs, S. J., Bown, R., Ward, B. A., Alvarez, A., Kim, H., Archontikis, O. A., Sauterey, B., Poulton, A., Wilson, J., and Ridgwell, A. Supplementary material for algal plankton turn to hunting to survive and recover from end-cretaceous impact darkness. *Science Advances*, 6(44), 2020b.

Gillooly, J. F., Brown, J. H., West, G. B., Savage, V. M., and Charnov, E. L. Effects of size and temperature on metabolic rate. *science*, 293(5538):2248–2251, 2001.

Godrijan, J., Drapeau, D., and Balch, W. Mixotrophic uptake of organic compounds by coccolithophores. *Limnology and Oceanography*, 65, 01 2020.

González-Olalla, J. M., Medina-Sánchez, J. M., and Carrillo, P. Mixotrophic trade-off under warming and uvr in a marine and a freshwater alga. *Journal of phycology*, 55 (5):1028–1040, 2019.

Grigoratou, M., Monteiro, F. M., Wilson, J. D., Ridgwell, A., and Schmidt, D. N. Exploring the impact of climate change on the global distribution of non-spinose planktonic foraminifera using a trait-based ecosystem model. *Global change biology*, 2021.

Guidi, L., Stemmann, L., Jackson, G. A., Ibanez, F., Claustre, H., Legendre, L., Picheral, M., and Gorskya, G. Effects of phytoplankton community on production, size, and export of large aggregates: A world-ocean analysis. *Limnology and Oceanography*, 54 (6):1951–1963, 2009.

Hain, M. P., Sigman, D., and Haug, G. The biological pump in the past. *Reference Module in Earth Systems and Environmental Sciences, Treatise on Geochemistry (Second Edition), The Oceans and Marine Geochemistry*, 8:485–517, 2014.

Halac, S., Villafañe, V. E., Gonçalves, R. J., and Helbling, E. W. Photochemical responses of three marine phytoplankton species exposed to ultraviolet radiation and increased temperature: role of photoprotective mechanisms. *Journal of Photochemistry and Photobiology B: Biology*, 141:217–227, 2014.

Hallegraeff, G. M. Ocean climate change, phytoplankton community responses, and harmful algal blooms: a formidable predictive challenge 1. *Journal of phycology*, 46 (2):220–235, 2010.

Halsey, K. H. and Jones, B. M. Phytoplankton strategies for photosynthetic energy allocation. *Annual review of marine science*, 7:265–297, 2015.

Hammer, A. C. and Pitchford, J. W. The role of mixotrophy in plankton bloom dynamics, and the consequences for productivity. *ICES Journal of Marine Science*, 62(5): 833–840, 2005.

Hansen, B., Bjornsen, P. K., and Hansen, P. J. The size ratio between planktonic predators and their prey. *Limnology and Oceanography*, 39(2):395–403, 1994.

Hansen, P., Bjørnsen, P., and Hansen, B. Zooplankton grazing and growth: Scaling within the 2-2,000-m body size range. *Limnology and Oceanography*, 42(4):687–704, January 1997. ISSN 0024-3590.

Hartmann, M., Grob, C., Tarran, G. A., Martin, A. P., Burkill, P. H., Scanlan, D. J., and Zubkov, M. V. Mixotrophic basis of atlantic oligotrophic ecosystems. *Proceedings of the National Academy of Sciences*, 109(15):5756–5760, 2012. ISSN 0027-8424.

Hausfather, Z. and Peters, G. P. Emissions–the 'business as usual'story is misleading. *Nature*, 577(7792):618–620, 2020.

Hays, G. C., Richardson, A. J., and Robinson, C. Climate change and marine plankton. *Trends in Ecology Evolution*, 20(6):337–344, 2005. ISSN 0169-5347. SPECIAL ISSUE: BUMPER BOOK REVIEW.

Heinze, C., Maier-Reimer, E., and Winn, K. Glacial pco2 reduction by the world ocean: Experiments with the hamburg carbon cycle model. *Paleoceanography*, 6(4):395–430, 1991.

Heinze, M. and Ilyina, T. Ocean biogeochemistry in the warm climate of the late paleocene. *Climate of the Past*, 11(1):63–79, 2015.

Hendry, K. R., Marron, A. O., Vincent, F., Conley, D. J., Gehlen, M., Ibarbalz, F. M., Quéguiner, B., and Bowler, C. Competition between silicifiers and non-silicifiers in the past and present ocean and its evolutionary impacts. *Frontiers in Marine Science*, 5:22, 2018.

Henson, S. A., Laufkötter, C., Leung, S., Giering, S. L., Palevsky, H. I., and Cavan, E. L. Uncertain response of ocean biological carbon export in a changing world. *Nature Geoscience*, 15(4):248–254, 2022.

Holling, C. S. The components of predation as revealed by a study of small-mammal predation of the european pine sawfly1. *The Canadian Entomologist*, 91(5):293–320, 1959.

Hollowed, A. B., Barange, M., Beamish, R. J., Brander, K., Cochrane, K., Drinkwater, K., Foreman, M. G., Hare, J. A., Holt, J., Ito, S.-i., et al. Projected impacts of climate change on marine fish and fisheries. *ICES Journal of Marine Science*, 70(5): 1023–1037, 2013.

Hu, Y. O., Karlson, B., Charvet, S., and Andersson, A. F. Diversity of pico- to mesoplankton along the 2000 km salinity gradient of the baltic sea. *bioRxiv*, 2015.

IPCC. *Climate Change 2021 – The Physical Science Basis: Working Group I Contribution to the Sixth Assessment Report of the Intergovernmental Panel on Climate Change*, page 673–816. Cambridge University Press, 2023.

Irigoien, X., Flynn, K., and Harris, R. Phytoplankton blooms: a 'loophole'in microzooplankton grazing impact? *Journal of Plankton Research*, 27(4):313–321, 2005.

Jassey, V. E., Signarbieux, C., Hättenschwiler, S., Bragazza, L., Buttler, A., Delarue, F., Fournier, B., Gilbert, D., Laggoun-Défarge, F., Lara, E., et al. An unexpected role for mixotrophs in the response of peatland carbon cycling to climate warming. *Scientific reports*, 5(1):16931, 2015.

Jin, X., Gruber, N., Dunne, J., Sarmiento, J. L., and Armstrong, R. Diagnosing the contribution of phytoplankton functional groups to the production and export of particulate organic carbon, caco3, and opal from global nutrient and alkalinity distributions. *Global Biogeochemical Cycles*, 20(2), 2006.

Jones, R. I. Mixotrophy in planktonic protists: an overview. *Freshwater biology*, 45(2): 219–226, 2000.

Kalinkat, G., Rall, B. C., Uiterwaal, S. F., and Uszko, W. Empirical evidence of type iii functional responses and why it remains rare. *Frontiers in Ecology and Evolution*, 11, 2023.

Karl, D. M., Björkman, K. M., Dore, J. E., Fujieki, L., Hebel, D. V., Houlihan, T., Letelier, R. M., and Tupas, L. M. Ecological nitrogen-to-phosphorus stoichiometry at station aloha. *Deep Sea Research Part II: Topical Studies in Oceanography*, 48(8-9): 1529–1566, 2001.

Key, R. M., Kozyr, A., Sabine, C. L., Lee, K., Wanninkhof, R., Bullister, J. L., Feely, R. A., Millero, F. J., Mordy, C., and Peng, T.-H. A global ocean carbon climatology: Results from global data analysis project (glodap). *Global biogeochemical cycles*, 18 (4), 2004.

Kiørboe, T. A mechanistic approach to plankton ecology. *ASLO Web Lectures*, 1(2): 1–91, 2009.

Kleypas, J. Nutrients, chlorophyll, primary production and related biogeochemical properties in the ocean mixed layer. a compilation of data collected at nine jfofs sites. 2001.

Koeve, W., Kähler, P., and Oschlies, A. Does export production measure transient changes of the biological carbon pump's feedback to the atmosphere under global warming? *Geophysical Research Letters*, 47(22):e2020GL089928, 2020.

Kriest, I., Oschlies, A., and Khatiwala, S. Sensitivity analysis of simple global marine biogeochemical models. *Global Biogeochemical Cycles*, 26(2), 2012.

Kritzberg, E. and Ekström, S. Increasing iron concentrations in surface waters–a factor behind brownification? *Biogeosciences*, 9(4):1465–1478, 2012.

Kwiatkowski, L., Torres, O., Bopp, L., Aumont, O., Chamberlain, M., Christian, J. R., Dunne, J. P., Gehlen, M., Ilyina, T., John, J. G., et al. Twenty-first century ocean warming, acidification, deoxygenation, and upper-ocean nutrient and primary production decline from cmip6 model projections. *Biogeosciences*, 17(13):3439–3470, 2020.

Kwon, E. Y., Primeau, F., and Sarmiento, J. L. The impact of remineralization depth on the air–sea carbon balance. *Nature Geoscience*, 2(9):630–635, 2009.

Laws, E. A. The importance of respiration losses in controlling the size distribution of marine phytoplankton. *Ecology*, 56(2):419–426, 1975.

Layman, C. A., Giery, S. T., Buhler, S., Rossi, R., Penland, T., Henson, M. N., Bogdanoff, A. K., Cove, M. V., Irizarry, A. D., Schalk, C. M., et al. A primer on the history of food web ecology: fundamental contributions of fourteen researchers. *Food Webs*, 4:14–24, 2015.

le Quéré, C., Harrison, S. P., Colin Prentice, I., Buitenhuis, E. T., Aumont, O., Bopp, L., Claustre, H., Cotrim Da Cunha, L., Geider, R., Giraud, X., Klaas, C., Kohfeld, K. E., Legendre, L., Manizza, M., Platt, T., Rivkin, R. B., Sathyendranath, S., Uitz, J., Watson, A. J., and Wolf-Gladrow, D. Ecosystem dynamics based on plankton functional types for global ocean biogeochemistry models. *Global Change Biology*, 11 (11):2016–2040, 2005.

Leander, B. S. A hierarchical view of convergent evolution in microbial eukaryotes 1. *Journal of eukaryotic microbiology*, 55(2):59–68, 2008.

Lenton, T., Williamson, M., Edwards, N., Marsh, R., Price, A., Ridgwell, A., Shepherd, J., Cox, S., and team, G. Millennial timescale carbon cycle and climate change in an efficient earth system model. *Climate Dynamics*, 26:687–711, 2006.

Lepori-Bui, M., Paight, C., Eberhard, E., Mertz, C. M., and Moeller, H. V. Evidence for evolutionary adaptation of mixotrophic nanoflagellates to warmer temperatures. *Global Change Biology*, 28(23):7094–7107, 2022.

Lévy, M., Iovino, D., Resplandy, L., Klein, P., Madec, G., Tréguier, A.-M., Masson, S., and Takahashi, K. Large-scale impacts of submesoscale dynamics on phytoplankton: Local and remote effects. *Ocean Modelling*, 43:77–93, 2012.

Levy, M., Memery, L., and Madec, G. The onset of a bloom after deep winter convection in the northwestern mediterranean sea: mesoscale process study with a primitive equation model. *Journal of Marine Systems*, 16(1-2):7–21, 1998.

Lévy, M., Resplandy, L., and Lengaigne, M. Oceanic mesoscale turbulence drives large biogeochemical interannual variability at middle and high latitudes. *Geophysical Research Letters*, 41(7):2467–2474, 2014.

Li, W. K. W. and Dickie, P. M. Temperature characteristics of photosynthetic and heterotrophic activities: Seasonal variations in temperate microbial plankton. *Applied and Environmental Microbiology*, 53(10):2282–2295, 1987.

Litchman, E. and Klausmeier, C. Trait-based community ecology of phytoplankton. *Annual Review of Ecology Evolution and Systematics*, 39:615–639, 12 2008.

Litchman, E., Klausmeier, O., Christopher, A., Schofield, M., and Falkowski, P. G. The role of functional traits and trade-offs in structuring phytoplankton communities: scaling from cellular to ecosystem level. *Ecology Letters*, 10:1170–1181, 2007.

Lochte, K., Ducklow, H., Fasham, M., and Stienen, C. Plankton succession and carbon cycling at 47 n 20 w during the jgofs north atlantic bloom experiment. *Deep Sea Research Part II: Topical Studies in Oceanography*, 40(1-2):91–114, 1993.

Longhurst, A., Sathyendranath, S., Platt, T., and Caverhill, C. An estimate of global primary production in the ocean from satellite radiometer data. *Journal of plankton Research*, 17(6):1245–1271, 1995.

Mahowald, N. M., Baker, A. R., Bergametti, G., Brooks, N., Duce, R. A., Jickells, T. D., Kubilay, N., Prospero, J. M., and Tegen, I. Atmospheric global dust cycle and iron inputs to the ocean. *Global biogeochemical cycles*, 19(4), 2005.

Manabe, S., Stouffer, R. J., Spelman, M. J., and Bryan, K. Transient responses of a coupled ocean–atmosphere model to gradual changes of atmospheric co2. part i. annual mean response. *Journal of Climate*, 4(8):785–818, 1991.

Marañón, E., Cermeño, P., López-Sandoval, D. C., Rodríguez-Ramos, T., Sobrino, C., Huete-Ortega, M., Blanco, J. M., and Rodríguez, J. Unimodal size scaling of phytoplankton growth and the size dependence of nutrient uptake and use. *16*, 3(371-379), 2013.

Marsh, R., Müller, S., Yool, A., and Edwards, N. Incorporation of the c-goldstein efficient climate model into the genie framework:" eb_go_gs" configurations of genie. *Geoscientific Model Development*, 4(4):957–992, 2011.

Martiny, J., Bohannan, B., Brown, J., Colwell, R., Fuhrman, J., Green, J., Horner-Devine, C., Kane, M., Krumins, J., Kuske, C., Morin, P., Naeem, S., Øvreås, L., Reysenbach, a.-l., Smith, V., and Staley, J. Microbial biogeography: putting microorganisms on the map. *Nature reviews. Microbiology*, 4:102–12, 03 2006.

Menden-Deuer, S. and Lessard, E. J. Carbon to volume relationships for dinoflagellates, diatoms, and other protist plankton. *Limnology and oceanography*, 45(3):569–579, 2000.

Michael, A. F., M, K. D., and Capone, D. G. Element stoichiometry, new production and nitrogen fixation. *Oceanography*, 14(4):68, 2001.

Millette, N. C., Gast, R. J., Luo, J. Y., Moeller, H. V., Stamieszkin, K., Andersen, K. H., Brownlee, E. F., Cohen, N. R., Duhamel, S., Dutkiewicz, S., et al. Mixoplankton and mixotrophy: future research priorities. *Journal of Plankton Research*, page fbad020, 2023.

Mitra, A., Flynn K. J. Burkholder, J. M., Berge, T., Calbet, A., Raven, J. A., Granéli, E., Glibert, P. M., Hansen, P. J., Stoecker, D. K., Thingstad, F., Tillmann, U., Våge, S., Wilken, S., and Zubkov, M. V. The role of mixotrophic protists in the biological carbon pump. *Biogeosciences*, 11:995–1005, 2014.

Mitra, A., Flynn, K. J., Stoecker, D. K., and Raven, J. A. Trait trade-offs in phagotrophic microalgae: the mixoplankton conundrum. *European Journal of Phycology*, pages 1–20, 2023.

Moloney, C. L., Field, J. G., and Lucas, M. I. The size-based dynamics of plankton food webs. II. Simulations of three contrasting southern Benguela food webs. *Journal of Plankton Research*, 13(5):1039–1092, 09 1991.

Monod, J. Recherches sur la croissance des cultures bacteriennes. 1942.

Monod, J. Biosynthese eines enzyms. information, induktion, repression. *Angewandte Chemie*, 71(22):685–691, 1959.

Moore, C., Mills, M., Arrigo, K., Berman-Frank, I., Bopp, L., Boyd, P., Galbraith, E., Geider, R., Guieu, C., Jaccard, S., et al. Processes and patterns of oceanic nutrient limitation. *Nature geoscience*, 6(9):701–710, 2013.

Moore, J. K., Doney, S. C., Kleypas, J. A., Glover, D. M., and Fung, I. Y. An intermediate complexity marine ecosystem model for the global domain. *Deep Sea Research Part II: Topical Studies in Oceanography*, 49(1-3):403–462, 2001.

Moore, J. K., Fu, W., Primeau, F., Britten, G. L., Lindsay, K., Long, M., Doney, S. C., Mahowald, N., Hoffman, F., and Randerson, J. T. Sustained climate warming drives declining marine biological productivity. *Science*, 359(6380):1139–1143, 2018.

Najjar, R. G., Sarmiento, J. L., and Toggweiler, J. Downward transport and fate of organic matter in the ocean: Simulations with a general circulation model. *Global Biogeochemical Cycles*, 6(1):45–76, 1992.

Nguyen, N.-P., Warnow, T., Pop, M., and White, B. A perspective on 16s rrna operational taxonomic unit clustering using sequence similarity. *NPJ biofilms and microbiomes*, 2(1):1–8, 2016.

Nygaard, K. and Tobiesen, A. Bacterivory in algae: a survival strategy during nutrient limitation. *Limnology and Oceanography*, 38(2):273–279, 1993.

Olsen, A., Key, R. M., Van Heuven, S., Lauvset, S. K., Velo, A., Lin, X., Schirnick, C., Kozyr, A., Tanhua, T., Hoppema, M., et al. The global ocean data analysis project version 2 (glodapv2)–an internally consistent data product for the world ocean. *Earth System Science Data*, 8(2):297–323, 2016.

Oschlies, A., Koeve, W., and Garçon, V. An eddy-permitting coupled physical-biological model of the north atlantic: 2. ecosystem dynamics and comparison with satellite and jgofs local studies data. *Global Biogeochemical Cycles*, 14(1):499–523, 2000.

Pachauri, R. K., Allen, M. R., Barros, V. R., Broome, J., Cramer, W., Christ, R., Church, J. A., Clarke, L., Dahe, Q., Dasgupta, P., et al. *Climate change 2014: synthesis report. Contribution of Working Groups I, II and III to the fifth assessment report of the Intergovernmental Panel on Climate Change*. Ipcc, 2014.

Pahlow, M. and Riebesell, U. Temporal trends in deep ocean redfield ratios. *Science*, 287(5454):831–833, 2000.

Palevsky, H. I. and Doney, S. C. Sensitivity of 21st century ocean carbon export flux projections to the choice of export depth horizon. *Global Biogeochemical Cycles*, 35 (2):e2020GB006790, 2021.

Parekh, P., Dutkiewicz, S., Follows, M., and Ito, T. Atmospheric carbon dioxide in a less dusty world. *Geophysical research letters*, 33(3), 2006.

Pérez, M., Dolan, J., and Fukai, E. Planktonic oligotrich ciliates in the nw mediterranean: growth rates and consumption by copepods. *Marine Ecology Progress Series*, 155:89–101, 1997.

Prentice, I. C., Farquhar, G., Fasham, M., Goulden, M. L., Heimann, M., Jaramillo, V., Kheshgi, H., Le Quéré, C., Scholes, R., Wallace, D. W., et al. The carbon cycle and atmospheric carbon dioxide, 2001.

Princiotta, S. D., Smith, B. T., and Sanders, R. W. Temperature-dependent phagotrophy and phototrophy in a mixotrophic chrysophyte. *Journal of phycology*, 52(3): 432–440, 2016.

Proctor, L. M. and Fuhrman, J. A. Viral mortality of marine bacteria and cyanobacteria. *Nature*, 343(6253):60–62, 1990.

Raven, J. A. Phagotrophy in phototrophs. *Limnology and Oceanography*, 42(1):198–205, 1997.

Redfield, A. C. *On the proportions of organic derivatives in sea water and their relation to the composition of plankton*, volume 1. university press of liverpool Liverpool, 1934.

Reinhard, C. T., Planavsky, N. J., Ward, B. A., Love, G. D., Le Hir, G., and Ridgwell, A. The impact of marine nutrient abundance on early eukaryotic ecosystems. *Geobiology*, 18(2):139–151, 2020.

Ridgwell, A., Hargreaves, J., Edwards, N. R., Annan, J., Lenton, T. M., Marsh, R., Yool, A., and Watson, A. Marine geochemical data assimilation in an efficient earth system model of global biogeochemical cycling. *Biogeosciences*, 4(1):87–104, 2007.

Rose, J. M. and Caron, D. A. Does low temperature constrain the growth rates of heterotrophic protists? evidence and implications for algal blooms in cold waters. *Limnology and Oceanography*, 52(2):886–895, 2007.

Roxburgh, S., Berry, S. L., Buckley, T., Barnes, B., and Roderick, M. What is npp? inconsistent accounting of respiratory fluxes in the definition of net primary production. *Functional Ecology*, 19(3):378–382, 2005.

Roy, S., Sathyendranath, S., Bouman, H., and Platt, T. The global distribution of phytoplankton size spectrum and size classes from their light-absorption spectra derived from satellite data. *Remote Sensing of Environment*, 139:185–197, 2013.

Sanders, R. W., Porter, K. G., and Caron, D. A. Relationship between phototrophy and phagotrophy in the mixotrophic chrysophyte poterioochromonas malhamensis. *Microbial Ecology*, 19(1):97–109, 1990.

Sarkar, S., Cotton, L. J., Valdes, P. J., and Schmidt, D. N. Shallow water records of the petm: Novel insights from ne india (eastern tethys). *Paleoceanography and Paleoclimatology*, 37(7):e2021PA004257, 2022.

Sarmiento, J. L. *Ocean biogeochemical dynamics*. Princeton university press, 2006.

Sarmiento, J. L., Slater, R., Barber, R., Bopp, L., Doney, S., Hirst, A., Kleypas, J., Matear, R., Mikolajewicz, U., Monfray, P., et al. Response of ocean ecosystems to climate warming. *Global Biogeochemical Cycles*, 18(3), 2004.

Schwalm, C. R., Glendon, S., and Duffy, P. B. Rcp8. 5 tracks cumulative co2 emissions. *Proceedings of the National Academy of Sciences*, 117(33):19656–19657, 2020.

Semtner Jr, A. J. A model for the thermodynamic growth of sea ice in numerical investigations of climate. *Journal of Physical Oceanography*, 6(3):379–389, 1976.

Shigesada, N. and Okubo, A. Analysis of the self-shading effect on algal vertical distribution in natural waters. *Journal of Mathematical Biology*, 12:311–326, 1981.

Sigman, D. M. and Haug, G. The biological pump in the past. *Treatise on geochemistry*, 6:625, 2003.

Simberloff, D. and Dayan, T. The guild concept and the structure of ecological communities. *Annual review of ecology and systematics*, 22(1):115–143, 1991.

Six, K. D. and Maier-Reimer, E. Effects of plankton dynamics on seasonal carbon fluxes in an ocean general circulation model. *Global Biogeochemical Cycles*, 10(4):559–583, 1996.

Stabile, T. A., Zollo, A., Vassallo, M., and Iannaccone, G. Underwater acoustic channel properties in the gulf of naples and their effects on digital data transmission. *Annals of Geophysics*, 50:313–328, 01 2007.

Steinacher, M., Joos, F., Frölicher, T., Bopp, L., Cadule, P., Cocco, V., Doney, S., Gehlen, M., Lindsay, K., Moore, J., et al. Projected 21st century decrease in marine productivity: a multi-model analysis. *Biogeosciences*, 7(3):979–1005, 2010.

Stickney, H., Hood, R., and Stoecker, D. The impact of mixotrophy on planktonic marine ecosystems. *Ecological Modelling*, 125(2):203–230, 2000. ISSN 0304-3800.

Stoecker, D. K. Conceptual models of mixotrophy in planktonic protists and some ecological and evolutionary implications. *European Journal of Protistology*, 34(3): 281–290, 1998. ISSN 0932-4739.

Stoecker, D. K. Mixotrophy among dinoflagellates. *Journal of eukaryotic microbiology*, 46(4):397–401, 1999.

Stoecker, P. J., D. K. Hansen, Caron, D., and Mitra, A. Mixotrophy in the marine plankton. *Annual Review of Marine Science*, 9:311–35, 2017.

Tagliabue, A. and Arrigo, K. R. Anomalously low zooplankton abundance in the ross sea: An alternative explanation. *Limnology and Oceanography*, 48(2):686–699, 2003.

Tang, E. P. The allometry of algal growth rates. *Journal of Plankton Research*, 17(6): 1325–1335, 1995.

Telford, R. J., Vandvik, V., and Birks, H. J. B. Dispersal limitations matter for microbial morphospecies. *Science*, 312(5776):1015–1015, 2006. ISSN 0036-8075.

Thingstad, T. F., Havskum, H., Garde, K., and Riemann, B. On the strategy of 'eating your competitor': A mathematical analysis of algal mixotrophy. *Ecology*, 77(7):2108–2118, 1996.

Thingstad, T. F. and Lignell, R. Theoretical models for the control of bacterial growth rate, abundance, diversity and carbon demand. *Aquatic microbial ecology*, 13(1):19–27, 1997.

Troost, T. A., Kooi, B. W., and Kooijman, S. A. When do mixotrophs specialize adaptive dynamics theory applied to a dynamic energy budget model. *Mathematical Biosciences*, 193(2005):159–182, 2005.

Tyrrell, T. The relative influences of nitrogen and phosphorus on oceanic primary production. *Nature*, 400(6744):525–531, 1999.

Tyrrell, T. Anthropogenic modification of the oceans. *Philosophical Transactions of the Royal Society A: Mathematical, Physical and Engineering Sciences*, 369(1938): 887–908, 2011.

Vallina, S. M., Ward, B., Dutkiewicz, S., and Follows, M. Maximal feeding with active prey-switching: A kill-the-winner functional response and its effect on global diversity and biogeography. *Progress in Oceanography*, 120:93–109, 2014.

Van Donk, E. and Ringelberg, J. The effect of fungal parasitism on the succession of diatoms in lake maarsseveen i (the netherlands). *Freshwater biology*, 13(3):241–251, 1983.

Volk, T. and Hoffert, M. I. Ocean carbon pumps: Analysis of relative strengths and efficiencies in ocean-driven atmospheric co2 changes. pages 99–110, 1985.

Våge, S., Castellani, M., Giske, J., and Thingstad, T. F. Successful strategies in size structured mixotrophic food webs. *Aquat Ecol*, (47):329–347, 2013.

Ward, B. A. Mixotroph ecology: More than the sum of its parts. *Proceedings of the National Academy of Sciences*, 116(13):5846–5848, 2019. ISSN 0027-8424.

Ward, B. A., Dutkiewicz, S., Jahn, O., and Follows, M. J. A size-structured food-web model for the global ocean. *Limnol. Oceanogr*, 57(6):1877–1891, 2012.

Ward, B. A., Dutkiewicz, S., Barton, A. D., and Follows, M. J. Biophysical aspects of resource acquisition and competition in algal mixotrophs. *178*, 1, 2011.

Ward, B. A. and Follows, M. J. Marine mixotrophy increases trophic transfer efficiency, mean organism size, and vertical carbon flux. *Proceedings of the National Academy of Sciences*, 113(11):2958–2963, 2016.

Ward, B. A., Marañón, E., Sauterey, B., Rault, J., and Claessen, D. The size dependence of phytoplankton growth rates: A trade-off between nutrient uptake and metabolism. *The American Naturalist*, 189(2), 2017.

Ward, B. A., Wilson, J. D., Death, R. M., Monteiro, F. M., Yool, A., and Ridgwell, A. Ecogenie 1.0: plankton ecology in the cgenie earth system model. *Geoscientific Model Development*, 11(10):4241–4267, 2018.

Weaver, A. J., Eby, M., Wiebe, E. C., Bitz, C. M., Duffy, P. B., Ewen, T. L., Fanning, A. F., Holland, M. M., MacFadyen, A., Matthews, H. D., et al. The uvic earth system climate model: Model description, climatology, and applications to past, present and future climates. In *Data, Models and Analysis*, pages 169–236. Routledge, 2001.

Wieczynski, D. J., Moeller, H. V., and Gibert, J. P. Mixotrophic microbes create carbon tipping points under warming. *Functional Ecology*, 2023.

Wilken, S., Huisman, J., Naus-Wiezer, S., and Van Donk, E. Mixotrophic organisms become more heterotrophic with rising temperature. *Ecology Letters*, 16:225–233, 2013.

Wilken, S., Soares, M., Urrutia-Cordero, P., Ratcovich, J., Ekvall, M. K., Van Donk, E., and Hansson, L.-A. Primary producers or consumers? increasing phytoplankton bacterivory along a gradient of lake warming and browning. *Limnology and Oceanography*, 63(S1):S142–S155, 2018.

Wilken, S., Verspagen, J., Naus-Wiezer, S., Donk, E., and Huisman, J. Biological control of toxic cyanobacteria by mixotrophic predators: An experimental test of intraguild predation theory. *Ecological Applications*, 24:1235–1249, 07 2014.

Wilson, J. D., Andrews, O., Katavouta, A., de Melo Viríssimo, F., Death, R. M., Adloff, M., Baker, C. A., Blackledge, B., Goldsworth, F. W., Kennedy-Asser, A. T., et al. The biological carbon pump in cmip6 models: 21st century trends and uncertainties. *Proceedings of the National Academy of Sciences*, 119(29):e2204369119, 2022.

Wilson, J., Monteiro, F., Schmidt, D., Ward, B., and Ridgwell, A. Linking marine plankton ecosystems and climate: a new modeling approach to the warm early eocene climate. *Paleoceanography and Paleoclimatology*, 33(12):1439–1452, 2018.

Yutin, N., Wolf, M. Y., Wolf, Y. I., and Koonin, E. V. The origins of phagocytosis and eukaryogenesis. *Biology direct*, 4(1):1–26, 2009.

Zhang, C. L., Xie, W., Martin-Cuadrado, A.-B., and Rodriguez-Valera, F. Marine group ii archaea, potentially important players in the global ocean carbon cycle. *Frontiers in microbiology*, 6:1108, 2015.

Zingone, A., Dubroca, L., Iudicone, D., Margiotta, F., Corato, F., Ribera d'Alcalà, M., Saggiomo, V., and Sarno, D. Coastal phytoplankton do not rest in winter. *Estuaries and Coasts*, 33:342–361, 2010.